

Dissertation zur Erlangung des Doktorgrades
der Fakultät für Chemie und Pharmazie
der Ludwig-Maximilians-Universität München

Sequence-defined polycationic oligomers for nucleic acid
delivery

Christina Maria Troiber

aus

Deggendorf, Deutschland

2012

Erklärung

Diese Dissertation wurde im Sinne von § 7 der Promotionsordnung vom 28. November 2011 von Herrn Prof. Dr. Ernst Wagner betreut.

Eidesstattliche Versicherung

Diese Dissertation wurde eigenständig und ohne unerlaubte Hilfe erarbeitet.

München, 12.12.2012

(Unterschrift des Autors)

Dissertation eingereicht am	13.12.2012
1. Gutachter:	Prof. Dr. Ernst Wagner
2. Gutachter:	Prof. Dr. Wolfgang Frieß
Mündliche Prüfung am	05.02.2013

Meinen Eltern

TABLE OF CONTENTS

I.	INTRODUCTION.....	1
1.	Nucleic acids as pharmaceutical tools	1
2.	Delivery systems for nucleic acids.....	2
2.1.	Polydisperse delivery systems	2
2.2.	Precise delivery systems.....	3
2.2.1.	Dendrimers.....	3
2.2.2.	Peptidic carriers	4
3.	Precise conjugation techniques	6
4.	Polyplex stability.....	8
5.	Polyplex size.....	9
6.	Aims of the thesis	10
II.	MATERIALS AND METHODS.....	11
1.	Chemicals and reagents	11
2.	Solid phase assisted peptide synthesis.....	12
2.1.	Synthesis of 3-Fmoc-4-diaminobenzoic acid (Fmoc-Dbz).....	12
2.2.	Synthesis of ICH-CAMP	12
2.3.	Attachment of the first amino acid	12
2.3.1.	Loading of a chlorotriyl chloride resin with Fmoc-Tyr(tBu)-OH	12
2.3.2.	Loading of a chlorotriyl chloride resin with Fmoc-Cys(trt)-OH	13
2.3.3.	Loading of a chlorotriyl chloride resin with Fmoc-Glu-OtBu	13
2.3.4.	Loading of a chlorotriyl chloride resin with dde-Lys(Fmoc)-OH	13
2.3.5.	Loading of a MBHA Rink amide resin with Dbz-Fmoc.....	14
2.4.	Convergent fragment synthesis.....	14
2.4.1.	Convergent synthesis of Fmoc-Tyr(tBu) ₃ -OH.....	14
2.4.2.	Convergent synthesis of Boc-Tyr(tBu) ₃ -OH.....	14
2.4.3.	Convergent synthesis of Fola(trt)-OH	14
2.4.4.	Cleavage conditions	15
2.5.	Oligomer synthesis.....	15
2.5.1.	Synthesis of the T-Shape 464: H ₂ N-C-Y ₃ -Stp ₂ -[(Y ₃) ₂]-K]K-Stp ₂ -Y ₃ -C-OH	15

2.5.2.	Reverse synthesis of 408: [(ICH-CAMP-Stp ₅) ₂ K]K[K(OleA) ₂]-OH	16
2.5.3.	Synthesis of Nbz-PEG ₂ -A.....	17
2.5.4.	Cleavage conditions	17
2.6.	Proton NMR spectra.....	18
2.7.	Native chemical ligation	18
3.	Biophysical characterization.....	18
3.1.	DNA and siRNA polyplex formation	18
3.2.	Gel shift assays.....	19
3.2.1.	DNA binding assay.....	19
3.2.2.	siRNA binding assay	19
3.2.3.	Gel shift assay of siRNA polyplexes in 90% FBS.....	19
3.3.	Methods for particle size determination.....	19
3.3.1.	Dynamic laser light scattering	19
3.3.2.	Fluorescence correlation spectroscopy.....	20
3.3.3.	Atomic force microscopy	21
3.3.4.	Nanoparticle tracking analysis.....	22
3.4.	Buffer capacity	22
3.5.	Erythrocyte leakage assay	22
4.	In vitro analysis	23
4.1.	Cell culture	23
4.2.	Flow cytometry	23
4.3.	Luciferase gene silencing.....	24
4.4.	Luciferase reporter gene expression.....	24
4.5.	Cell viability assay (MTT)	24
5.	In vivo experiments.....	25
5.1.	Polyplex distribution	25
5.2.	N2A tumor treatment.....	25
6.	Statistical analysis	26
III.	RESULTS	27
1.	Stabilizing effects of tyrosine trimers on pDNA and siRNA polyplexes.....	27
1.1.	Design and synthesis of oligotyrosine containing oligomers	27
1.1.1.	Convergent building block synthesis	29

1.1.2.	Structural overview.....	29
1.2.	Biophysical characterization.....	32
1.3.	Uptake and transfection efficiency	36
1.4.	Serum stability.....	39
1.5.	In vivo experiments	44
2.	Further stabilizing motifs for pDNA and siRNA polyplexes	51
2.1.	Ureido-pyrimidinone containing oligomers	51
2.1.1.	Building block synthesis	52
2.1.2.	Oligomer synthesis.....	52
2.1.3.	In vitro characterization	53
2.2.	Pyridyl-thiourea containing oligomers	54
2.2.1.	Oligomer synthesis.....	55
2.2.2.	Transfection efficiency	55
2.3.	Stabilizing effect of C-R-C motifs on pDNA and siRNA polyplexes	56
2.3.1.	Oligomer synthesis and structures	57
2.3.2.	Biophysical characterization.....	57
2.3.3.	Transfection efficiency	60
2.3.4.	Serum stability.....	62
3.	Comparison of four different particle sizing methods for siRNA polyplex characterization	64
3.1.	Synthesis of oligomers	65
3.2.	Dynamic laser light scattering	66
3.3.	Atomic force microscopy	69
3.4.	Nanoparticle tracking analysis.....	70
3.5.	Fluorescence correlation spectroscopy	72
4.	Native chemical ligation	76
4.1.	Principles of NCL	76
4.1.1.	Synthesis of model oligomers for NCL	77
4.1.2.	Ligation of model oligomers	78
4.2.	Synthesis of shielded and targeted oligomers for NCL	79
IV.	DISCUSSION.....	80
1.	Stabilizing effects of tyrosine trimers on pDNA and siRNA polyplexes.....	80

2.	Further stabilizing motifs for pDNA and siRNA polyplexes	82
3.	Comparison of four different particle sizing methods for siRNA polyplex characterization	85
4.	Native chemical ligation	89
V.	SUMMARY	91
VI.	REFERENCES	93
VII.	APPENDIX	102
1.1.	Abbreviations	102
1.2.	Analytical data	106
1.3.	Publications	114
1.3.1.	Original paper	114
1.3.2.	Reviews	115
1.3.3.	Patents	115
1.3.4.	Poster presentations	115
1.3.5.	Oral abstracts	115
VIII.	ACKNOWLEDGEMENTS	116

I. INTRODUCTION

1. Nucleic acids as pharmaceutical tools

Genetic disorders like mucoviscidosis¹, severe combined immunodeficiency (SCID)², haemophilia³ and acquired viral infections⁴⁻⁵ have their origin at gene level. Classical gene therapy addresses these diseases by inserting functional DNA into the human genome in order to replace defect gene sections. DNA based therapy has been extended to other areas like cancer therapy⁶ and vaccination⁷. However, safety concerns about interference with the human genome and incidence of side effects remain.

Consequently, the focus of nucleic acid research shifted to the application of RNA. RNA interference (RNAi), discovered by Fire et al.⁸, leads to specific gene silencing and hence, the inhibition of the cellular expression of a protein. Tuschl et al.⁹ demonstrated that double stranded, small synthetic interfering RNA (siRNA) mediates target specific RNA interference without significant side effects. After reaching the cytosol with help of appropriate carriers, siRNAs are incorporated in a multiprotein complex called RNA induced silencing complex (RISC). Thereafter, the enzyme Argonaute 2 unwinds the siRNA and the sense strand of the siRNA is cleaved¹⁰⁻¹¹. The RISC is activated by the guide strand (antisense strand) which remains incorporated¹² and hence, cleaves repeatedly the complementary mRNA. As a result, the gene of interest is silenced for several days.

A prerequisite for successful delivery of genetic information into target cells of patients is the existence of appropriate carriers. Efficient viral and synthetic vectors already exist for ex vivo nucleic acid delivery, whereas efficient and successful in vivo transport of DNA, RNA or siRNA to target cells is still limited. In terms of efficiency, viral vectors are still the most potent systems. Nonetheless synthetic vectors possess distinct advantages, like lower immunogenic potential, reduced mutagenic risk, and easier handling and manufacturing¹³⁻¹⁷. A combination of both worlds, the design of 'synthetic viruses', might be most advantageous¹⁸⁻²¹.

2. Delivery systems for nucleic acids

Anionic charge, large size and degradability of nucleic acids by nucleases make administration of naked nucleic acids rather inefficient in reaching the target location²²⁻²³. For these reasons, special carriers have been developed to aid the delivery of genetic material. They are designed to protect nucleic acids in the extracellular environment and to mediate their transport into the cytoplasm²⁴. Several barriers including stickiness to non-target cells, extracellular fluids, and matrix have to be overcome²⁵. Cell entry, endolysosomal escape, cytoplasmic trafficking and vector unpacking are further bottlenecks for successful delivery²⁶⁻²⁸. In case of gene delivery, the functional plasmid DNA (pDNA) encoding the protein has to be delivered into the nucleus²⁹.

The most common synthetic vectors are cationic lipids and polymers which form electrostatic complexes with the negatively charged nucleic acid. The payload is packaged into nanosized structures enabling uptake into cells^{27, 30}. In case of polymers, the polyplex stability and transfection efficiency depends on the chemical type, molecular weight and topology of the cationic polymer, as well as the ratio of polymer to nucleic acid³¹⁻³³. Polyamine structures, including poly-*L*-lysine, linear and branched polyethylenimines (PEIs) or polyamidoamine (PAMAM) dendrimers, are an often used class of artificial vector systems. In some polymers such as PEI or PAMAM, only a fraction of amine groups are protonated at physiological pH. The remaining basic groups may exhibit a buffering effect (proton-sponge effect) upon entry into the endosome. The pH-mediated creation of new cationic polymer charges triggers an influx of chloride counter-ions followed by water. The resulting osmotic pressure, together with interactions of the cationic polymer with the membrane, is assumed to rupture the lysosome/endosome releasing the carrier and its cargo into the cytosol³⁴⁻³⁶.

2.1. Polydisperse delivery systems

Polyethylenimine, a polydisperse delivery system, has been one of the gold standards for polymeric pDNA transfer in vitro and in vivo³⁷. Various forms of branched PEI (bPEI) with molecular weights between 2 kDa and 800 kDa have been used frequently. bPEI contains primary, secondary, and tertiary amino

groups. These amines have pK_a values spanning a broad pH range, resulting in high buffering capacity. The degree of protonation of the amines increases from roughly 20 to 45%, as pH decreases from 7 to 5³⁴. bPEI is synthesized by polymerization of aziridine and hence, has a very heterogeneous and polydisperse structure.

Branched PEI and many other related polymers and their derivatives show a heterogeneous distribution of molecular weight and isomers, what significantly influences physicochemical properties, biological efficiency, and cytotoxicity³⁸⁻⁴¹. Moreover, random attachment of one or even several different functional domains results in heterogeneous conjugates that might be useful in experimental approaches, but are rather unsuitable for clinical developments⁴².

2.2. Precise delivery systems

A possible solution to the inherent drawbacks of macromolecules derived by random polymerization is the synthesis of defined polymeric systems as nucleic acid carriers. The precise structure definition allows the evaluation of structure activity relationships.

2.2.1. Dendrimers

Dendritic structures are built from a series of branches extending outward from an inner core. Each iteration leads to a higher generation material and therefore to dendrimers with higher molecular weight. They consist of three distinct parts: A core, branching units and branches which can be chemically altered independently. As a result, an enormous variety of possible dendrimers exist⁴³.

Denkewalter⁴⁴ reported the synthesis of *L*-lysine based dendrimers in the early 1980s which are usually synthesized by means of solid phase peptide synthesis (SPPS) introduced by Merrifield in 1963⁴⁵. Boc-protected lysines were coupled to the core repeatedly after TFA deprotection resulting in dendritic polylysine structures of different generations. Multiple antigen peptide (MAP) systems are a distinct type of dendritic structures containing an inner oligolysine core, multiple copies of synthetic peptide antigens and a simple amino acid, such as alanine or

glycine, as internal standard for monitoring the synthesis process⁴⁶. These systems are used in vaccines to induce immunoreactions.

Starburst polyamidoamine (PAMAM) dendrimers are spherical, highly ordered, dendritic polymers with positively charged primary amino groups on their surface at physiological pH. The manufacturing process is a series of repetitive steps starting with a central initiator core. This core may consist of either an ammonium as trivalent initiator or an alkylenediamine as tetravalent initiator. Methyl acrylates are added to the core by exhaustive Michael addition followed by amidation of the resulting ester with an excess of alkylenediamine. Each complete growth step represents a new generation of polymer with a larger molecular diameter, twice the number of reactive surface sites, and approximately twice the molecular weight of the preceding generation⁴⁷.

2.2.2. Peptidic carriers

Monodispersity and exact composition, defined by peptide sequence, are key advantages of peptidic carriers. This structural definition allows the evaluation of structure activity relationships. Natural amino acids with cationic or protonated side chains are able to bind nucleic acids through electrostatic interactions and build positively charged polyplexes which are taken up through endocytosis.

Solid phase peptide synthesis (SPPS) provided important technology such as orthogonal protective groups which can be very useful for synthesizing monodisperse sequence-defined polymers⁴⁸. Instead of applying only protected natural amino acids in SPPS, artificial monomer building blocks are introduced to precisely position various functionalities within the peptide sequence. Natural and artificial amino acids, but also monomers of completely different chemistries, chemical targeting ligands, polyethylene glycol (PEG) molecules or lipophilic domains can be used as functional groups. Hartmann and Börner applied SPPS for generating sequence-defined multifunctional polyamidoamines (PAA)⁴⁹⁻⁵². Alternate coupling steps of diacids (succinic anhydride, Suc) and diamines, like diamino-*N*-methyldipropylamine (Damp) or (*tBoc*)-spermine (*tBoc*-Spe), led to stepwise assembly of polyamidoamines (Figure 1)⁵³. Within the single component PAA-block segment, functionalities were positioned precisely along the polymer allowing local control of the chain properties.

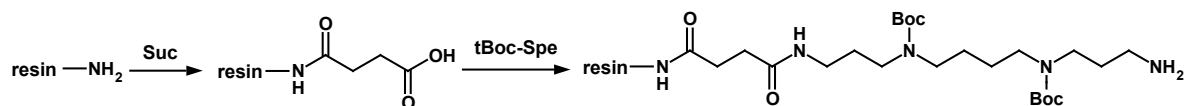


Figure 1: Alternate coupling steps of Suc and *t*Boc-Spe on solid phase

As a variation of the concept, Schaffert et al.⁵⁴ introduced novel Fmoc/Boc-protected polyamino acids (Stp, Gtp, Gtt, Ptp, Figure 2) fully compatible with standard Fmoc-peptide synthesis. Fmoc-polyamino acids contain diacids as well as diamines in one building block. The secondary amines of tetraethylenepentamine (tp) or triethylenetetramine (tt) were protected with di-*tert*-butyl dicarbonate (Boc_2O). The symmetrical Boc-protected diamines were monoacetylated in the first step with various cyclic anhydrides: Succinic (S), phthalic (P) or glutaric (G) anhydride, followed by subsequent Fmoc-protection. The novel building blocks were assembled by standard Fmoc/Boc SPPS, optionally in combination with natural amino acids (Figure 2) to provide defined polycations⁵⁴. The presented strategy has been applied for synthesis of a library of over 600 defined polycationic carriers for nucleic acid delivery, including efficient pDNA and siRNA carriers⁵⁵⁻⁵⁶. The artificial amino acids Stp, Gtp, or Gtt were applied together with lysines as branching units, cysteines as bioreversible disulfide forming units, and various fatty acids as domains providing hydrophobic stabilization, but also endosomal membrane destabilization.

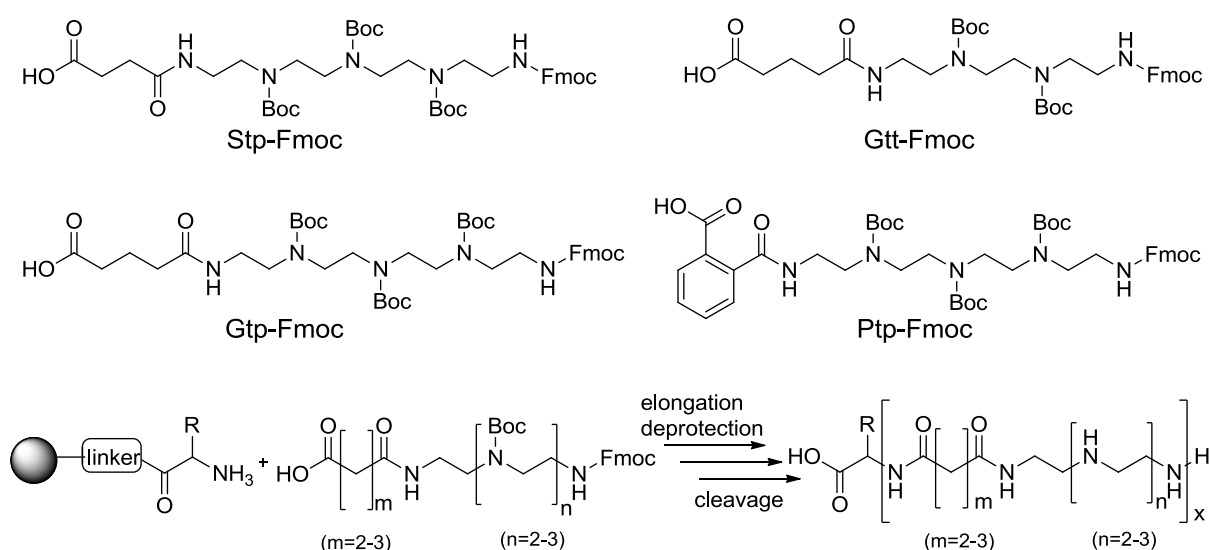


Figure 2: SPPS compatible building blocks and SPPS-based polymer assembly

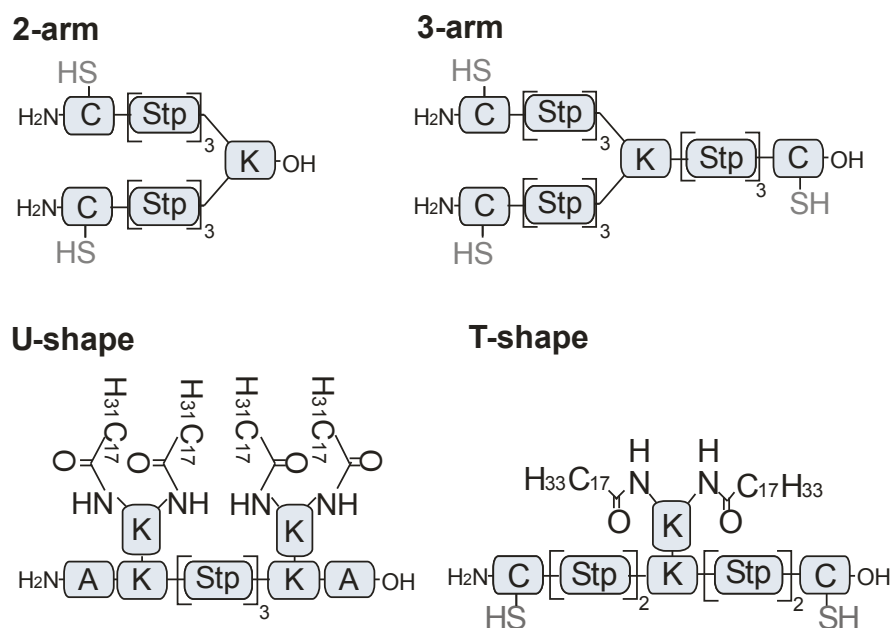


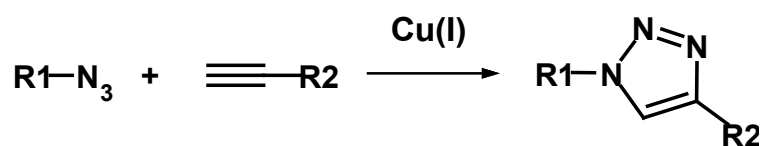
Figure 3: Classes of oligomer structures.

As topology can influence biophysical and biological properties, branched polymers (2-arm, 3-arm, 4-arm and 5-arm) or linear polymers optionally with modification in the center (T-shapes) or the end of chains (i-shapes, U-shapes) were designed and tested (Figure 3).

3. Precise conjugation techniques

A plain polymer, even when optimized and modified with lipid or hydrophobic domains, may not be the ideal carrier for overcoming all delivery steps. Therefore, conjugation of additional natural or artificial biometric transport functionalities such as cell targeting ligand or shielding domains may further improve the carrier system. In order to modify the conjugates at a defined position, precise conjugation techniques are needed.

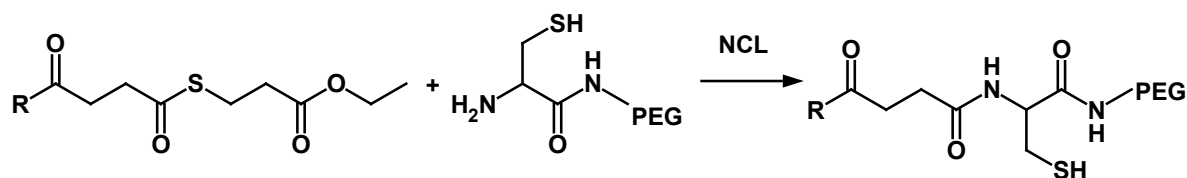
A series of 'click chemistry' conjugation techniques have become available⁵⁷⁻⁶⁰ which are useful tools for precise conjugation at selected sites of macromolecules. As a variation of the Huisgen 1,3-dipolar cycloaddition the Cu(I)-catalyzed cycloaddition of terminal alkynes and azides (CuAAC)⁶¹⁻⁶³ proceeds efficiently and selectively under aqueous reaction conditions and in presence of various other functionalities or biomolecules⁶⁴⁻⁶⁵ (Scheme 1).



Scheme 1: Cu(I)-catalyzed 1,3-dipolar cycloaddition reaction

Click chemistry is fully compatible with the reaction conditions used for solid phase synthesis, in the synthesis of peptides, and for modification of oligonucleotides. Copper-free click chemistries were even performed in living organisms⁶⁶. Several applications for polymer polymerizations and conjugations for nucleic acid delivery have been reported⁶⁷⁻⁷⁰. Copper-assisted or copper-free click chemistry can also be used for the synthesis of siRNA conjugates⁷¹.

Another conjugation technique is native chemical ligation (NCL, Scheme 2). Native chemical ligation was originally developed to connect two unprotected peptides for the total synthesis of proteins⁷². An amide bond is formed by transthioesterification followed by intramolecular nucleophilic rearrangement between thioester and cysteine. The chemoselective reaction occurs in mild aqueous solution, is simple and gives almost quantitative yields⁷³. Byun attached cysteine-PEG to a titanium surface with thioester containing phosphonic acid conjugates⁷⁴. This approach indicates the usefulness of NCL as toolkit for surface bioconjugation and functionalization. The potential of NCL in the synthesis of precise polymers or conjugates for nucleic acid delivery has to be further investigated.



Scheme 2: Native chemical ligation

4. Polyplex stability

Intracellular localization of nucleic acid targets and the inability of siRNA and other oligonucleotides to diffuse across cellular membranes require formulation with carriers^{13, 15, 75-76}. High stability is an important requirement for in vivo administration of polyplexes, because free nucleic acids i) are degraded by DNases or RNases, ii) cannot enter cells, because of their negative charge, and iii) in case of small oligonucleotides are rapidly cleared through the urinary tract due to their size⁷⁷. Tumor vessels are leaky, resulting in enhanced permeability. Therefore, particles are taken up into the interstitium and remain there for a long time due to the poor lymph drainage for tumors. This phenomenon is known as the tumor-selective enhanced permeability and retention (EPR) effect⁷⁸. Macromolecules with a molecular weight > 40 kDa, as well as some nanoparticles exhibit the EPR effect⁷⁹⁻⁸⁰. After intravenous (i.v.) injection, serum proteins or blood cells interact with the polyplexes potentially leading to aggregation or dissociation. Therefore, stable and neutral particles in a range of ~ 100 nm⁸¹ are considered as ideal for i.v. injection, because they can benefit from the EPR effect⁷⁸. In contrast, other polyplex properties are required for intratumoral (i.t.) injections. Nomura et al. showed that larger and positively charged liposomes are superior for i.t. injections compared to smaller and uncharged liposomes⁸². Therefore, precise changes in the oligomer structure can affect size, charge and stability of the polyplexes leading to differences in biodistribution, cellular uptake, and release of the nucleic acid in the cytoplasm.

5. Polyplex size

Polyplex size influences the clearance and biodistribution to a great extent. After intravenous administration, very small particles (< 6 nm) are quickly eliminated by renal excretion⁸³, whereas larger particles are taken up by the monomolecular phagocytic system cells, which are predominantly present in liver and spleen. Particles between 150 and 300 nm are distributed in the liver and spleen, whereas 30-150 nm particles are found in the bone marrow, heart, kidney and stomach⁸⁴. For intravenous administrations, particle size is a particularly important polyplex characteristic. The upper end of a size distribution is crucial to prevent clogging of capillaries. Extravasation of siRNA complexes through fenestrations of tumor capillaries dictates certain size requirements⁸⁵. The EPR effect leads to an accumulation of nanoparticles in the tumor because of the leaky tumor vessels and the poor lymph drainage of tumors⁷⁸. Depending on tumor type, the size of gaps between tumor endothelial cells ranges from 100 to 780 nm⁸⁶. On the contrary, the tight endothelial junctions of normal vessels are between 5 and 10 nm. The diameter of those fenestrations in the liver are around 100 nm, hence particles < 100 nm improve circulation half-life^{79, 87}. Therefore, the ideal particle size for cancer treatment heavily depends on the type of administration.

Ideal carrier systems reach the target tissue avoiding all other tissues, thereby preventing side effects. In addition, polyplexes should be stable in the blood stream after injection. Binding of negatively charged proteins, like serum albumin, or blood cells can lead to aggregation. Serum components may also disassemble the polyplexes, leading to degradation of the siRNA. These changes in the polyplex properties can affect biodistribution, cellular uptake and siRNA release in the cytoplasm.

Particle size data from literature is difficult to compare, if determined with different methods due to the different underlying principles⁸⁸. Up to now, no standard technique is available, as the choice of methods largely depends on availability, application, and required measurement. However, good understanding of the polyplex characteristics may allow prediction of in vivo performance, as well as particle design and formulation development in a rational fashion. As a result, reliable size determination is important.

6. Aims of the thesis

High stability is an important requirement for in vivo administration of polyplexes, because DNases or RNases degrade free nucleic acids. Moreover, nucleic acids cannot enter the cells because of their negative charge, and they are rapidly cleared through the urinary tract due to their size. Consequently, the first aim of the thesis was to increase the stability of polyplexes, based on precise, polycationic oligomers. This should be achieved by integration of stabilizing components into the oligomer sequences which lead to stabilization through π - π interactions, hydrogen bonds, hydrophobic interactions or covalent bonds. Biodegradability of the polyplexes should be maintained after chemical modification for a low toxicity profile of the nanoparticle. The optimal stabilizing domain should display maximal delivery performance in vitro and in vivo. Biophysical and biological properties of such stabilized particles were examined for their potential as effective nucleic acid delivery systems.

Nanoparticle size is important for in vivo delivery as it influences clearance and biodistribution to a great extent. Hence, the second aim of the thesis was the comparison of four particle sizing methods for the characterization of siRNA polyplexes. Therefore, the assembly of three sequence-defined oligomers into polyplexes was investigated with dynamic light scattering, atomic force microscopy, nanoparticle tracking analysis, and fluorescence correlation spectroscopy. In this way, the suitability, advantages and disadvantages of these methods to determine polyplex sizes was evaluated.

Interaction of the carrier surface with blood components and off-target cells influences the choice of carrier. Therefore, the surface of polycationic delivery systems should be shielded to avoid interactions during blood circulation. As maximally shielded particles do not interact with their targets, the incorporation of an active targeting domain into the structure of the carrier system is necessary. As a result, the third aim of the thesis was the synthesis of activated ligands with shielding and targeting domains. Afterwards, those ligands should be attached to already existing, polycationic structures with the help of native chemical ligation.

II. MATERIALS AND METHODS

1. Chemicals and reagents

Amino acids and resins were purchased from Iris Biotech (Marktredwitz, Germany) and Novabiochem GmbH (Hohenbrunn, Germany). Pybop®, HBTU and syringe reactors (PP reactor with PE frit) were bought from Mulitsyntech GmbH (Witten, Germany). HOBt was purchased from Sigma Aldrich (München, Germany). *N*¹⁰-(Trifluoroacetyl)pteroic acid was obtained from Clausen & Kaas (Fraum, Denmark) and Fmoc-*N*-amido-dPEG®24-acid from Quanta Biodesign (Powell, USA). All solvents and small molecule reagents were purchased in high quality from Sigma-Aldrich (Steinheim, Germany), Iris Biotech (Marktredwitz, Germany), Merck (Darmstadt, Germany) or AppliChem (Darmstadt, Germany), unless stated otherwise.

All cell culture consumables (dishes, well plates, flasks) were obtained from NUNC (Langenselbold, Germany) or TPP (Trasadingen, Switzerland). Fetal bovine serum (FBS), cell culture media and antibiotics were purchased from Invitrogen (Karlsruhe, Germany), glucose from Merck (Darmstadt, Germany), HEPES from Biomol GmbH (Hamburg, Germany) and sodium chloride from Prolabo (Haasrode, Belgium). Luciferase cell culture 5x lysis buffer and D-luciferin sodium salt were obtained from Promega (Mannheim, Germany). pCMVLuc plasmid DNA (pDNA) was purchased from PlasmidFactory (Bielefeld, Germany). Cy5-labeling kit for pDNA labeling was obtained from Mirus Bio (Madison, USA). Ready to use siRNA duplexes (small letters: 2'methoxy-RNA; s: Phosphorothioate, dT: Deoxythymidine) were kindly provided by Axolabs GmbH (formerly Roche Kulmbach, Kulmbach, Germany), or in case of RAN siRNA was purchased from Dharmacon (Thermo Fischer Scientific Inc., Lafayette, USA) in case of RAN siRNA:

Control siRNA (Mut):	sense: 5'-AuGuAuuGGccuGuAuuAGdTsdT-3'
	antisense: 5'-CuAAuAcAGGCcAAuAcAUdTsdT-3'
Cy5-labeled siRNA	sense: (Cy5)-5'-cuuAcGcuGAGuAcuucGAdTsdT-3'
	antisense: 5'-UCGAAGuACUcAGCGuAAGdTsdT-3'
GFP-siRNA	sense: 5'-AuAucAuGGccGAcAAGcAdTsdT-3'
(silencing of eGFPLuc protein)	antisense: 5'-UGCUUGUCGGCcAUGAuAUdTsdT-3'
Cy7-labeled siAHA1	sense: 5'-(Cy7)(NHC ₆)-GGAuGAAGuGGAGAuAGudTsdT-3'
	antisense: 5'-ACuAAUCUCcACUUC AUCCdTsdT-3'
RAN siRNA	antisense: 5'-AGAAGAAUCUUCAGUACUAUU-3'
	sense: 5'-UAGUACUGAAGAUUCUUCUUU-3'

Dilutions of siRNA and polymers were prepared in 20 mM HEPES pH 7.4 and 20 mM HEPES with 5% glucose (HBG) pH 7.4. All buffer components were solved in MilliQ water with a conductance below 0.06 μ S and the pH was adjusted, if necessary. Afterwards, the buffers were filtered with a sterile filter with 0.2 μ m pore size. Succinoyl tetraethylenepentamine (Stp) based, sequence-defined oligomers were synthesized as described below.

2. Solid phase assisted peptide synthesis

2.1. Synthesis of 3-Fmoc-4-diaminobenzoic acid (Fmoc-Dbz)

The synthesis of 3-Fmoc-4-diaminobenzoic acid was performed as described by Blanco-Canosa et al.⁷³. 3,4-diaminobenzoic acid was solved in a 1:1 mixture of sodium bicarbonate $\text{NaHCO}_{3(\text{aq})}$ (0.1 M, pH 7.9) and ACN. *N*-(9-fluorenylmethoxycarbonyloxy)succinimide was added to the turbid solution in small portions over 30 min. After one hour, three drops of 1 M NaOH solution were added. Reaction progress was monitored with thin layer chromatography in ethyl acetate. After 6 h, acidification with HCl (1 M) formed a precipitate that was filtered and washed with cooled MtBE, *n*-hexane and methanol. The white solid was dried under vacuum.

2.2. Synthesis of ICH-CAMP

2-Amino-4-hydroxy-6-methylpyrimidine was dissolved in 1,6-diisocyanatohexane and heated to 100°C for 17 h. The reaction mixture was cooled and 125 mL *n*-pentane were added. The resulting precipitate was filtered and thoroughly washed with 250 mL *n*-pentane. The product was dried at 50°C by means of vacuum distillation, yielding 2-(6-Isocyanahexylaminocarbonylamino)-6-methyl-4(1*H*)pyrimidinone (ICH-CAMP) as white powder. The product was washed again with 350 mL *n*-pentane and dried in vacuo over night.

2.3. Attachment of the first amino acid

2.3.1. Loading of a chlorotriyl chloride resin with Fmoc-Tyr(tBu)-OH

After swelling 1.2 mmol of a chlorotriyl chloride resin (750 mg) in DCM for 10 min, Fmoc-Tyr(tBu)-OH (0.75 eq) and DIPEA (1.5 eq) were added to the resin for 1 h. The

reaction solvent was drained and a mixture of DCM/MeOH/DIPEA (80/15/5) was added twice for 10 min. After the removal of the reaction mixture, the resin was washed 5 times with DCM.

About 30 mg of the resin were removed and dried to determine the loading of the resin. Therefore, an exact amount of resin was treated with 1 mL deprotection solution (20% piperidine in DMF) for 1 h. Afterwards, the solution was diluted and absorption was measured at 301 nm. The loading was then calculated according to the equation

$$\text{loading}[\text{mmol} / \text{g}] = \frac{1000 \times A_{301}}{m[\text{mg}] \times 7800 \times D}$$

with D as dilution factor.

The residual resin was treated twice with 20% piperidine in DMF and twice with 20% piperidine DMF with 2% DBU to remove the Fmoc protection group. Reaction progress was monitored by Kaiser test⁸⁹. Afterwards, the resin was washed with DMF, DCM and *n*-hexane, and dried in vacuo.

2.3.2. Loading of a chlorotriyl chloride resin with Fmoc-Cys(trt)-OH

The loading was performed analogously to the loading of a chlorotriyl chloride resin with Fmoc-Tyr-(tBu)-OH. Instead of Fmoc-Tyr-(tBu)-OH, Fmoc-Cys(trt)-OH was used as amino acid.

2.3.3. Loading of a chlorotriyl chloride resin with Fmoc-Glu-OtBu

The loading was performed analogously to the loading of a chlorotriyl chloride resin with Fmoc-Tyr-(tBu)-OH. Instead of Fmoc-Tyr-(tBu)-OH, Fmoc-Glu-OtBu was used as amino acid.

2.3.4. Loading of a chlorotriyl chloride resin with dde-Lys(Fmoc)-OH

The loading was performed analogously to the loading of a chlorotriyl chloride resin with Fmoc-Tyr-(tBu)-OH. Instead of Fmoc-Tyr-(tBu)-OH, dde-Lys(Fmoc)-OH was used as amino acid.

2.3.5. Loading of a MBHA Rink amide resin with Dbz-Fmoc

After swelling 0.05-0.3 mmol of a MBHA Rink amide resin in DCM for 10 min, the Fmoc protection group was removed. Therefore, the resin was treated four times with 20% piperidine in DMF. After washing of the resin, four equivalents of Fmoc-Dbz, DIPEA (8 eq) and PyBOP®/HOBt (4 eq) were added for 1.5 h. Reaction progress was monitored with Kaiser test. The reaction solvent was drained and the resin was washed with DMF, DCM and *n*-hexane, and dried in vacuo.

2.4. Convergent fragment synthesis

2.4.1. Convergent synthesis of Fmoc-Tyr(tBu)₃-OH

After swelling 1.2 mmol of a Tyr(tBu) chlorotrityl resin in DCM for 30 min, four equivalents of Fmoc-Tyr(tBu)-OH, DIPEA (8 eq) and PyBOP®/HOBt (4 eq) were added for 30 min. The reaction solvent was drained and the resin was washed five times with DMF and DCM. Reaction progress was monitored by Kaiser test. To remove the Fmoc protection group, the resin was treated twice with 20% piperidine in DMF and twice with 20% piperidine DMF with 2% DBU. After a positive Kaiser test, the resin was washed with DMF and DCM. Afterwards, Fmoc-Tyr(tBu)-OH, DIPEA (8 eq) and PyBOP®/HOBt (4 eq) were added for 30 min to the resin. After a negative Kaiser test, the resin was washed with DMF, DCM and *n*-hexane, and dried in vacuo.

2.4.2. Convergent synthesis of Boc-Tyr(tBu)₃-OH

The first part was performed as described for the synthesis of Fmoc-Tyr(tBu)₃-OH. After the second coupling of Fmoc-Tyr(tBu)-OH, the resin was washed and the Fmoc protection group was removed. After a negative Kaiser test, four equivalents of di-*tert*-carbonyl dicarbonate (Boc₂O) and DIPEA (8 eq) were added twice for 30 min to the resin. After a negative Kaiser test, the resin was washed with DMF, DCM and *n*-hexane, and dried in vacuo.

2.4.3. Convergent synthesis of Fola(trt)-OH

After swelling 0.2 mmol of a Glu-OtBu chlorotrityl resin in DCM for 30 min, four equivalents of *N*¹⁰-(Trifluoroacetyl)pteroic acid, DIPEA (16 eq) and PyBOP®/HOBt (4 eq) in DMF were added for 2.5 h. The reaction solvent was drained and the resin was washed five times with

DMF. Reaction progress was monitored by Kaiser test. To remove the trifluoroacetyl protection group, the resin was treated with 50% ammonia in DMF for 30 min. Afterwards, the resin was washed with DMF. This deprotection cycle was repeated three times. Trityl chloride (20 eq) and DIPEA (20 eq) in DCM were added for 2 h in order to protect the pteric acid with an acid labile protection group. The resin was washed with DMF, DCM and *n*-hexane, and dried in vacuo.

2.4.4. Cleavage conditions

For cleavage of the protected building block, the resin was treated with 10 mL/g_(resin) cleavage solution: The building blocks were treated with a DCM/TFE (7.5:2.5) mixture 5-10 times for 20 min till no absorption was detectable on a thin layer chromatography plate. The solvents of the combined filtrates were removed and the residue was dried in vacuo.

2.5. Oligomer synthesis

2.5.1. Synthesis of the T-Shape 464: H₂N-C-Y₃-Stp₂-[(Y₃)₂]-K]K-Stp₂-Y₃-C-OH

After swelling of 0.05-0.20 mmol of Cys(trt) chlorotriptyl resin in DCM for 30 min, three equivalents of Fmoc-Y(tBu)₃-OH, DIPEA (6 eq) and PyBOP®/HOBt (3 eq) were added for 50 min. The reaction solvent was drained and the resin was washed five times with DMF and DCM. Reaction progress was monitored with Kaiser test. To remove the Fmoc protection group, the resin was treated twice with 20% piperidine in DMF and twice with 20% piperidine DMF with 2% DBU. After a positive Kaiser test, the resin was washed with DMF and DCM. Four equivalents of a solution of Fmoc-Stp(Boc)₃-OH (Synthesis described in ⁵⁴) in DCM/DMF, DIPEA (8 eq) and PyBOP®/HOBt (4 eq) were added to the resin and the vessel was agitated until Kaiser test indicated complete conversion (normally 40 min). The reaction solvent was drained and the resin was washed five times with DMF and DCM. This cycle was repeated. To introduce a branching point Fmoc-Lys(dde)-OH was used in the next coupling step. Fmoc-Lys(dde)-OH (4 eq), DIPEA (8 eq) and PyBOP®/HOBt (4 eq) dissolved in DMF/DCM were added and the synthesis vessel was agitated for 40 min. After a negative Kaiser test, the resin was washed with DMF. After treatment with 20% piperidine in DMF, 20% piperidine in DMF with 2% DBU and washing the resin with DMF and DCM, Fmoc-Stp(Boc)₃-OH (4 eq), DIPEA (8 eq) and PyBOP®/HOBt (4 eq) in DMF were added for 30 min. After successful reaction the resin was treated twice with 20% piperidine in DMF and twice with 20% piperidine in DMF with 2% DBU. The reaction

solvent was drained and the resin was washed five times with DMF and DCM. This cycle was repeated. Three equivalents of Fmoc-Y(tBu)₃-OH, DIPEA (6 eq) and PyBOP®/HOBt (3 eq) were added for 50 min. The reaction solvent was drained and the resin was washed five times with DMF and DCM. To remove the Fmoc protection group, the resin was treated twice with 20% piperidine in DMF and twice with 20% piperidine DMF with 2% DBU. After a positive Kaiser test and washing of the resin, Boc-Cys(trt)-OH (4 eq) dissolved in DMF/DCM, DIPEA (8 eq) and PyBOP®/HOBt (4 eq) were added for 40 min. After a negative Kaiser test, the dde protecting group was cleaved using 2% hydrazine monohydrate in DMF (10-15 times for 5 min) till no significant A₃₀₁ was measurable in the deprotection mixture. Fmoc-Lys(Fmoc)-OH (4 eq), DIPEA (8 eq) and PyBOP®/HOBt (4 eq) were added to the resin for 40 min. In order to cap unreacted primary amino groups, the resin was acetylated using 10 equivalents of acetic anhydride and 20 equivalents of DIPEA before the subsequent removal of the Fmoc protecting group. After removal of the Fmoc protecting group, 4 equivalents of the Boc-Tyr(tBu)₃-OH dissolved in DMF/DCM, 8 equivalents of DIPEA and 4 equivalents of PyBOP®/HOBt were added to the resin for 60 min. After completion of the reaction, the resin was washed with DMF, DCM and *n*-hexane, and dried in vacuo.

2.5.2. Reverse synthesis of 408: [(ICH-CAMP-Stp₅)₂K]K[K(OleA)₂]-OH

After swelling of 0.05-0.20 mmol of dde-Lys chlorotriyl resin in DCM for 30 min, four equivalents of Fmoc-Lys(Fmoc)-OH, DIPEA (8 eq) and PyBOP®/HOBt (4 eq) were added for 40 min. The reaction solvent was drained and the resin was washed five times with DMF and DCM. Reaction progress was monitored with Kaiser test. To remove the Fmoc protection group, the resin was treated twice with 20% piperidine in DMF and twice with 20% piperidine DMF with 2% DBU. After a positive Kaiser test, the resin was washed with DMF and DCM. Eight equivalents of a solution of oleic acid in DCM/DMF, DIPEA (16 eq) and PyBOP®/HOBt (8 eq) were added to the resin and the vessel was agitated until Kaiser test indicated complete conversion (normally 40 min). The reaction solvent was drained and the resin was washed five times with DMF and DCM. Afterwards, the dde protecting group was cleaved using 2% hydrazine monohydrate in DMF (10-15 times for 5 min) till no significant A₃₀₁ was measurable in the deprotection mixture. After washing the resin five times with DMF and DCM, Fmoc-Lys(Fmoc)-OH (4 eq), DIPEA (8 eq) and PyBOP®/HOBt (4 eq) dissolved in DMF/DCM were added and the synthesis vessel was agitated for 40 min. After a negative Kaiser test, the resin was washed with DMF and DCM. After treatment with 20% piperidine in DMF and washing the resin with DMF and DCM, Fmoc-Stp(Boc)₃-OH (4 eq), DIPEA (8 eq) and PyBOP®/HOBt (4 eq) in DMF were added

for 30 min. After successful reaction, the resin was treated twice with 20% piperidine in DMF. The reaction solvent was drained and the resin was washed five times with DMF and DCM. This cycle was repeated four times. ICH-CAMP (15 eq) was solved in DMF and added to the resin for 48 h. After completion of the reaction, the resin was washed with DMF, DCM and *n*-hexane, and dried in vacuo.

2.5.3. Synthesis of Nbz-PEG₂-A

After swelling of 0.025 mmol of Dawson-Dbz AM resin in DCM for 30 min, the Fmoc protection group was removed. Therefore, the resin was treated twice with 20% piperidine in DMF and twice with 20% piperidine DMF with 2% DBU. After washing of the resin, four equivalents of Fmoc-*N*-amido-dPEG₂ acid, DIPEA (8 eq) and PyBOP®/HOBt (4 eq) were added for 1.5 h. The reaction solvent was drained and the resin was washed five times with DMF and DCM. Reaction progress was monitored with Kaiser test. To remove the Fmoc protection group, the resin was treated twice with 20% piperidine in DMF and twice with 20% piperidine DMF with 2% DBU. After a positive Kaiser test, the resin was washed with DMF and DCM. Four equivalents of a solution of Boc-Ala-OH in DCM/DMF, DIPEA (8 eq) and PyBOP®/HOBt (4 eq) were added to the resin and the vessel was agitated until Kaiser test indicated complete conversion (normally 40 min). The reaction solvent was drained and the resin was washed five times with DMF and DCM. Afterwards, 10 equivalents of *p*-nitrophenyl chloroformate in DCM were added for 60 min. After removal of the solution and washing of the resin with DCM, DIPEA (10 eq) in DMF was added twice for 15 min. After completion of the reaction, the resin was washed with DMF, DCM and *n*-hexane and dried in vacuo.

2.5.4. Cleavage conditions

For cleavage, the resin was treated with 10 mL/g_(resin) cleavage solution: The resin was treated with a TFA/Water/TIS (95:2.5:2.5) mixture for 1.5-2.5 h. The resin was filtered off and washed twice using pure TFA, followed by one DCM wash. The combined filtrates were concentrated and either precipitated by dropwise addition into ice-cold MTBE or other suitable mixtures. The precipitate was collected by centrifugation. The precipitate/film was dissolved in 10 mM HCl with 30% acetonitrile unless stated otherwise and purified with size exclusion chromatography (G 10 column). The collected fractions were snap frozen and lyophilized.

2.6. Proton NMR spectra

^1H NMR spectra were recorded using a Jeol JNMR-GX 400 (400 MHz) unit produced by Jeol. All spectra were recorded without tetramethylsilane (TMS) as internal standard and therefore all signals were calibrated to the residual proton signal of the solvent. The coupling constant had an accuracy of 0.3 Hz. Chemical shifts are reported in ppm and refer to the solvent as internal standard (D_2O at 4.80, CDCl_3 at 7.26, DMSO-d_6 at 2.50, and DMF-d_6 at 2.73, 2.91 and 8.01). Data are reported as s = singlet, d = doublet, t = triplet, m = multiplet; integration was performed manually. The spectra were analyzed using MestreNova (Ver. 5.2.5-4119 by MestReLab Research).

2.7. Native chemical ligation

Native chemical ligation was performed at room temperature with the following ligation buffer: 6 M guanidine hydrochloride, 200 mM disodium hydrogen phosphate, 20 mM tris(2-carboxyethyl)phosphine hydrochloride (TCEP*HCl) and 200 mM 4-mercaptophenylacetic acid (MPAA). The pH was adjusted to 7.0 with 3 M sodium hydroxide solution. Ligations were carried out with a 1.3-fold molar excess of polycation over the Nbz-oligomer and a reaction time of 2-3 h. Afterwards, the product was purified with size exclusion chromatography (G 10 or G 25 column) in 10 mM HCl with 30% acetonitrile. The collected fractions were snap frozen and lyophilized.

3. Biophysical characterization

3.1. DNA and siRNA polyplex formation

Polyplex formulations for transfection and gel shift experiments were prepared as follows: 100-200 ng of pDNA or 500 ng of siRNA and the calculated amount of oligomer were diluted in separate tubes in 10 μL of 20 mM HEPES buffered 5% glucose pH 7.4 (HBG) each. The nucleic acid and the polycation solution were mixed by rapidly pipetting up and down (at least 5 times) and incubated for 30-40 min at RT in order to form the polyplexes necessary for transfection and gel shift experiments.

3.2. Gel shift assays

3.2.1. DNA binding assay

A 1% agarose gel was prepared by dissolving agarose in TBE buffer (trizma base 10.8 g, boric acid 5.5 g, disodium EDTA 0.75 g, and 1 L of water) and boiling everything up to 100°C. After cooling down to about 50°C and addition of GelRed, the agarose gel was cast in the electrophoresis unit. Polyplexes, containing 100 ng pDNA in 20 µL HBG and loading buffer (prepared from 6 mL of glycerine, 1.2 mL of 0.5 M EDTA, 2.8 mL of H₂O, 0.02 g of bromophenol blue) were placed into the sample pockets. Electrophoresis was performed at 120 V for 80 min.

3.2.2. siRNA binding assay

A 2.5% agarose gel was prepared containing GelRed as described above. Polyplexes containing 500 ng siRNA in 20 µL HBG and loading buffer (containing xylene cyanol) were placed into the sample pockets. Electrophoresis was performed at 120 V for 40 min.

3.2.3. Gel shift assay of siRNA polyplexes in 90% FBS

2.5 µg of control siRNA and the oligomer at N/P 12 were diluted in separate tubes to a total volume of 12.5 µL in 20 mM HEPES pH 7.4. The nucleic acid solution was added to the diluted polycation, mixed and incubated for 30-40 min at room temperature. Afterwards, fetal bovine serum (FBS) was added to the samples. All samples had a final concentration of 90% FBS. The samples were incubated either at room temperature or 37°C for different time points. Meanwhile, a 2.5% agarose gel was prepared, by dissolving agarose in TBE buffer and heating the suspension up to 100°C. After cooling down to about 50°C and addition of GelRed, the clear agarose gel solution was cast into an electrophoresis unit. After 0, 10, 30 and 90 min, 20 µL of the samples and 4 µL loading buffer were carefully mixed and placed into the sample pockets. Electrophoresis was performed at 120 V for 40 min.

3.3. Methods for particle size determination

3.3.1. Dynamic laser light scattering

pDNA and siRNA polyplexes were formed as follows: 10 µg of nucleic acid and the

calculated amount of oligomer (N/P 12) were diluted in separate tubes in a total volume of 50 μL of buffer. The siRNA solution was added to the oligomer solution and mixed by rapidly pipetting up and down for at least 5 times resulting in a final nucleic acid concentration of 200 $\mu\text{g}/\text{mL}$. The incubation time was 30-40 min in order to complete polyplex formation. For DLS measurement, the polyplex solution was diluted 1:20 with buffer and measured in a folded capillary cell (DTS1060) with laser light scattering using a Zetasizer Nano ZS with backscatter detection (Malvern Instruments, Worcestershire, UK). The viscosity influences the diffusion of the particles, hence the hydrodynamic diameter, and therefore, an accurately known viscosity and constant temperature was needed. For size measurements, equilibration time was 0 min, temperature was 25°C, and an automatic attenuator was used. The refractive index of the solvent, in our case water, was 1.330 and the viscosity was 0.8872 mPa/s.

The DLS set up for the size measurements was calibrated with narrow distributed polystyrene latex nanoparticles with a size of 60 and 200 nm and a refractive index of 1.590 from Thermo Scientific (formerly Duke Scientific Corp.). Each sample was measured 3 times with 10 subruns of 10 seconds. A single exponential was fit to the correlation function with Cumulants analysis to obtain the Z-average diameter and the polydispersity index (PDI). The standard deviation after data analysis was not the distribution of the size around the mean, but the variation of the median amongst n measurements of the same sample⁸⁴. The DLS set up for the zeta potential measurements was calibrated with a zeta potential transfer standard of -50 mV from Malvern Instruments. The zeta potential was calculated by the Smoluchowski equation⁹⁰. Therefore, 10 up to 30 subruns of 10 s at 25°C ($n = 3$) were measured.

3.3.2. Fluorescence correlation spectroscopy

Unlabeled control siRNA was spiked with Cy5-labeled siRNA in formulation buffer (20 mM HEPES pH 7.4) in order to determine the size of the polyplexes with FCS. The calculated amount of oligomer (N/P) diluted in formulation buffer, was mixed with siRNA solution to concentrations of 200 μg siRNA per mL. Afterwards, the polyplexes were incubated at room temperature for 30 min. For the size measurements in buffer and FBS, the samples were diluted 1:40 in buffer or fetal bovine serum. Undiluted samples were analyzed to investigate polyplex self-assembly over time. For serum measurements, FBS was added to a final concentration of 90%, after polyplex formation. Afterwards, the polyplexes were incubated at room temperature or 37°C and measured at different time points. The minimal volume for polyplex analysis was 200 μL for all measurements with a final concentration of Cy5-labeled siRNA of 50 nM in each sample. FCS measurements were performed on an

Axiovert 200 microscope with a ConfoCor 2 unit (Carl Zeiss, Jena, Germany). A HeNe laser (633 nm, average power of 50 μ W at the sample) was used for excitation. The objective was a 40x (NA = 1.2) water immersion apochromat (Carl Zeiss, Jena, Germany). Samples were measured in eight well LabTek I chamber slides (NUNC, Wiesbaden, Germany). The laser beam focused at about 200 μ m above the bottom of the wells containing the samples. Autocorrelation and analysis were performed using a ConfoCor 2 software. Starting value for analysis was 3-18 μ s to cut off photo-physical effects. To determine the structural parameter and measurement parameters, Cy5 dye in water was analyzed before each data acquisition. All data were evaluated with a one component fit, unless stated otherwise. The hydrodynamic radius was calculated with the help of the data evaluation program FCS-R v0.7. Measurements in fetal bovine serum were viscosity corrected. Therefore, the viscosity of FBS was determined using a microviscosimeter (AMVn, Anton Paar, Ostfildern, Germany), resulting in a viscosity of 1.18 mPa/s. As a result, the hydrodynamic radii of all samples, obtained with the data evaluation program FCS-R v0.7, were multiplied with 0.75 (viscosity of water/ viscosity of FBS).

3.3.3. Atomic force microscopy

Polyplex preparation was performed in 20 mM HEPES buffer pH 7.4 with a siRNA concentration of 100 μ g/mL and a N/P ratio of 12. Polyplexes were prepared by mixing the siRNA stock solution (200 μ g/mL) with the oligomer stock solution 1:1 through pipetting. Samples were incubated for 30 min to ensure complete complex formation. Samples were diluted 1:200 (**49** polyplexes) and 1:50 (**332** and **279** polyplexes) for AFM measurements in the formulation buffer (20 mM HEPES buffer pH 7.4). The particles had to be attached onto a flat substrate. Therefore, a freshly cleaved mica sheet was used, as an atomically flat substrate, which was negatively charged. After complex formation, 5 μ L of the diluted polyplexes with positive surface charge were deposited onto the freshly cleaved mica sheet, which was glued to a metal puck (Plano, Dresden, Germany) and incubated for \sim 3 min, resulting in a surface coated with nanoparticles. After mounting the metal puck onto the AFM, the cantilever fluid cell was installed into the device and filled with approximately 30 μ L buffer solution. Samples were imaged in the tapping mode on a Multimode VIII AFM (Bruker AXS, Santa Barbara, USA). Imaging at room temperature was performed in formulation buffer with DNP-S oxide-sharpened silicon nitride cantilevers and SNL sharp nitride levers (Bruker Probes, Camarillo, USA) using resonance frequencies between 7-9 kHz of the narrow 100 μ m, 0.32 N/m cantilever spring constant. Imaging parameters were optimized for best image quality, in combination with the maintenance of the highest possible set point to minimize damage to the samples. Images were

post-processed by subtracting a 3rd order polynomial from each scan line. Drive amplitudes were ~0.11 V, integral gains ~ 2, and proportional gains ~ 4. Atomic force microscopy was performed by Julia Kasper and Max Scheible.

3.3.4. Nanoparticle tracking analysis

The calculated amount of oligomer (N/P 12) and the siRNA were diluted in 20 mM HEPES pH 7.4 in two separate tubes. The siRNA solution and the oligomer solution were mixed 1:1 resulting in a final siRNA concentration of 100 µg/mL. For nanoparticle tracking analysis experiments, all samples were diluted 1:5000 with formulation buffer. NTA was performed with a digital microscope LM20 System (NanoSight, Salisbury, UK). The diluted samples were injected with sterile syringes (BD Discardit II, USA) into the sample chamber equipped with a 640 nm diode laser. All samples were measured in the single shutter and gain mode for 40 s with manual shutter, gain, brightness and threshold adjustments at room temperature. The extended dynamic range mode, which splits the capture video into two videos with independent shutter and gain settings, was not useful to monitor a broader size range of the particles, as in this case the maximum shutter level was limited to 700. The video images of the particles, moving under Brownian motion, were captured and analyzed by the NTA 2.0 image analysis software (NanoSight, Salisbury, UK). Three measurements of each, always newly injected, sample were performed. The mean size and SD values obtained by the NTA software are based on the arithmetic values calculated with the sizes of all the particles analyzed by the software. Nanoparticle tracking analysis measurements were made by Julia Kasper.

3.4. Buffer capacity

The oligomer sample, containing 15 µmol protonable amines, was diluted in a total volume of 3.5 mL sodium chloride solution (50 mM) and the pH was adjusted to 2 by addition of hydrochloric acid. Afterwards, a back titration with 0.05 M sodium hydroxide (NaOH) was performed with an automatic titration system (Titrand 905 from Metrohm, Germany), until a pH of 11 was reached.

3.5. Erythrocyte leakage assay

Fresh, citrate buffered murine blood was washed with phosphate-buffered saline (PBS). The washed murine erythrocyte suspension was centrifuged and the pellet was diluted to

5×10^7 erythrocytes per mL with PBS (pH 7.4, 6.5, and 5.5). A volume of 75 μL of erythrocyte suspension and 75 μL of oligomer solution were added to each well of a V-bottom 96-well plate (NUNC, Denmark) resulting in final concentrations of 2.5 μM , 5 μM and 7.5 μM oligomer per well. All samples were pipetted in quadruplicates. The plates were incubated at 37°C under constant shaking for 1 h. After centrifugation, 80 μL of the supernatant were analyzed for hemoglobin release at 405 nm using a microplate plate reader (Spectrafluor Plus, Tecan Austria GmbH, Grödig, Austria).

4. In vitro analysis

4.1. Cell culture

Mouse neuroblastoma cells Neuro2A and Neuro2A/EGFPLuc cells, stably expressing the CMV-eGFPLuc cassette (Clontech) encoding a fusion of enhanced green fluorescent protein and GL3 firefly luciferase under the control of the CMV promoter⁹¹⁻⁹², were grown in Dulbecco's modified Eagle's medium (DMEM) supplemented with 10% FBS, 4 mM stable glutamine, 100 U/mL penicillin, and 100 $\mu\text{g}/\text{mL}$ streptomycin.

4.2. Flow cytometry

Neuro2A cells were seeded into 24-well plates coated with collagen at a density of 5×10^4 cells/well. After 24 h, culture medium was replaced with 400 μL fresh growth medium containing 10% FBS. Transfection complexes for pDNA or siRNA delivery at N/P ratio of 12 in 100 μL HBG, containing either 2.5 μg siRNA or 1 μg pDNA (20% of the nucleic acids were Cy5-labeled) were added to each well and incubated at 37°C for 4 h. All experiments were performed in triplicates. Subsequently, cells were washed twice with 500 μL PBS containing 100 I.U. of heparin for 15 min to remove any polyplexes sticking to the cell surface. Cells were detached with trypsin/EDTA and taken up in PBS with 10% FBS. Cellular uptake was assayed by excitation of Cy5 at 635 nm and detection of emission at 665 nm. Cells were appropriately gated by forward/sideward scatter and pulse width for exclusion of doublets. DAPI (4',6-diamidino-2-phenylindole) was used to discriminate between viable and dead cells. Data were recorded by Cyan™ ADP flow Cytometer (Dako, Hamburg, Germany) using Summit™ acquisition software (Summit, Jamesville, USA) and analyzed by FlowJo® 7.6.5 flow cytometric analysis software. Flow cytometry studies were performed by Petra Kos.

4.3. Luciferase gene silencing

Gene silencing experiments were performed in stably transfected Neuro2A/EGFP_{Luc} cells using 0.5 µg/well of either GFP-siRNA for silencing of the eGFP_{Luc} protein, or control-siRNA as a control. siRNA delivery was performed in 96-well plates with 5000 cells/well in triplicates. Cells were seeded 24 h prior to transfection and then medium was replaced with 80 µL fresh growth medium containing 10% FBS. Transfection complexes for siRNA delivery (20 µL formed in HBG) at different N/P ratios were added to each well and incubated at 37°C. At 48 h after transfection, cells were treated with 100 µL cell lysis buffer (25 mM Tris, pH 7.8, 2 mM EDTA, 2 mM DTT, 10% glycerol, 1% Triton X-100). Luciferase activity in the cell lysate was measured using a luciferase assay kit (100 µL Luciferase Assay buffer, Promega, Mannheim, Germany) and a Lumat LB9507 luminometer (Berthold, Bad Wildbad, Germany). The relative light units (RLU) were presented as percentage of the luciferase gene expression obtained with only buffer treated control cells. Luciferase gene silencing experiments were performed by Daniel Edinger and Thomas Fröhlich.

4.4. Luciferase reporter gene expression

Neuro2A cells were seeded 24 h prior to pDNA delivery using 1×10^4 cells/well in 96-well plates. In vitro transfection efficiency of the polymers was evaluated using 200 ng pCMV_{Luc} per well. All experiments were performed in quintuplicates. Before transfection, medium was replaced with 80 µL fresh medium containing 10% FBS. Transfection complexes formed at different protonable nitrogen/phosphate (N/P) ratios in 20 µL HBG were added to each well and incubated at 37°C. At 24 h after transfection, luciferase activity was determined as described above. Luciferase reporter gene expression experiments were performed by Petra Kos.

4.5. Cell viability assay (MTT)

Neuro2A cells were seeded into 96-well plates at a density of 1×10^4 cells/well. After 24 h, culture medium was replaced with 80 µL fresh growth medium containing 10% FBS and transfection complexes (20 µL in HBG) at different N/P ratios were added. All studies were performed in quintuplicates. 24 h post-transfection, 10 µL MTT (3-(4,5-Dimethylthiazol-2-yl)-2,5-diphenyltetrazolium bromide; 5 mg/mL) were added to each well reaching a final concentration of 0.5 mg MTT/mL. After an incubation time of 2 h, unreacted dye and medium were removed. The purple formazan product was dissolved in 100 µL/well DMSO

(dimethyl sulfoxide) and quantified by a microplate reader (Tecan, Switzerland) at 530 nm with background correction at 630 nm. The relative cell viability (%) related to control wells containing cell culture medium with 20 μ L HBG was calculated by $[A]_{\text{test}}/[A]_{\text{control}} \times 100$. Cell viability was determined by Petra Kos.

5. In vivo experiments

For all in vivo experiments female Rj:NMRI-nu (nu/nu) (Janvier, Le Genest-St-Isle, France) mice were chosen, housed in isolated vented cages with a 12 h day/night interval and food and water ad libitum. Animal experiments were performed according to guidelines of the German law of protection of animal life and were approved by the local animal experiments ethical committee.

5.1. Polyplex distribution

Different polyplexes (N/P 12) containing 50 μ g siRNA including 50% Cy7-labeled siAHA1 were mixed in a total volume of 250 μ L (HBG). Fluorescence imaging was performed utilizing the IVIS Lumina system with Living Image software 3.2 (Caliper Life Sciences, Hopkinton, USA). After anesthetizing the mice with 3% isoflurane in oxygen, polyplexes were injected into the tail vein and the distribution was measured after 0, 0.25, 0.5, 1, 4, and 24 h with a CCD camera (IVIS Lumina™). Experiments were performed in triplicates by Laura Schreiner, Annika Herrmann and Daniel Edinger and pictures were analyzed using the Living Image software.

5.2. Neuro2A tumor treatment

Mice were injected subcutaneously with 5×10^6 Neuro2A-eGFPLuc cells into their left flank at day 0. Two days later, the mice were separated into 6 groups ($n = 5$) based on their bioluminescence signal (Caliper Life Sciences, Hopkinton, USA). Bioluminescence imaging was performed 15 min after intraperitoneal injection of 100 μ L luciferin solution ($c = 60$ mg/mL), recorded by a CCD camera (IVIS Lumina™) and analyzed using Living Image software 3.2. Intratumoral treatment with polyplexes, containing oligomers **49** and **332** complexing either 50 μ g RAN siRNA or control siRNA (N/P 12) in a total volume of 50 μ L (HBG) was also started at day 2 and repeated at day 4, 8, 11, 14. Tumor growth was recorded with bioluminescence imaging at day 8, 11, 14, 16 and 18. Caliper measurements were performed twice every week. Mice were sacrificed after their tumors reached a size of

1500 mm³ (length x width²/2). Bioluminescence signals were analyzed with the IVIS Lumina system with Living Image software 3.2 (Caliper Life Sciences, Hopkinton, USA). Neuro2A treatment experiments were performed by Raphaela Kläger and Daniel Edinger.

6. Statistical analysis

Results are presented as mean \pm standard deviation (SD), unless stated otherwise. Statistical significance of differences was evaluated by t-test. P-values < 0.05 were considered significant. Statistics were performed with Graph Pad Prism 5[®].

III. RESULTS

1. Stabilizing effects of tyrosine trimers on pDNA and siRNA polyplexes

Several modifications of the pDNA transfection agent polyethylenimine (PEI) have been reported to convert it into a suitable siRNA carrier⁹²⁻⁹⁶. Creusat et al. modified PEI with hydrophobic natural amino acids⁹⁴ and showed that the random modification of 10-20% of PEI nitrogens with tyrosines was beneficial in regards of buffer capacity, reduced cytotoxicity, and siRNA⁹⁷ or oligonucleotide⁹⁸ delivery. Modification of PEI with tyrosines occurred at random positions and only one single tyrosine was attached per nitrogen. Tyrosine modified PEI showed favorable properties: It did not display hemolytic activity, but polyplexes nevertheless escaped endosomes due to their endosomal protonation capacity. Moreover, those polyplexes displayed an increased stability in glucose solution, favorable for in vivo application. Self-assembly of tyrosine containing biopolymers into nanostructures has been described in a different context to be facilitated through the π - π interactions of the aromatic rings of single neighboring tyrosines or tyrosine dimers⁹⁹⁻¹⁰⁰. As a result, we aimed at optimizing the serum stability of polyplexes based on sequence-defined carriers^{55-56, 101}. For this purpose, we evaluated the effect of three consecutive tyrosines as stabilizing components and synthesized various oligomers containing oligotyrosine motifs at defined positions.

1.1. Design and synthesis of oligotyrosine containing oligomers

Solid phase assisted synthesis, first published by Merrifield⁴⁵, enables the use of a high excess of educts which drives the coupling reaction to completion. Moreover, the excess of reagents and by-products during synthesis could be easily separated from the growing oligomer by filtration and washings.

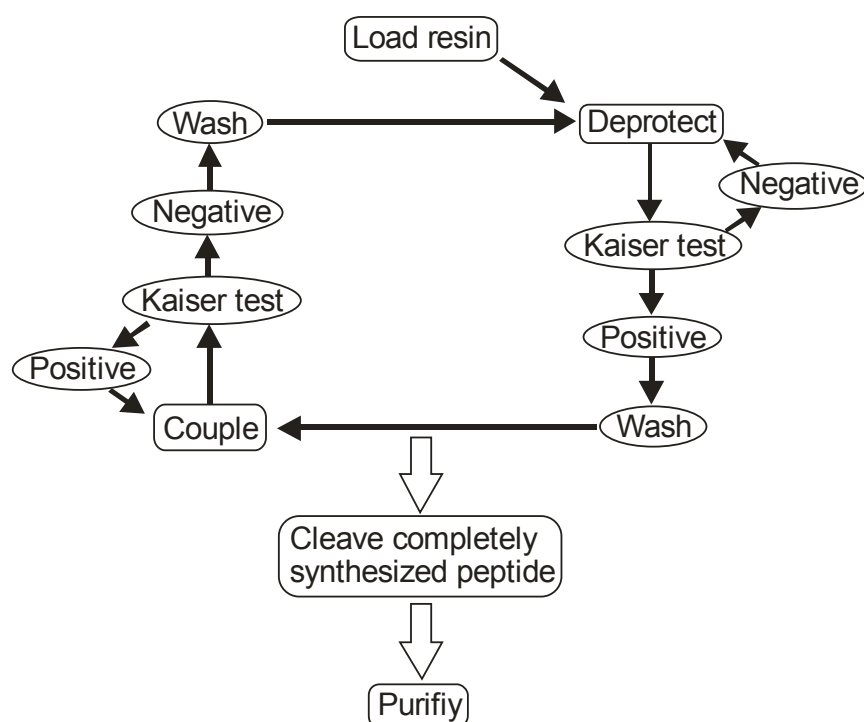


Figure 4: Solid phase peptide synthesis

Solid phase assisted synthesis involves numerous repetitive steps (Figure 4): After loading the resin with a *N*-protected amino acid, the desired sequence is assembled from *C*-terminus to *N*-terminus by alternate cycles of deprotection and coupling. Reaction progress is monitored through Kaiser test. The functional groups of the side chains are protected with permanent, acid labile groups like trityl (trt), *tert*-butyl (tBu), 2,2,4,6,7-pentamethyldihydrobenzofuran-5-sulfonyl (Pbf), or *tert*-butyloxycarbonyl (Boc) which are stable at the reaction conditions used during peptide elongation. The α -amino group is shielded by the temporary protecting groups 1-(4,4-dimethyl-2,6-dioxocyclohex-1-ylidene)-ethyl (dde) or fluorenyl-methoxycarbonyl (Fmoc). The temporary protection groups are removed under mild basic conditions that preserve the integrity of the oligomer and reduce the rate of epimerization. The temporary *N*-terminal protecting group is removed allowing the addition of the next amino acid through activation of its α -carboxylic group. In a final step, the peptide is released from the resin and the acid labile side chain protecting groups are simultaneously removed.

1.1.1. Convergent building block synthesis

Fully protected, repeating tyrosine sequences Fmoc-Y(tBu)₃-OH and Boc-Y(tBu)₃-OH were synthesized first by means of convergent synthesis. After assembly of the desired Y3 fragment on a 2-chlorotrityl chloride resin with solid phase assisted synthesis, the side chain protected fragments were released under mild acid conditions. Thereafter, the cleavage solution was removed under vacuum. The convergent building blocks were used like side chain protected amino acids for synthesis of the following oligotyrosine containing oligomers. Consequently, synthesis times were shortened and the abundance of deletion sequences was reduced.

1.1.2. Structural overview

Various precise, polycationic oligomers containing 1,2-diaminoethane subunits (Stp) were synthesized applying solid phase assisted synthesis and purified by means of size exclusion^{55-56, 101}. We demonstrated that crosslinking domains (cysteines) at the periphery of the oligomer and the lytic and stabilizing domain (dioleic acid motif) in the oligomer center were essential structural prerequisites for oligonucleotide transfer activity. Tyrosine motifs were introduced as new stabilizing building blocks. Initially, we synthesized linear oligomers X_n-Stp₃-C with one, three, or six aromatic amino acids (X = phenylalanine (F), tryptophan (W) or tyrosine (Y)). The oligomer Y₆-Stp₃-C was the only one which showed a silencing tendency if complexed with eGFP-siRNA (Figure 5).

Elongation of the aromatic amino acid chain to 9 or 12 consecutive tyrosines did not improve transfection efficiency. As a result, we introduced at least six tyrosines in our structures divided in tyrosine motifs with three consecutive tyrosines which should stabilize the polyplexes through π - π interactions.

On the one hand, Y3 motifs were introduced to replace the terminal cysteines at the periphery, or the hydrophobic domain in the center. On the other hand, additional tyrosine trimers were added just before the terminal cysteines. Consequently, the resulting oligomers (schematic overview Figure 6 and sequences listed in Table 1) contain an oligotyrosine motif either in the periphery, the center, or both, whereas the oligomer **49** and controls (**216** and **413**) lack aromatic amino acids.

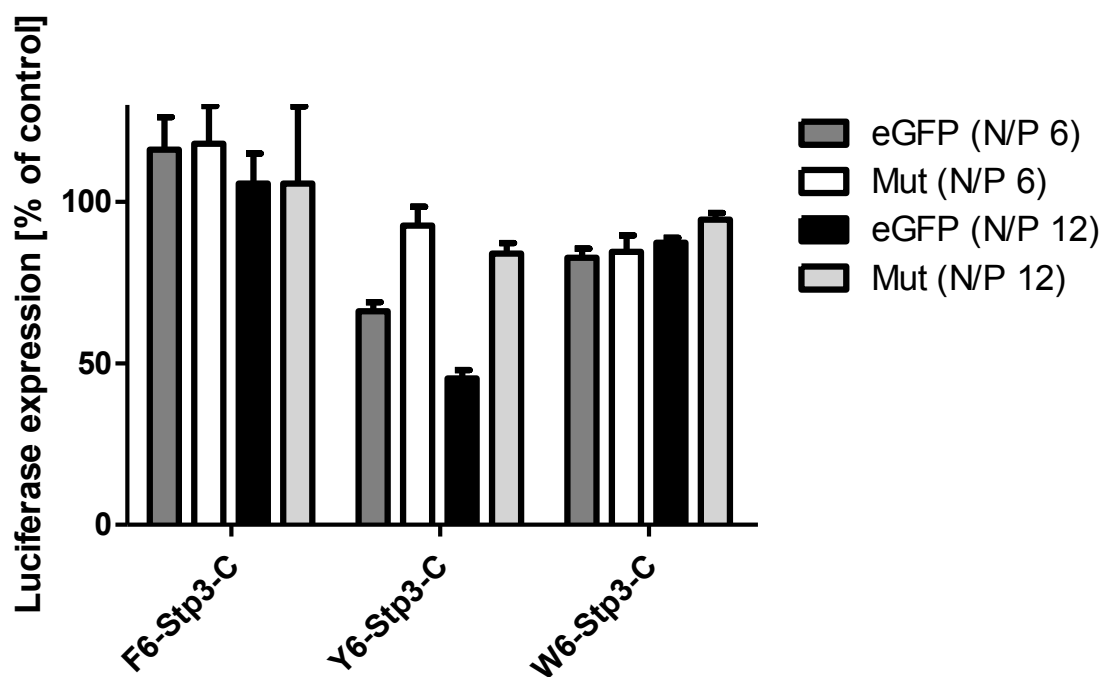


Figure 5: Gene silencing in neuroblastoma cells. eGFP-targeted siRNA (eGFP) or control siRNA (Mut) polyplexes were used for eGFPLuc gene silencing in Neuro2A-eGFPLuc cells, polyplexes were tested at N/P 6 and 12. Transfection experiments were performed by Thomas Fröhlich and Daniel Edinger.

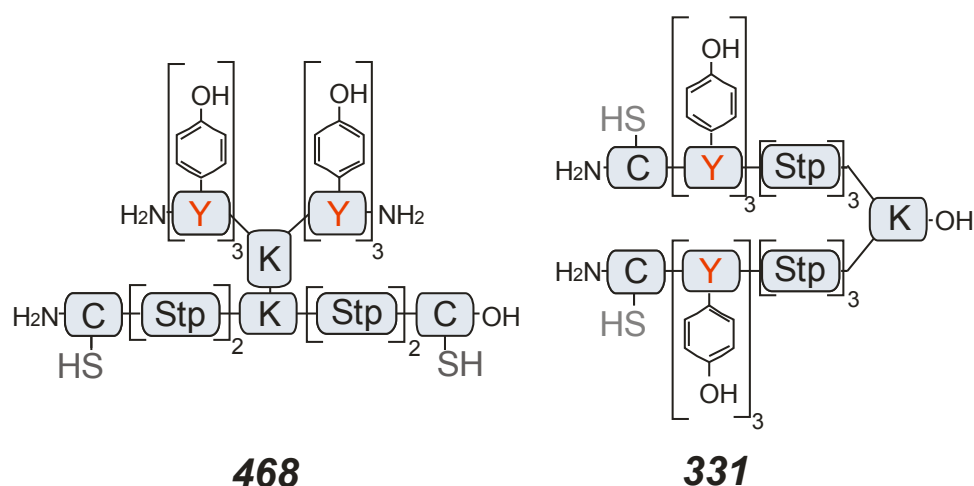


Figure 6: Schematic overview of structures with oligotyrosine motifs in the center or the periphery of the succinyl tetraethylenepentamine (Stp) oligomer chains.

Table 1: Selected oligomer sequences (*N*- to *C*-terminus).

	Oligomer	Sequence
	49	C-Stp ₂ -[(OleA) ₂ -K]K-Stp ₂ -C
controls	216	A-Stp ₂ -[(OleA) ₂ -K]K-Stp ₂ -A
	413	C-Stp ₂ -[K]K-Stp ₂ -C
peripheral tyrosines	331	[C-Y ₃ -Stp ₃] ₂ K
	332	Y ₃ -Stp ₂ -[(OleA) ₂ -K]K-Stp ₂ -Y ₃
	454	C-Y ₃ -Stp ₂ -[(OleA) ₂ -K]K-Stp ₂ -Y ₃ -C
	465	C-Y ₃ -Stp ₂ -[K]K-Stp ₂ -Y ₃ -C
	589	[C-Y ₃ -Stp ₃] ₂ K-Stp ₃ -Y ₃ -C
	590	[Y ₃ -Stp ₃] ₂ K-Stp ₃ -Y ₃
central and peripheral tyrosines	333	Y ₃ -Stp ₂ -[(Y ₃) ₂ -K]K-Stp ₂ -Y ₃
	464	C-Y ₃ -Stp ₂ -[(Y ₃) ₂ -K]K-Stp ₂ -Y ₃ -C
central tyrosines	468	C-Stp ₂ -[(Y ₃) ₂ -K]K-Stp ₂ -C

]K represent branching points with branching at the α, ϵ -amino group of lysine.

1.2. Biophysical characterization

Agarose gel shift assays were performed to assess siRNA or pDNA binding ability of oligotyrosine containing polyplexes (Figure 7A and B, respectively). With regard to siRNA polyplexes, the control oligomer **413** with terminal cysteines, but without oligotyrosines and fatty acids, displayed the weakest siRNA binding ability, followed by control oligomer **216** containing fatty acids in the center, but without oligotyrosines and cysteines.

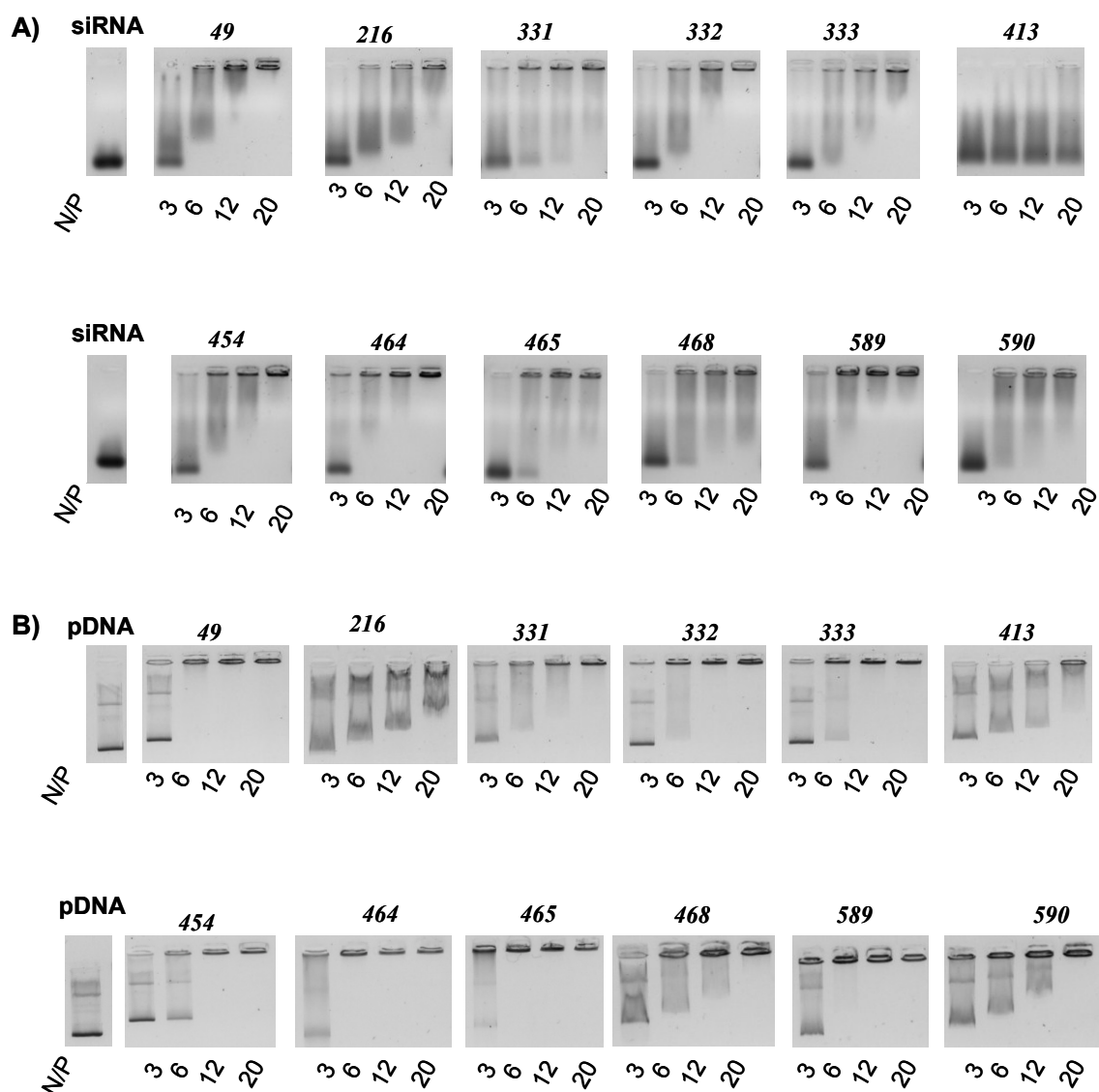


Figure 7: Nucleic acid binding ability of oligomers determined by agarose gel shift assay at different N/P ratios. Polyplex formation in HBG and 30 min incubation time. A) siRNA; B) pDNA.

Oligomers **331** and **465** having terminal oligotyrosines and cysteines, but lacking central fatty acids and oligotyrosines, showed complete siRNA binding only at high N/P ratios. Similarly, oligomers **468** with central tyrosines and terminal cysteines and the three arm structure **590** with only lateral oligotyrosines showed incomplete siRNA binding at low N/P ratios. The replacement of terminal cysteines (**49**) by oligotyrosines (**332**) or the substitution of terminal cysteines and central fatty acids (**49**) by oligotyrosines (**333**) displayed analogous gel-shift properties. This demonstrates that terminal oligotyrosines can substitute the stabilizing activity of either terminal cysteines or central fatty acids. Structures with a combination of terminal oligotyrosines and cysteines (**454**, **464**, **589**) independent of their central modification (fatty acid or oligotyrosines) led to an even better siRNA retardation compared to the oligomers **49**, **332**, and **333** (Figure 7). The results display that an addition of tyrosines before the terminal cysteines enhanced the stabilizing effect of cysteines.

In contrast, for pDNA all oligomers containing a combination of terminal oligotyrosines and cysteines with and without central modifications (without **331**, **465**; with **454**, **464**, **589**) led to complete pDNA binding comparable to oligomer **49**. In accordance to the findings for siRNA complexation, oligomers **216**, **413**, **468**, and **590** showed complete pDNA binding only at high N/P ratios (Figure 7B). These data revealed that siRNA requires a combination of terminal cysteines and oligotyrosines, as well as a central modification (oligotyrosines or fatty acids) for stable polyplex formation. Contrary, the much larger pDNA only required a combination of terminal oligotyrosines and cysteines for stable polyplex formation.

For further characterization, particle size and zeta potential of polyplexes were analyzed with DLS (Table 2). siRNA polyplexes of oligomer **468** with solely central tyrosines could not be analyzed, because no signal was measurable. Polyplexes with **331**, **465**, and **590** were over 600 nm in diameter. The size of all other siRNA polyplexes at N/P 12 was in a range applicable for further evaluations. Contrary to siRNA formulation, all oligomers formed polyplexes with pDNA with sizes between 90 and 540 nm.

Table 2: Particle size (Z-average) and zeta potential of polyplexes (N/P 12) formed in HEPES buffer determined with DLS. Polyplexes were diluted 1:20 before measurement. Variations refer to the median of three measurements of the same sample.

siRNA	Z-average [nm]	Zeta potential [mV]	DNA	Z-average [nm]	Zeta potential [mV]
49 polyplexes	23 ± 4	24.9 ± 1.0	49 polyplexes	114 ± 1	43.6 ± 1.3
216 polyplexes	32 ± 2	5.1 ± 0.3	216 polyplexes	139 ± 3	27.0 ± 1.6
331 polyplexes	644 ± 15	21.7 ± 0.9	331 polyplexes	175 ± 3	21,6 ± 1.6
332 polyplexes	150 ± 2	38.1 ± 0.8	332 polyplexes	93 ± 1	43.8 ± 0.9
333 polyplexes	334 ± 46	16.7 ± 0.3	333 polyplexes	287 ± 46	20.7 ± 0.5
413 polyplexes	n. d.*	n. d.*	413 polyplexes	358 ± 8	16.2 ± 1.3
454 polyplexes	99 ± 2	50.7 ± 0.8	454 polyplexes	99 ± 1	53.2 ± 2.8
464 polyplexes	243 ± 12	13.3 ± 0.4	464 polyplexes	180 ± 5	21.5 ± 1.8
465 polyplexes	1570 ± 194	11.8 ± 0.7	465 polyplexes	244 ± 18	14.0 ± 2.5
468 polyplexes	n. d.*	n. d.*	468 polyplexes	542 ± 22	12.7 ± 1.8
589 polyplexes	233 ± 3	33.4 ± 0.6	589 polyplexes	115 ± 2	19.6 ± 1.4
590 polyplexes	703 ± 44	18.0 ± 0.4	590 polyplexes	144 ± 2	17.8 ± 0.6

*not detectable (no measurable signal).

The buffer capacity of the oligomers was investigated with the help of acidimetric back titration (Table 3). Therefore, the differential buffer capacities of the oligomers were determined between the endosomal pH of 5.5 and the physiological pH of 7.4. In comparison to oligomer **49**, the buffer capacity of oligotyrosine containing oligomers was higher due to the phenolic group within the amino acid. Moreover, the pH-specific lytic potential of oligomers was investigated with the help of an erythrocyte leakage assay (Figure 8).

Table 3: Buffer capacity of oligomers determined between pH 5.5 and 7.4 by acidification to pH 2 and back titration with NaOH.

Oligomer	Buffer capacity [%]
49	19.0
331	21.0
332	24.3
333	24.1
454	22.2
464	21.4
465	19.0
468	21.1
589	17.4
590	18.0

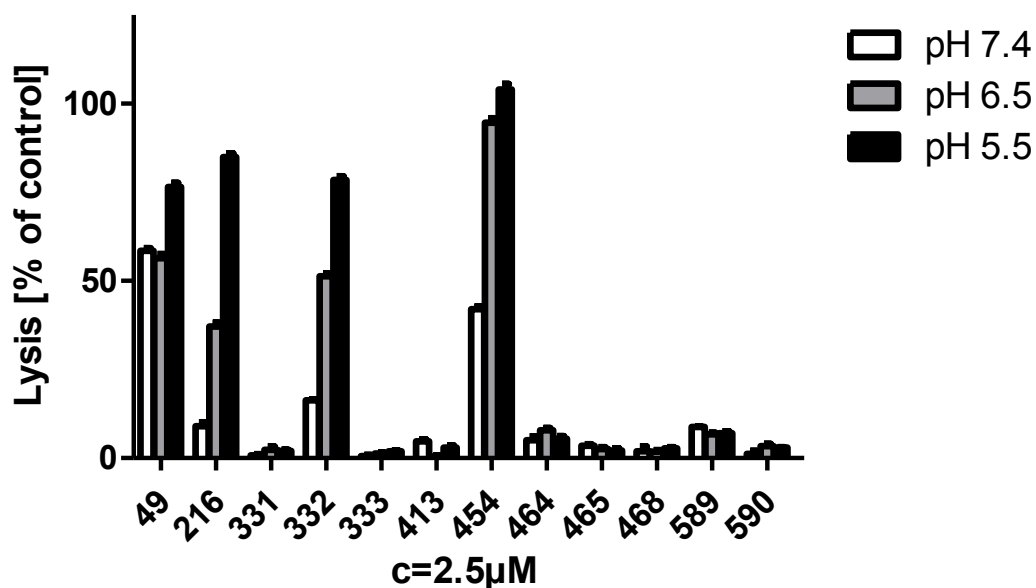


Figure 8 Erythrocyte leakage assay at different pH values. Erythrocytes were incubated with 2.5 μ M oligomer solutions at 37°C and the indicated pH values. Hemoglobin release was measured after 1 h.

Only dioleic acid modified oligomers showed significant pH-specific lytic potential, whereas tyrosine-containing oligomers without fatty acid modification did not mediate any significant lysis. The endosomal escape of oligomers with fatty acids is therefore a combination of “proton sponge” effect and lytic activity, whereas oligomers without fatty acids lack lytic activity illustrated in the leakage assay. Oligotyrosine modified oligomers apparently (based on the subsequently demonstrated bioactivity) form polyplexes with improved “proton sponge” effect sufficient for endosomal escape, as already pointed out with the acidimetric titrations.

1.3. Uptake and transfection efficiency

After their biophysical characterization, the cellular uptake of selected oligomers was investigated using Neuro2A cells (Figure 9).

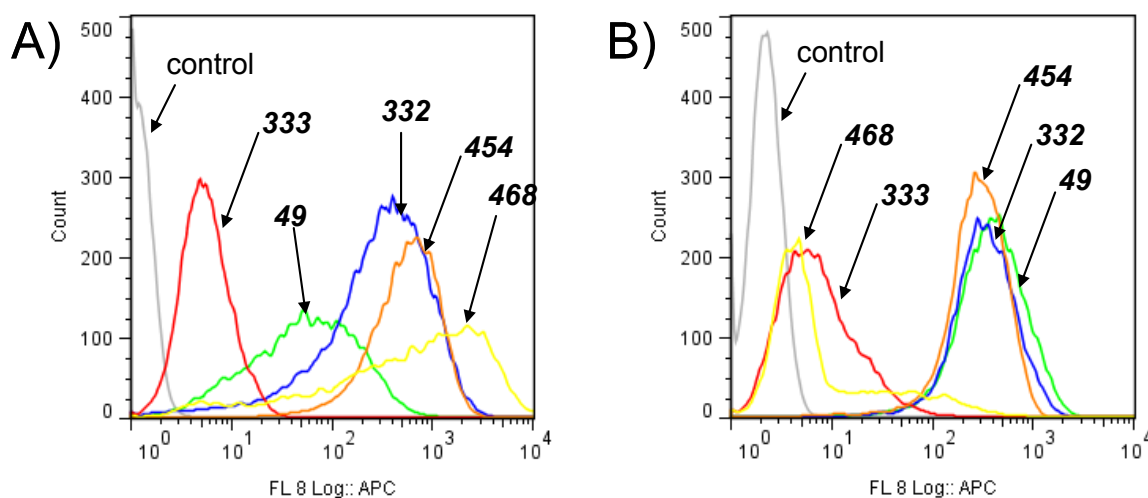


Figure 9: Cellular internalization study using flow cytometry. Cellular uptake of Cy5-labeled siRNA or pDNA, complexed with oligomer **49**, **332**, **333**, **454**, and **468** (N/P 12) was determined by the means of flow cytometry. The intensity of the Cy5 signal resembles the amount of polyplexes taken up into Neuro2A cells. “Count” represents cumulative counts of cells with indicated Cy5 fluorescence after appropriate gating by forward/sideward scatter and pulse width. Dead cells (DAPI positive, less than 2%) were excluded from analysis. All experiments were performed in triplicates. A) siRNA; B) pDNA. Flow cytometry studies were performed by Petra Kos.

Polyplexes with **333** displayed the lowest siRNA uptake (Figure 9A), whereas **468** polyplexes displayed the strongest shift compared to control treated cells. Nevertheless, the uptake curve for **468** polyplexes did not follow the Gaussian distribution showing a broad shoulder with a low count rate. Connecting this data with the DLS data, **468** polyplexes seemed to form undesirable aggregates leading to a strong uptake in a small subpopulation of cells. pDNA complexed with oligomer **333** or **468** displayed the lowest uptake. The reason for the different uptake profiles of oligomer **468** is its ability to form large aggregates with siRNA, but not with pDNA, as observed with DLS measurements. In general, a correlation between zeta potential and nucleic acid uptake could be seen: The lower the positive charge of the polyplexes, the lower the uptake.

Nearly all tested polyplexes showed efficient pDNA transfection activity except the control oligomers (**216** and **413**) and oligomers where terminal cysteines as well as central lytic domains had been replaced by oligotyrosine motifs (**333** and **590**). Replacing terminal cysteines by oligotyrosines (**332**) or adding oligotyrosines to the terminal cysteines or replacing the central lytic domain with oligotyrosines (**464**) led to improved luciferase expression comparable to oligomer **49** (Figure 10A).

Oligomer **468** with oligotyrosines instead of fatty acids as lytic domains showed equivalent pDNA transfection compared to oligomer **49**. Three-arm structures required terminal cysteines in order to mediate gene transfer (oligomer **589** compared to **590**). The pDNA transfection data were in accordance with the biophysical characterization and uptake studies. Moreover, they confirmed the favorable effect of tyrosine trimer integration. The cell viability assay (Figure 11) did not reveal any cytotoxicity for all tested pDNA polyplexes.

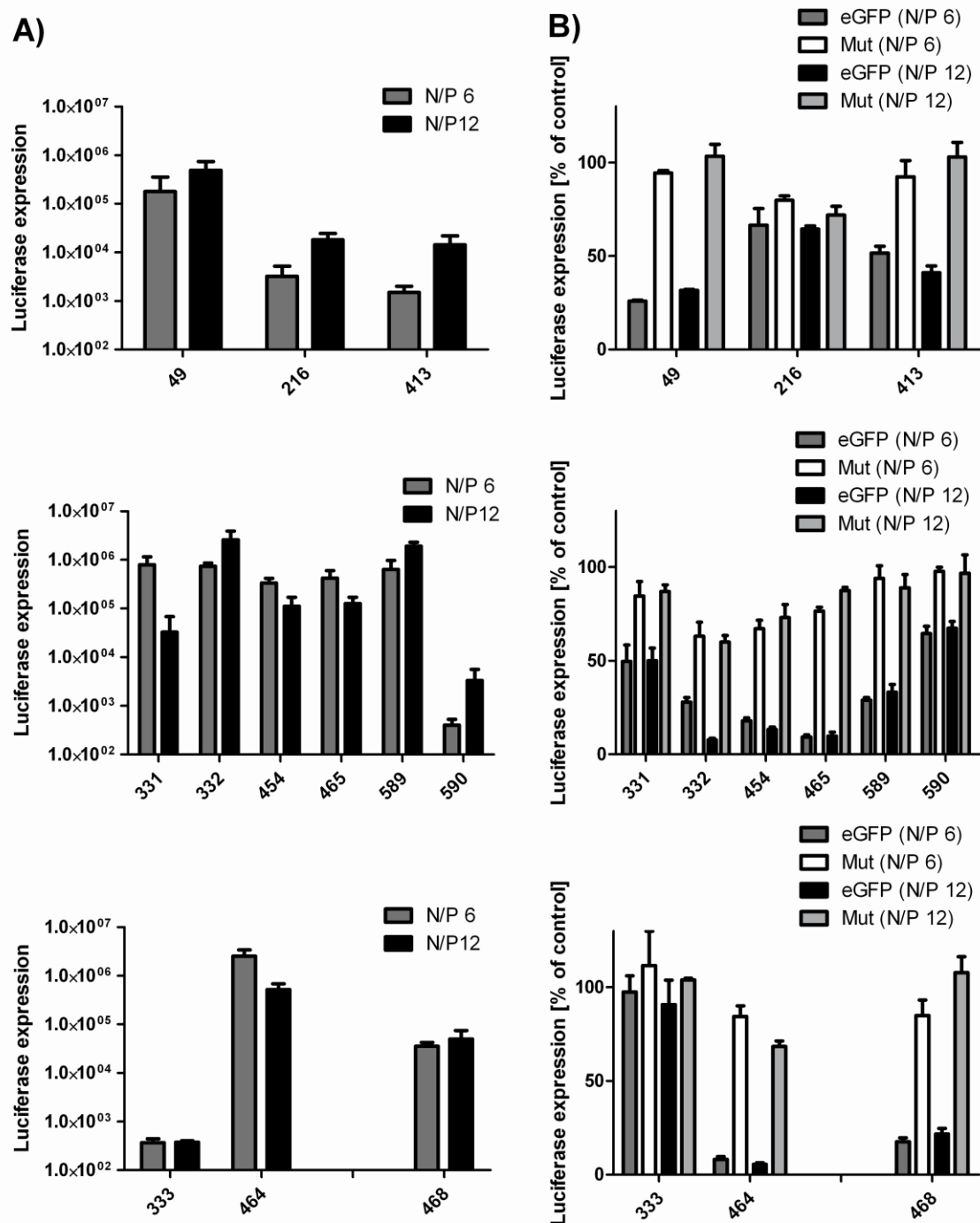


Figure 10: Gene transfer (A) and gene silencing (B) in neuroblastoma cells. Luciferase pDNA polyplexes were tested for luciferase expression in Neuro2A cells, eGFP-targeted siRNA (eGFP) or control siRNA (Mut) polyplexes for eGFPLuc gene silencing in Neuro2A-eGFPLuc cells, polyplexes were tested at N/P 6 and 12. *Top:* Polyplexes without tyrosines. *Center:* Polyplexes with tyrosine motif in the periphery. *Bottom:* Polyplexes with central and peripheral tyrosines or only central tyrosines. Transfection experiments were performed by Petra Kos, Thomas Fröhlich and Daniel Edinger.

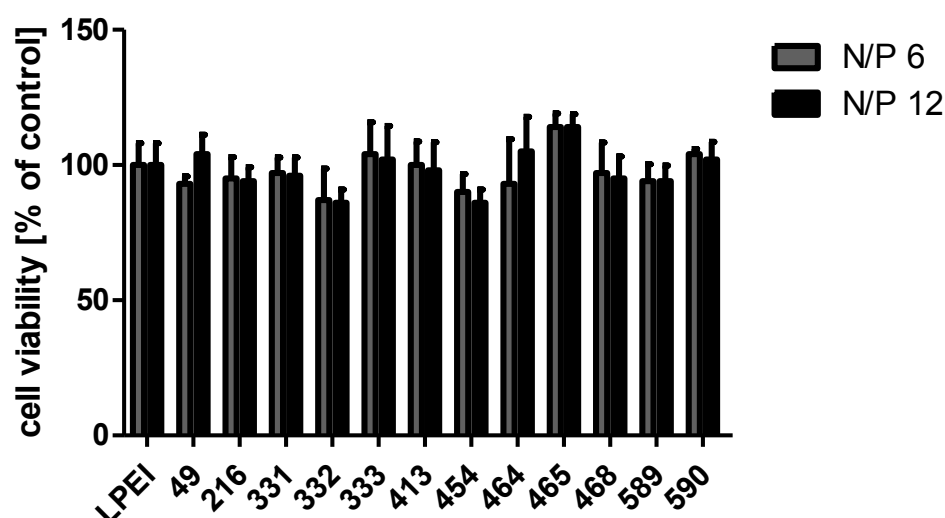


Figure 11: Metabolic activity of Neuro2A cells after transfection with pDNA polyplexes (N/P 12). Positive control: Linear PEI (LPEI). MTT assay was made by Petra Kos.

For siRNA transfection, the addition of oligotyrosines to the terminal cysteines was a favorable modification (oligomers **454**, **464**, **465**, **589**) leading to stronger target gene knockdown compared to oligomer **49**. The alteration of the central domain (fatty acid **454**, oligotyrosine **464**, and lysine **465**) showed only moderate influence on the transfection efficiency. Solely, the substitution of the central fatty acid by oligotyrosines (oligomer **468**) improved transfection efficiency, whereas replacing both the terminal cysteines and the central hydrophobic domain by oligotyrosines led to an inactive polyplex (oligomer **333** and **590**) (Figure 10B). In summary, the new class of oligotyrosine containing oligomers was efficient in pDNA and siRNA transfection, in most cases superior to oligomer **49**.

1.4. Serum stability

For simulating in vivo conditions, the polyplexes were analyzed for their stability in fetal bovine serum (FBS). Therefore, polyplexes were first formed in HEPES buffer, followed by the addition of FBS. The samples were incubated at room temperature and 37°C for 0, 10, 30 and 90 min. Afterwards, gel electrophoresis was performed to investigate if the polyplexes were stable, partially stable or instable. Free siRNA migrates in the gel due to its negative charge, whereas intact polyplexes stay in the pockets of the agarose gel (Figure 12).

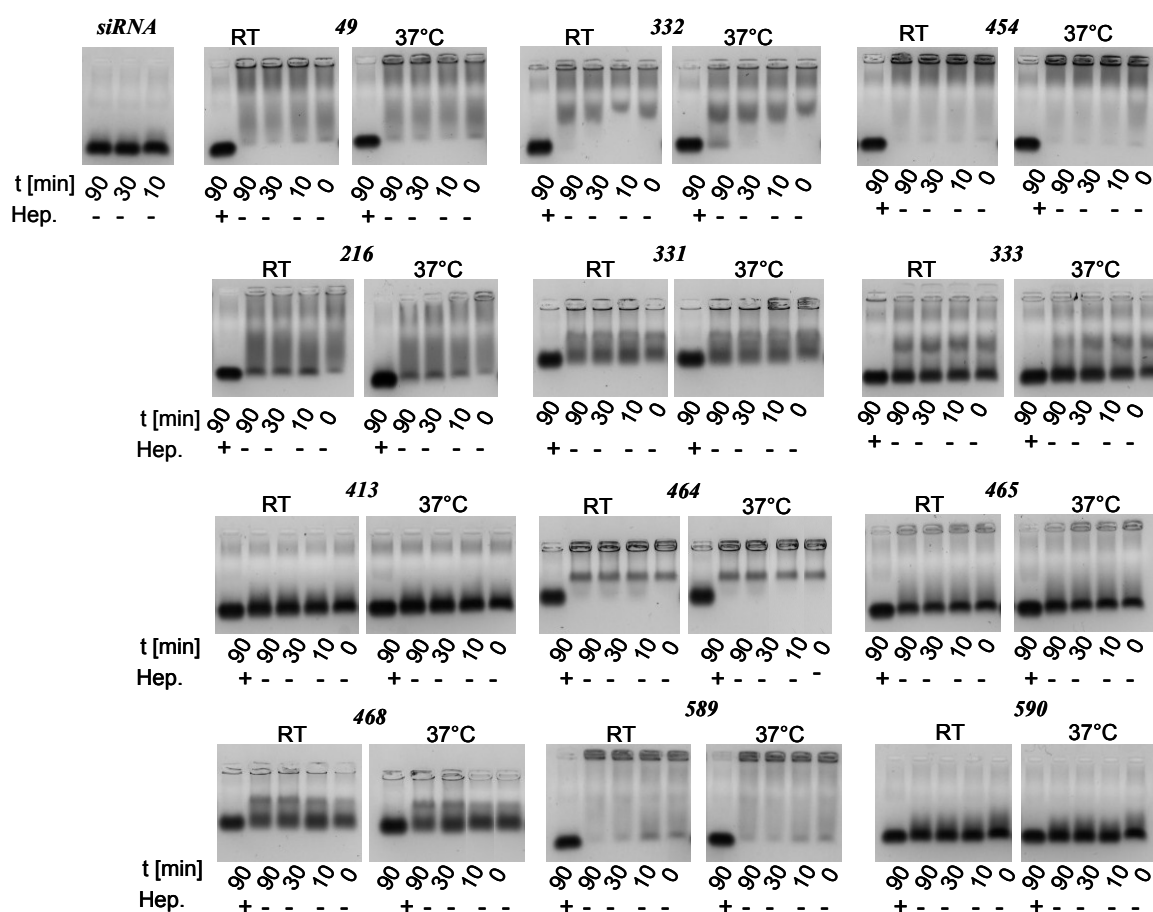


Figure 12: Polyplex stability in 90% FBS at RT and 37°C at different time points. Polyplexes, formed with stabilized control siRNA, were incubated at room temperature for 30 min before FBS was added. Heparin (50 I.U.) was added to dissociate polyplexes.

Moreover, polyplexes were treated with 50 I.U. of heparin per sample after 90 min in order to dissociate polyplexes, and to investigate whether the siRNA was degraded by serum proteins. The band of the stabilized siRNA of all heparin treated samples had comparable intensity to free siRNA at all time points. Hence, no degradation of the complexed or free siRNA occurred during the incubation time. This is not unexpected as 2'-methoxy stabilized siRNA was applied in our experiments. After gel electrophoresis, no siRNA migration was observable for **454**, **464**, and **589** polyplexes, confirming the serum stability of these polyplexes both at room temperature and 37°C. In contrast, **332** and **49** polyplexes dissociated partially at 37°C after 90 min, as a band at the free siRNA level appeared. This data showed that a combination of oligotyrosines and cysteines at the ends of our oligomers led to a favorable stabilization and improved resistance to serum protein mediated disassembly. The remaining oligomer polyplexes were instable in serum

and free siRNA was detected immediately after addition of serum.

Consequently, the stability of polyplexes in serum was investigated with fluorescence correlation spectroscopy (FCS). Therefore, oligotyrosine modified polyplexes with particle sizes smaller than 300 nm were investigated. The size limit was chosen due to the limited size of the confocal volume¹⁰². Table 4 shows the polyplex stability in serum after different time points at room temperature and 37°C. All radii were viscosity corrected for data analysis. The viscosity of serum was measured with a microviscosimeter.

Table 4: Hydrodynamic radii r , diffusion times, number of particles in the confocal volume, and fit χ^2 of polyplexes in serum at room temperature or 37°C determined with FCS. Samples were evaluated with one component fit, unless stated otherwise (2c. = two component fit).

RT	r [nm]	Diffusion time [μ s]	Number of particles	fit χ^2
free siRNA				
1 min	2.3	239.4	49.3	9.4E-09
49 polyplexes				
1 min	49.2	5464.1	2.2	6.4E-06
10 min	68.0	7560.2	2.0	2.1E-05
30 min	68.2	7581.8	2.2	1.1E-05
90 min 2c. (33.8%)	2.2	245.0	18.0	3.2E-07
90 min 2c. (66.2%)	77.1	8565.1		
332 polyplexes				
1 min	113.4	12600.4	0.6	1.9E-04
10 min	123.3	13700.3	0.5	3.5E-04
30 min	115.6	12844.3	1.0	1.7E-04
90 min	128.0	14222.9	0.3	5.6E-03

Table 4: Continued

RT	r [nm]	Diffusion time [μs]	Number of particles	fit χ^2
454 polyplexes				
1 min	82.8	8758.4	0.421	5.6E-03
10 min	84.6	8953.9	0.408	2.8E-03
30 min	105.2	11132.3	0.208	2.0E-03
90 min	91.8	9718.2	0.418	2.1E-03
464 polyplexes				
1 min	102.0	10797.2	0.254	1.7E-03
10 min	95.3	10085.5	0.245	3.7E-03
30 min	120.1	12709.9	0.193	6.2E-03
90 min	119.45	12640.8	0.235	1.8E-03
589 polyplexes				
1 min	164.4	17394.2	0.133	6.3E-02
10 min	165.2	17480.1	0.161	2.4E-02
30 min	165.6	17521.9	0.324	4.0E-03
90 min	188.0	19891.3	0.149	2.8E-02
37°C				
free siRNA				
1 min	2.4	272.2	86.0	7.8E-08
49 polyplexes				
1 min	52.3	5892.5	1.4	9.3E-05
10 min	59.4	6687.0	1.1	4.8E-04
30 min 2c.(6.0%)	2.4	272.2	5.9	1.6E-06
30 min 2c.(94.0%)	65.5	7372.7		
90 min 2c. (82.0%)	2.4	272.2	57.4	3.4E-08
90 min 2c. (18.0%)	52.6	5924.6		

Table 4: Continued

37°C	r [nm]	Diffusion time [μs]	Number of particles	fit χ^2
332 polyplexes				
1 min	110.5	12442.6	0.3	1.0E-02
10 min	109.0	12278.5	0.3	8.6E-04
30 min	114.2	12865.9	0.4	9.9E-04
90 min 2c. (52.8%)	2.4	272.2		
90 min 2c. (47.2%)	102.9	11588.6	21.6	1.7E-07
454 polyplexes				
1 min	103.7	10969.6	0.370	3.8E-03
10 min	103.1	10910.8	0.092	2.0E-01
30 min	86.8	9186.0	0.399	2.3E-03
90 min	121.2	12821.3	0.546	5.4E-04
464 polyplexes				
1 min	97.4	10310.0	0.251	3.8E-03
10 min	95.0	10056.8	0.186	9.0E-03
30 min	86.7	9178.7	0.171	2.7E-02
90 min	103.8	10988.8	0.252	8.8E-03
589 polyplexes				
1 min	164.4	17394.2	0.133	6.3E-02
10 min	174.7	18481.9	0.241	2.9E-03
30 min	165.6	17526.8	0.191	4.4E-02
90 min	157.9	16709.8	0.239	1.8E-02

49 polyplexes are stable for 30 min at room temperature, but dissociated at 37°C within the same time. After 90 min, dissociation of the polyplexes was observed for both temperatures. Contrary to **49** polyplexes, the new tyrosine-modified **332**, **454**, **464**, and **589** polyplexes displayed enhanced serum stability. Dissociation at room temperature was not observed at any time. Measurements at 37°C showed only a slightly decreased stability of the siRNA polyplexes. Terminal tyrosine and cysteine containing **454**, **464**, and **589** polyplexes remained stable at 37°C for 90 min. For the **332** polyplexes with tyrosines replacing cysteines, however, the number of observed particles in the confocal volume increased from < 1 to 21.6 after 90 min at 37°C, and free siRNA was detectable. Nevertheless, the stability of **332** was higher than stability of the **49** polyplexes. In contrast to **49** polyplexes with only 18% intact polyplexes after 90 min¹⁰³, as much as 47% intact **332** polyplexes were still detectable. This data fit very well to our gel shift findings, showing the improved stability of the new oligomers with peripheral oligotyrosines.

1.5. In vivo experiments

In a next step, the distribution of siRNA polyplexes after systemic administration was evaluated with the help of Cy7-labeled siRNA. Polyplexes were injected intravenously into mice (n = 3). Near-infrared (NIR) fluorescence imaging revealed a short circulation time followed by fast renal clearance of both uncomplexed siRNA, as well as the control (**216**, **413**) and **590** polyplexes due to polyplex dissociation in the blood (Figure 13).

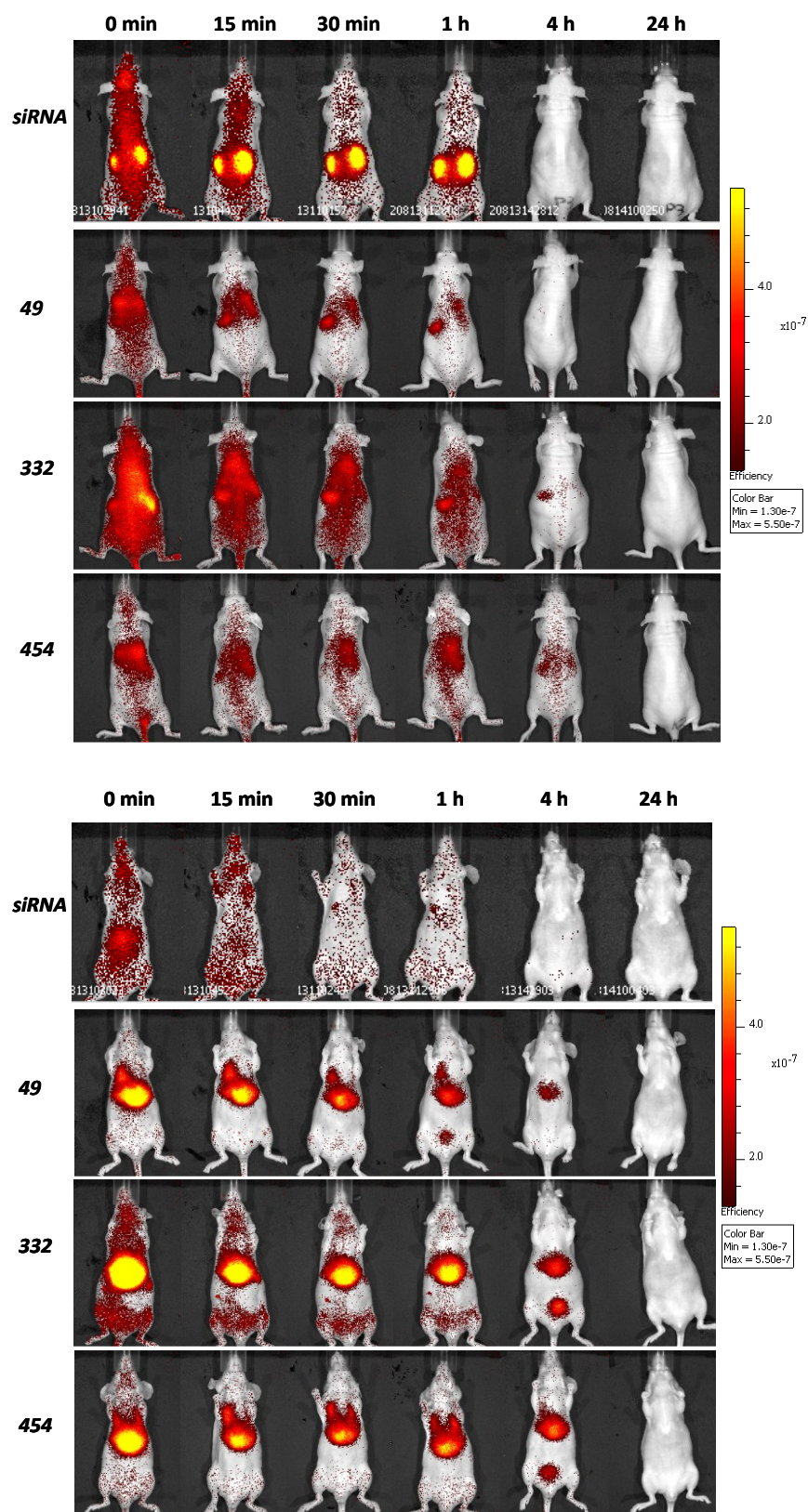


Figure 13: Intravenous administration of siRNA polyplexes. Time-dependent distribution of 50 µg Cy7-labeled siRNA after intravenous injection using no carrier, or oligomers as polyplex carrier. *Upper panel:* Ventral position. *Lower panel:* Dorsal position. Experiments were performed in triplicates by Laura Schreiner, Annika Herrmann and Daniel Edinger, one representative mouse per group is shown.

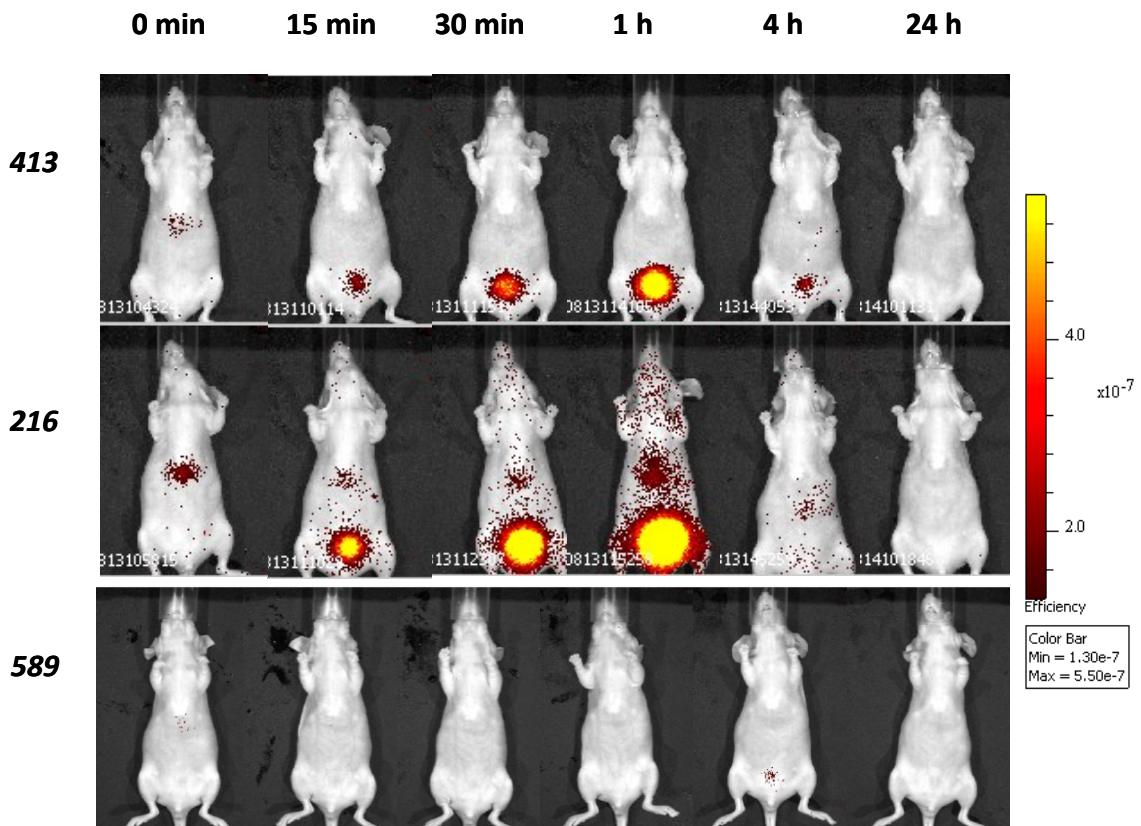
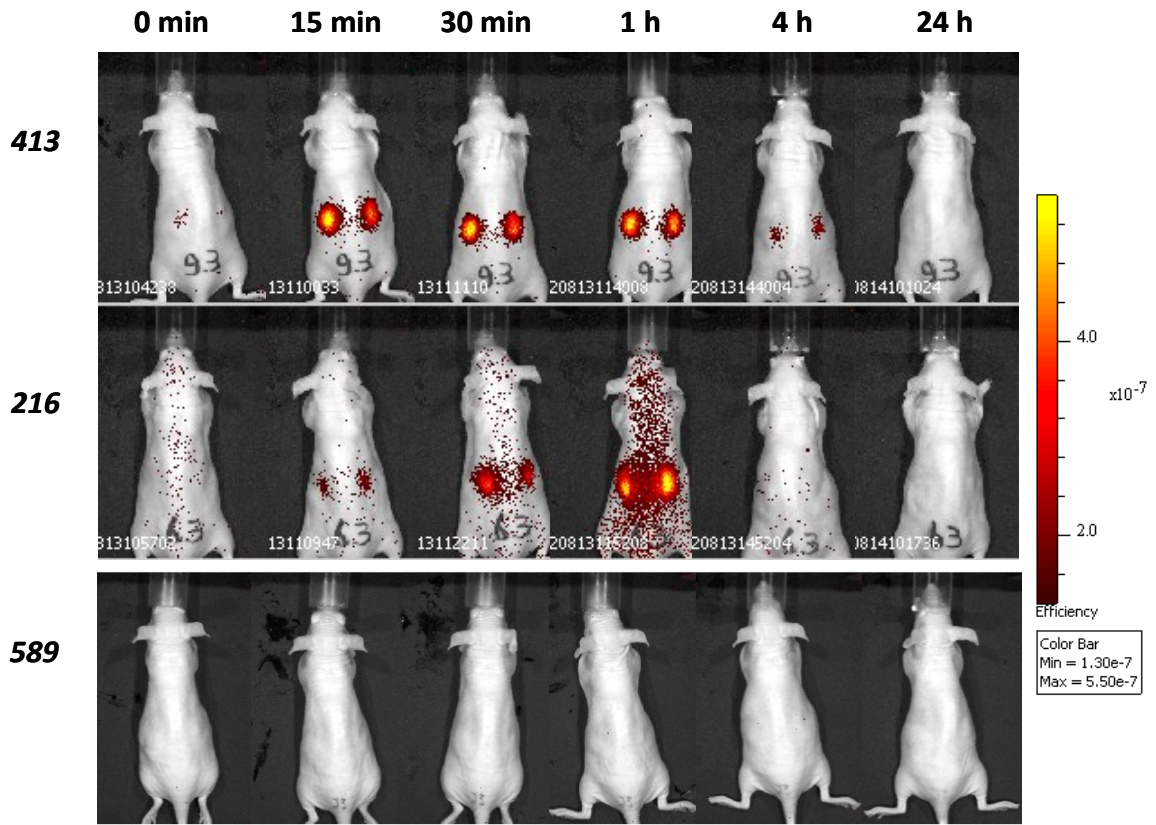


Figure 13: Continued.

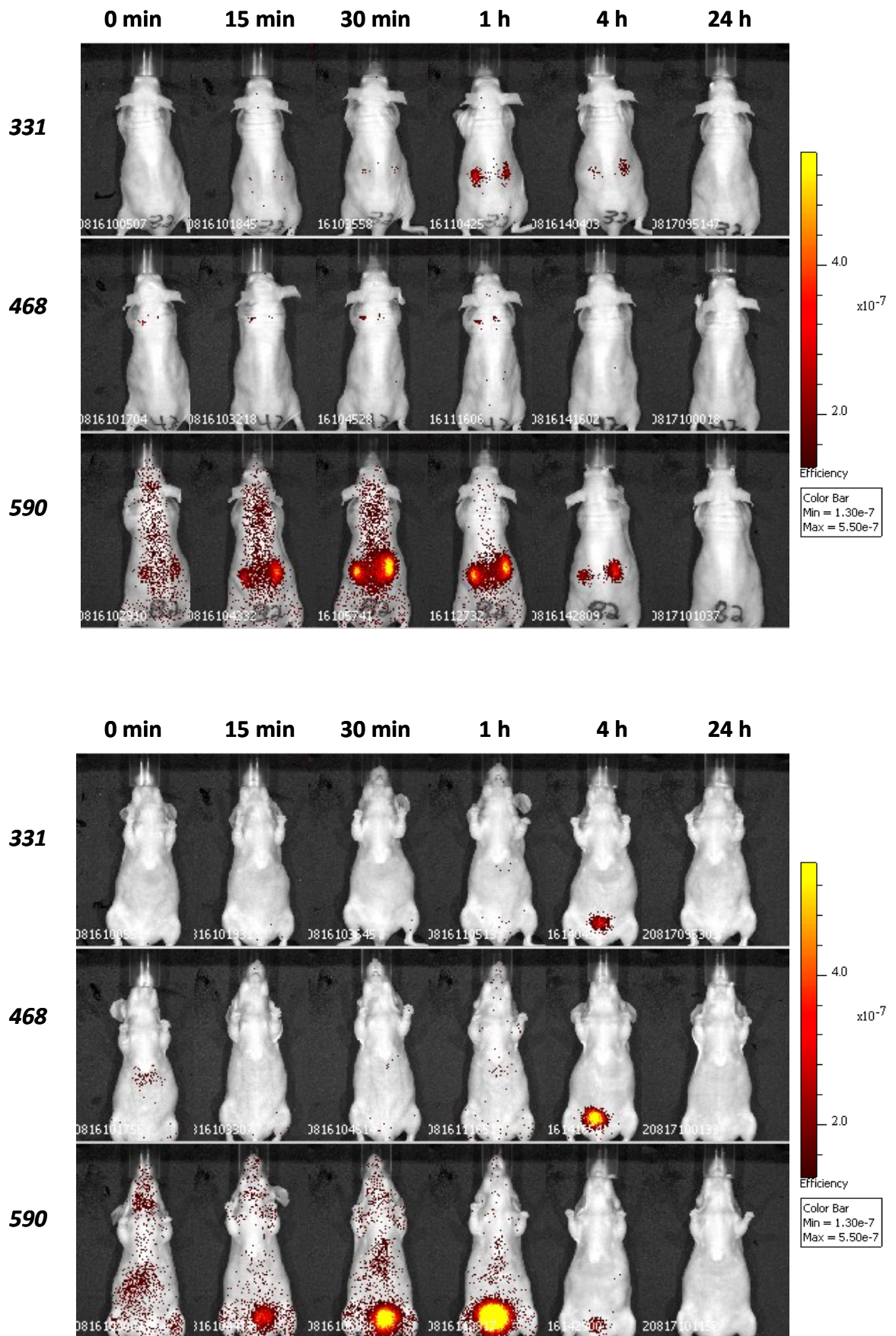


Figure 13: Continued.

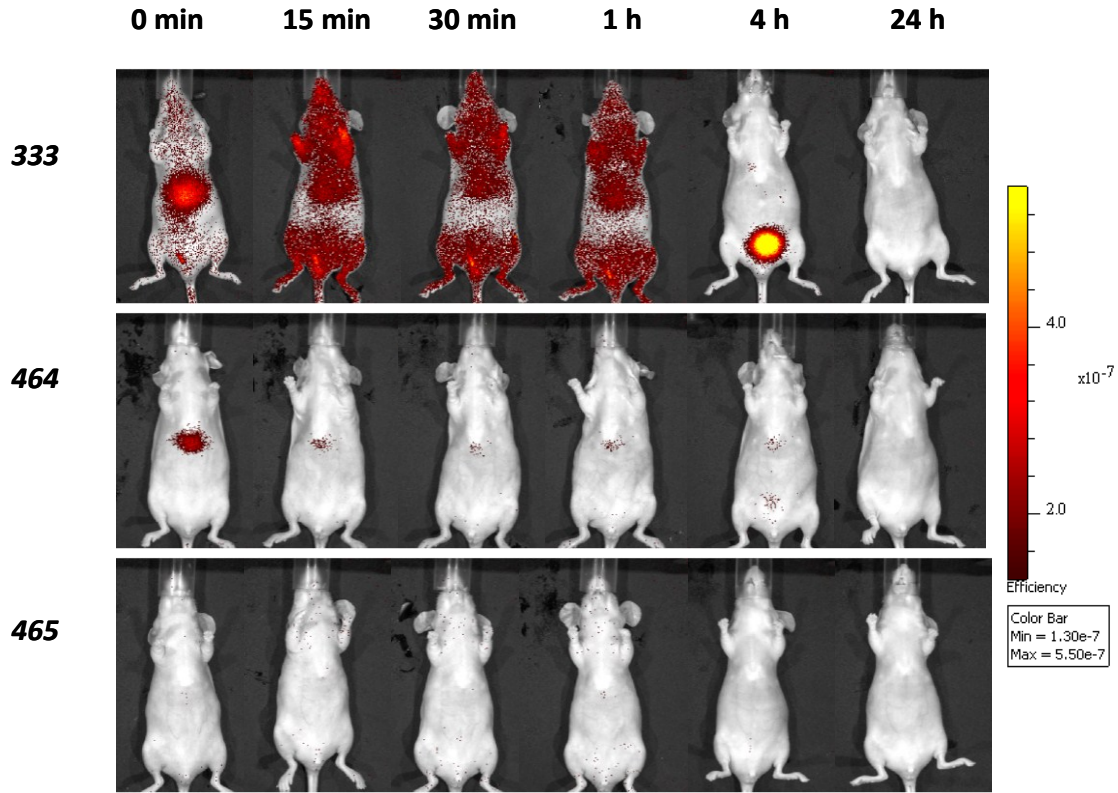
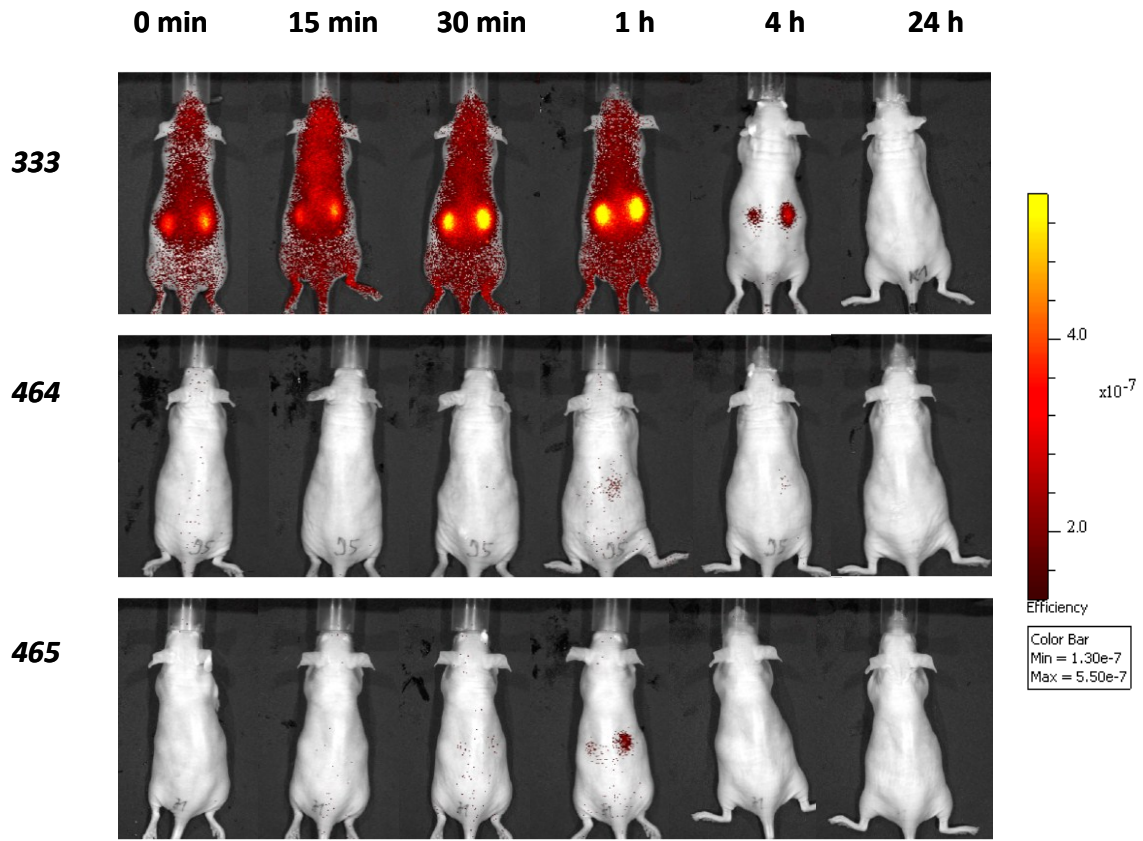


Figure 13: Continued.

Polyplexes of four oligomers (**331**, **464**, **465**, and **468**) showed a strong quenching of the fluorescent Cy7 signal upon polyplex formation. This hampered the monitoring of the siRNA distribution by NIR bioimaging. The lack of Cy7 signal over a long period (Figure 13) however suggests prolonged polyplex stability of these oligotyrosine oligomers. The oligomer **333** displayed a good systemic tissue distribution for at least 1 hour, though at 4 hours only a high signal in the kidneys and the bladder was seen (Figure 13). The agarose gel shift showed low serum stability, explaining the renal and bladder signal as probable consequence of the release of free siRNA.

49, **454**, and especially **332** polyplexes displayed initially a good systemic distribution of the polyplexes (Figure 13). Already right after injection, a signal in the liver was observed in the dorsal pictures. The liver signal was still visible at 4 hours, with a signal in the bladder appearing at this time point. The **332** polyplexes showed the most beneficial distribution, followed by **454** and then **49** polyplexes. **49** polyplexes displayed fastest clearance by the kidneys (at 1 h) and disappearance from the liver (at 4 h) which is consistent with lower polyplex stability.

Consequently, the polyplexes of **49** (as control) and **332** were investigated for their therapeutic potential. Mice were treated intratumorally with RAN siRNA and control siRNA polyplexes at day 2, 4, 8, 11 and 14 after inoculation of the eGFP-luciferase expressing Neuro2A tumor cells. Tumor growth was monitored by bioluminescence imaging (Figure 14), which was significantly reduced for mice treated with oligomer **332** RAN siRNA polyplexes compared to control siRNA treated animals. Only with **332** RAN siRNA polyplexes a significantly reduced tumor volume was found, whereas oligomer **49** RAN siRNA polyplexes did not show any reduction of the tumor burden in this experimental setting.

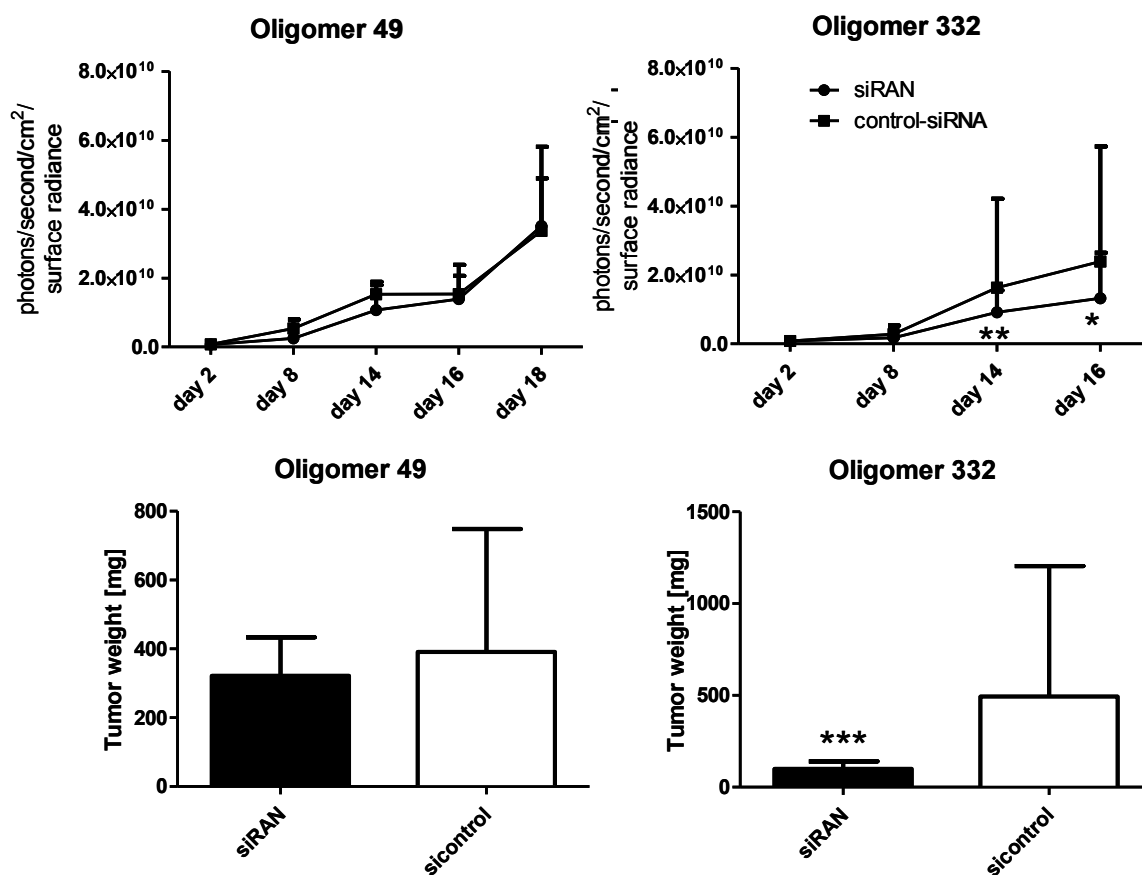


Figure 14: Tumor growth of subcutaneous Neuro2A-eGFPLuc tumors in mice after repeated intratumoral treatment (5 mice per group) with polyplexes of oligomers **49** or **332** and RAN siRNA or control siRNA (N/P 12). Animals were treated with 50 μ g siRNA per mouse at days 2, 4, 8, 11 and 14 after inoculation of the tumor cells. *Top:* Tumor development was determined by bioluminescent signal for the Neuro2A-eGFPLuc cells after intraperitoneal injection of luciferin. *Bottom:* Tumor weight of the mice at the time of termination of the experiment. The experiment was terminated when the first tumor of the oligomer group reached a size of 1500 mm³. Significance of 50 μ g RAN siRNA against 50 μ g control siRNA was evaluated by t-test (***) $p < 0.0005$; **) $p < 0.005$; *) $p < 0.05$). This experiment was performed by Raphaela Kläger and Daniel Edinger.

2. Further stabilizing motifs for pDNA and siRNA polyplexes

Stability of polyplexes plays an important role for in vivo delivery, as above-mentioned. Therefore, various further stabilizing components were integrated into the oligomer structures by means of solid phase assisted synthesis. Their stabilizing potential as well as the preservation in efficacy was investigated for pDNA or siRNA polyplexes.

A new synthetic procedure had to be introduced in order to attach certain motifs to the peripheral ends of T-shapes, as peptide elongation after coupling of these components was impossible. Therefore, these stabilizing motifs were incorporated as last synthesis step. The central component of the T-shape was synthesized first. Afterwards, the linear backbone was assembled. Therefore, this synthesis procedure was called 'reverse synthesis'. A chlorotrityl chloride resin was loaded with dde-Lys(Fmoc)-OH. After Fmoc deprotection and load determination, Fmoc-Lys(Fmoc)-OH as branching unit was coupled. After a negative Kaiser test, the central domain was attached to the resin. After dde deprotection with hydrazine hydrochloride in DMF, another branching point was introduced. After successful coupling and deprotection, the polycationic artificial amino acids were coupled, followed by the stabilizing motif. In a final step, the peptide was released from the resin and the acid labile side chain protecting groups were simultaneously removed.

2.1. Ureido-pyrimidinone containing oligomers

Dankers et al. ¹⁰⁴ introduced ureido-pyrimidinones which were coupled to peptides by means of solid phase peptide synthesis. Figure 15 shows the formation of non-covalent, hydrogen bonds between two ureido-pyrimidinone monomers.

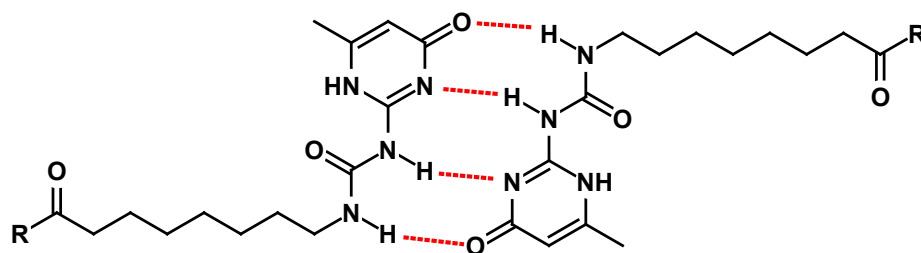


Figure 15: Hydrogen bond formation between two ureido-pyrimidinone monomers ¹⁰⁴.

2.1.1. Building block synthesis

The synthesis of 2-(6-isocyanahexylaminocarbonylamino)-6-methyl-4(1H)-pyrimidinone (ICH-CAMP) was described by Dankers et al. ¹⁰⁴. 2-Amino-4-hydroxy-6-methylpyrimidine was dissolved in 1,6-diisocyanatohexane and heated to 100°C for 17 h. The reaction mixture was cooled and *n*-pentane was added. The resulting precipitate was filtered and washed with *n*-pentane. After vacuum distillation of the product, ICH-CAMP was obtained as white powder. In order to determine identity and purity, mass spectroscopy and NMR spectroscopy were performed (page 106).

2.1.2. Oligomer synthesis

The ureido-pyrimidinone containing oligomer was synthesized with the help of solid phase assisted synthesis. Therefore, one T-shape oligomer was modified at the *N*-terminus with ICH-CAMP in order to investigate the effect of this modification on nucleic acid binding ability and transfection efficiency. The sequence of the oligomer with ureido-pyrimidinone motifs and its analog without stabilizing motifs are listed in Table 5.

Table 5: Selected oligomer sequence and its analog (*N*- to *C*-terminus).

Oligomer	Sequence
407	[(Stp ₅) ₂ K]K[K(OleA) ₂]
408	[(ICH-CAMP-Stp ₅) ₂ K]K[K(OleA) ₂]

2.1.3. In vitro characterization

Agarose gel shift assays were performed to assess siRNA binding ability of oligomer **407** and **408** polyplexes (Figure 16). The control oligomer **407** without ICH-CAMP motifs displayed a higher siRNA binding ability at N/P 6 than the oligomer **408** polyplexes with the ureido-pyrimidinone modification.

Both polyplexes showed efficient pDNA transfection activity compared to buffer treated cells. The ureido-pyrimidinone motif of oligomers **408** did not modify luciferase expression. As a result, oligomers **407** and **408** displayed comparable luciferase expression (Figure 17A).

For siRNA transfection, the addition of ureido-pyrimidinone motifs led to a slight increase in target gene knockdown compared to polyplexes without the ureido-pyrimidinone motifs (Figure 17B). However, the effect of the ureido-pyrimidinone modification on siRNA knockdown was lower than for analogs with cysteine modification⁵⁶.

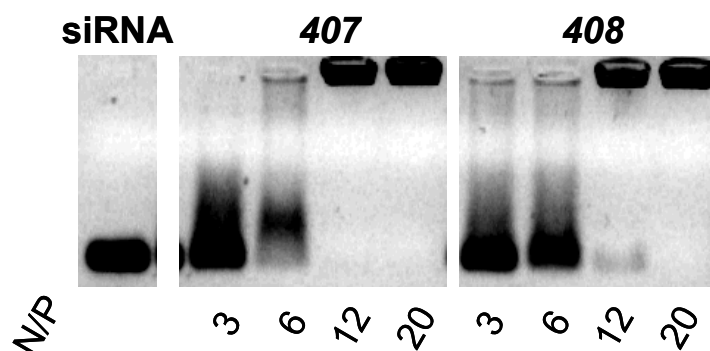


Figure 16: siRNA binding ability of oligomers determined by agarose gel shift assay at different N/P ratios. Polyplex formation in HBG and 30 min incubation time.

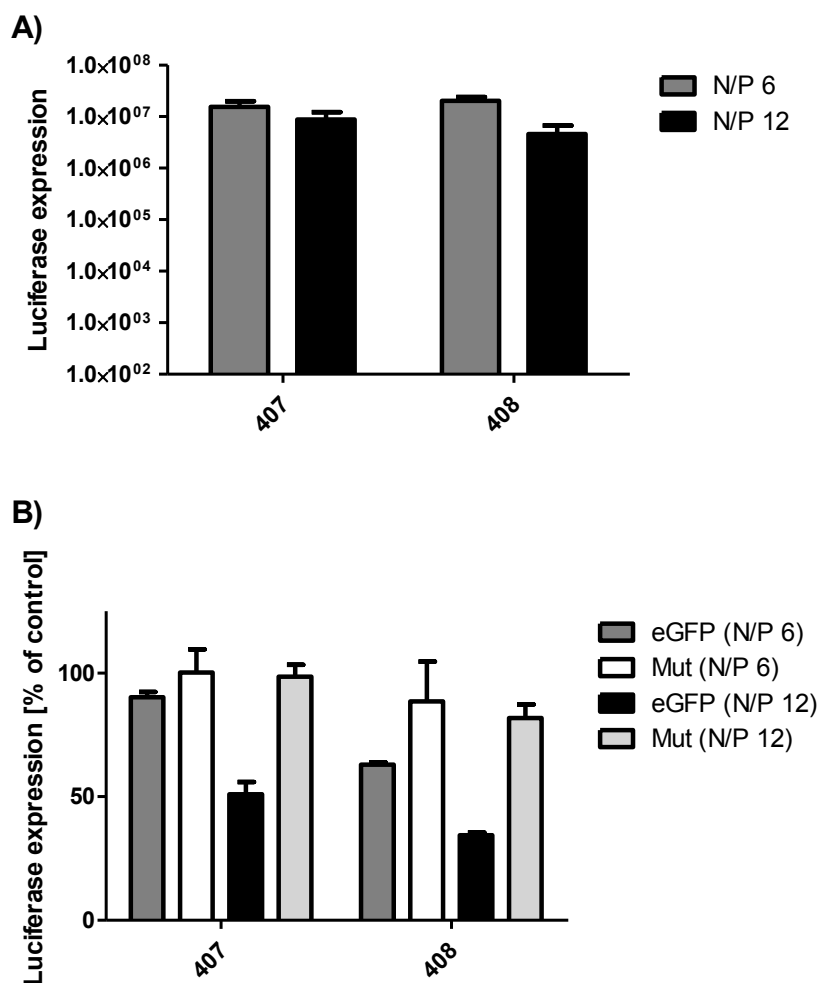


Figure 17: Gene transfer (A) and gene silencing (B) in neuroblastoma cells. Luciferase pDNA polyplexes were tested for luciferase expression in Neuro2A cells, eGFP-targeted siRNA (eGFP) or control siRNA (Mut) polyplexes for eGFPLuc gene silencing in Neuro2A-eGFPLuc cells, polyplexes were tested at N/P 6 and 12. Transfection experiments were performed by Petra Kos, Thomas Fröhlich and Daniel Edinger.

2.2. Pyridyl-thiourea containing oligomers

Creusat et al.¹⁰⁵ introduced pyridylthiourea grafted polyethylenimine which led to effective siRNA-mediated gene silencing in vitro and in vivo. The resulting polymers with a modification degree of 28% relative to ethylenimine did not have hemolytic activity. Moreover, the polyplexes were stable in 4.5% glucose for several hours.

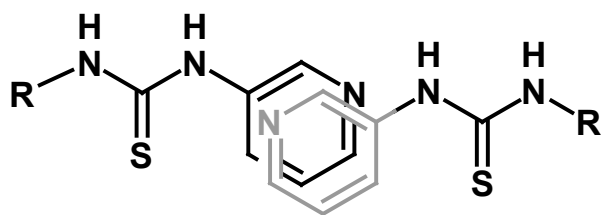


Figure 18: π - π interaction between two pyridyl thiourea containing monomers ¹⁰⁵.

2.2.1. Oligomer synthesis

One T-shape oligomer was modified at the *N*-terminus with 3-pyridyl isothiocyanate (PITC) in order to investigate the effect of this modification on transfection efficiency. Therefore, the T-shape **587** was synthesized by means of reverse synthesis as described above for the ICH-CAMP modified oligomers. The sequence of the oligomer with 3-pyridyl isothiocyanate motifs and its analog without stabilizing motifs are listed in Table 6.

Table 6: Selected oligomer sequence and its analog (*N*- to *C*-terminus).

Oligomer	Sequence
468	C-Stp ₂ -[(Y ₃) ₂ -K]K-Stp ₂ -C
587	[(PITC-Stp ₂) ₂ K]K[K(Y ₃) ₂]

2.2.2. Transfection efficiency

For siRNA transfection, the substitution of cysteines with 3-pyridyl isothiocyanate motifs like in oligomer **587** led to a complete loss of target gene knockdown compared to **468** polyplexes with cysteine motifs (Figure 19).

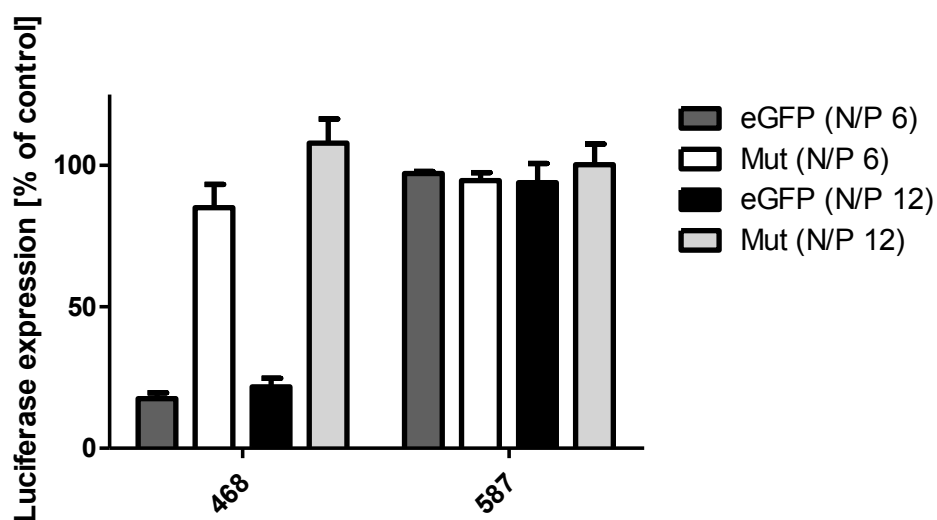


Figure 19: Gene silencing in neuroblastoma cells. eGFP-targeted siRNA (eGFP) or control siRNA (Mut) polyplexes for eGFPLuc gene silencing were tested in Neuro2A-eGFPLuc cells, polyplexes were tested at N/P 6 and 12. Transfection experiments were performed by Thomas Fröhlich and Daniel Edinger.

2.3. Stabilizing effect of C-R-C motifs on pDNA and siRNA polyplexes

Wu et al.¹⁰⁶ introduced twin disulfides C-X-C (cysteine-any-cysteine) for orthogonal disulfide pairing which led to the formation of stable dimers linked together by two disulfide bonds. As reduction of the disulfide bond of oligomers with twin disulfides was slower than of single cysteines, this motif might have a positive stabilizing effect on pDNA and siRNA polyplexes.

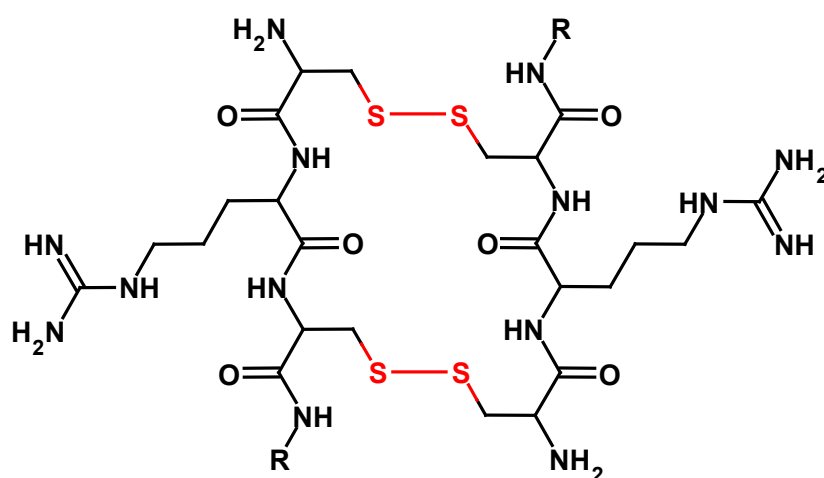


Figure 20: Orthogonal disulfide pairing between two oligomers with C-R-C motif¹⁰⁶.

2.3.1. Oligomer synthesis and structures

T-shape oligomers with cysteines in the periphery were chosen and further modified. Therefore, the cross-linking single cysteines were replaced by the C-R-C motifs which led to orthogonal disulfide pairing and directed folding as described by Wu et al.¹⁰⁶. All resulting oligomers had a constant number of protonable 1,2-diaminoethane motifs within the artificial amino acids providing electrostatic nucleic acid binding and endosomal buffering. Consequently, the resulting oligomers (sequences listed in Table 7) contain twin disulfide motifs in the periphery and dioleic acids, tyrosine trimers, or both as additional stabilizing components, either in the center, the periphery, or both.

Table 7: Selected oligomer sequences (*N*- to *C*-terminus) with twin disulfides and analogs with single cysteines.

Oligomer	Sequence	Analog
591	C-R-C-Stp ₂ -[K]K-Stp ₂ -C-R-C	413
592	C-R-C-Stp ₂ -[(OleA) ₂ -K]K-Stp ₂ -C-R-C	49
593	C-R-C-Stp ₂ -[(Y ₃) ₂ -K]K-Stp ₂ -C-R-C	468
594	C-R-C-Y ₃ -Stp ₂ -[K]K-Stp ₂ -Y ₃ -C-R-C	465
595	C-R-C-Y ₃ -Stp ₂ -[(OleA) ₂ -K]K-Stp ₂ -Y ₃ -C-R-C	454
596	C-R-C-Y ₃ -Stp ₂ -[(Y ₃) ₂ -K]K-Stp ₂ -Y ₃ -C-R-C	464

2.3.2. Biophysical characterization

Agarose gel shift assays were performed to assess siRNA or pDNA binding ability of C-R-C motif containing polyplexes (Figure 21A or B). With regard to siRNA polyplexes, the oligomer **591** with terminal C-R-C motif, but without oligotyrosines and fatty acids displayed the weakest siRNA binding ability, similar to oligomer **413** with single cysteines (Figure 7A). All other oligomers displayed complete siRNA binding at a N/P of 12, in contrast to the analogs with single cysteines (Figure 7A). These results show that the C-R-C motif is beneficial for siRNA binding compared to structures with terminal single cysteines and/or tyrosines. Stable siRNA polyplex formation is achieved by combining terminal C-R-C motifs and oligotyrosines, or a central modification with oligotyrosines or fatty acids.

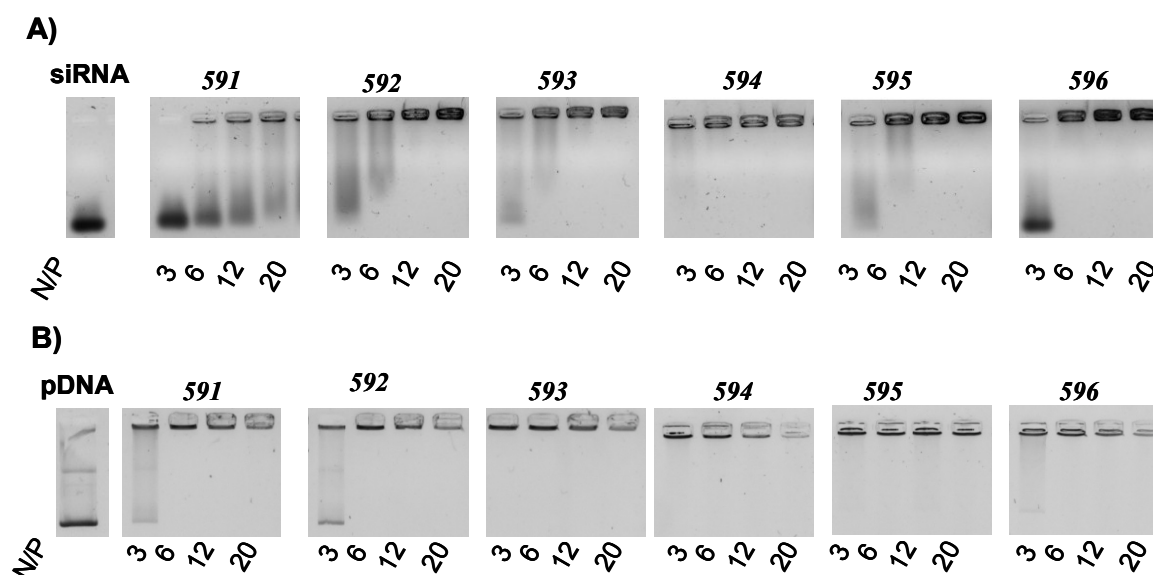


Figure 21: Nucleic acid binding ability of oligomers determined by agarose gel shift assay at different N/P ratios. Polyplex formation in HBG and 30 min incubation time. A) siRNA; B) pDNA.

Table 8: Particle size (Z-average) and zeta potential of polyplexes (N/P 12) formed in HEPES buffer determined with DLS. Polyplexes were diluted 1:20 before measurement. Variations refer to the median of three measurements of the same sample.

siRNA	Z-average [nm]	Zeta potential [mV]	DNA	Z-average [nm]	Zeta potential [mV]
591 polyplexes	n. d.*	n. d.*	591 polyplexes	285 ± 22	23.9 ± 0.5
592 polyplexes	672 ± 76	33.5 ± 0.9	592 polyplexes	121 ± 1	38.2 ± 1.2
593 polyplexes	160 ± 6	24.7 ± 0.9	593 polyplexes	105 ± 2	35.8 ± 0.4
594 polyplexes	197 ± 1	20.0 ± 1.2	594 polyplexes	188 ± 3	27.4 ± 1.3
595 polyplexes	162 ± 5	37.4 ± 1.4	595 polyplexes	100 ± 1	41.3 ± 1.2
596 polyplexes	192 ± 2	17.5 ± 0.6	596 polyplexes	115 ± 2	33.3 ± 0.8

*not detectable (no measurable signal).

In contrast, for pDNA, all twin disulfide containing oligomers showed complete binding at N/P > 3 independent of the additional stabilizing motifs (Figure 21B). All twin disulfide oligomers displayed therefore superior pDNA binding compared to oligomers with single cysteines (Figure 7B). In case of pDNA, stable polyplex formation was achieved with the help of twin disulfides.

For further characterization, particle size and zeta potential of polyplexes were analyzed with DLS (Table 8). No signal was measurable for siRNA polyplexes of oligomer **591** without central modification. Therefore, **519** polyplexes could not be analyzed just as their analogs **413**. Polyplexes of **592** were over 600 nm in diameter. Hence, the addition of the twin disulfides to the oligomer **49** led to a drastic increase in polyplex size. The size of all other siRNA polyplexes at N/P 12 was in a range applicable for further evaluations. Polyplexes of **593** formed particles with 160 nm in diameter, whereas siRNA particles of the single cysteine analog **468** could not be analyzed. Contrary to siRNA formulation, all oligomers formed polyplexes with pDNA with sizes between 100 and 300 nm.

The buffer capacity of the oligomers was investigated with the help of acidimetric back titration (Table 9). Therefore, the differential buffer capacities of the oligomers were determined between the endosomal pH of 5.5 and the physiological pH of 7.4. The buffer capacities of oligomers with single cysteines (Table 3) and twin disulfides were in the same order of magnitude.

Table 9: Buffer capacity of oligomers determined between pH 5.5 and 7.4 by acidification to pH 2 and back titration with NaOH.

Oligomer	Buffer capacity [%]
591	14.9
592	19.9
593	22.4
594	19.2
595	21.2
596	21.5

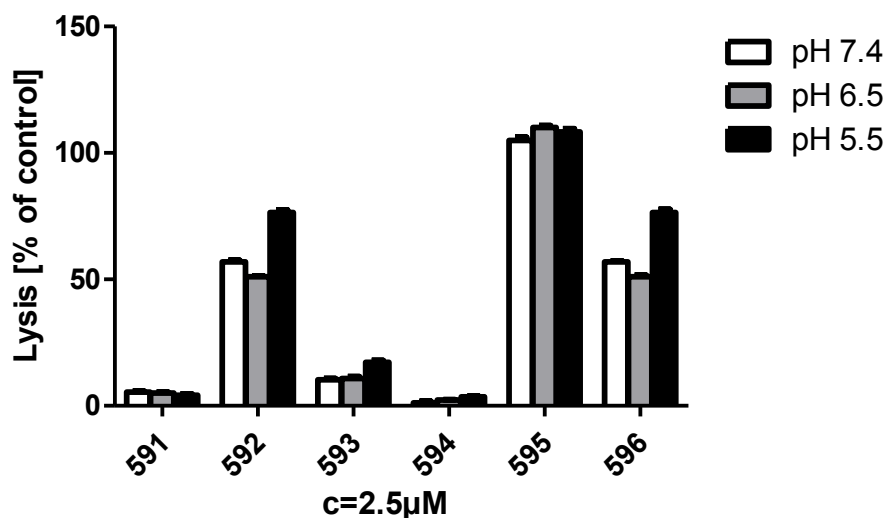


Figure 22: Erythrocyte leakage assay at different pH values. Erythrocytes were incubated with 2.5 μ M oligomer solutions at 37°C and the indicated pH values. Hemoglobin release was measured after 1 h.

Moreover, the pH-specific lytic potential of oligomers was investigated with the help of an erythrocyte leakage assay (Figure 22). Dioleic acid modified oligomers showed significant pH-specific lytic potential, whereas oligomers with twin disulfides or tyrosine containing oligomers without fatty acid modification did not mediate any significant lysis (Figure 22). The oligomer **596** was an exception to this rule. Combination of the C-R-C motif with terminal and central tyrosines led to significant lysis, even without fatty acid modifications. The oligomer **595** displayed the highest lytic activity due to the combination of terminal twin disulfides, oligotyrosines, and central fatty acids.

The endosomal escape of oligomers with fatty acids is therefore a combination of “proton sponge” effect and lytic activity. The additional arginines and cysteines in the oligomers with C-R-C motif did not influence buffer capacities.

2.3.3. Transfection efficiency

Nearly all tested polyplexes showed efficient pDNA transfection activity compared to buffer treated cells. Oligomers **593** and **596** with central oligotyrosine modification displayed the highest luciferase expression comparable to oligomer

464 and **468** without the twin disulfide modification (Figure 23A and Figure 10A). Oligomer **594** with a C-R-C motif showed equivalent pDNA transfection compared to oligomer **413** with only single cysteines. In contrast, gene transfer efficiency of oligomers **592**, **594** and **595** with the C-R-C motif was lower than for the structural analogs with single cysteines. Cell viability assay (Figure 24) did not reveal any cytotoxicity for all tested pDNA polyplexes.

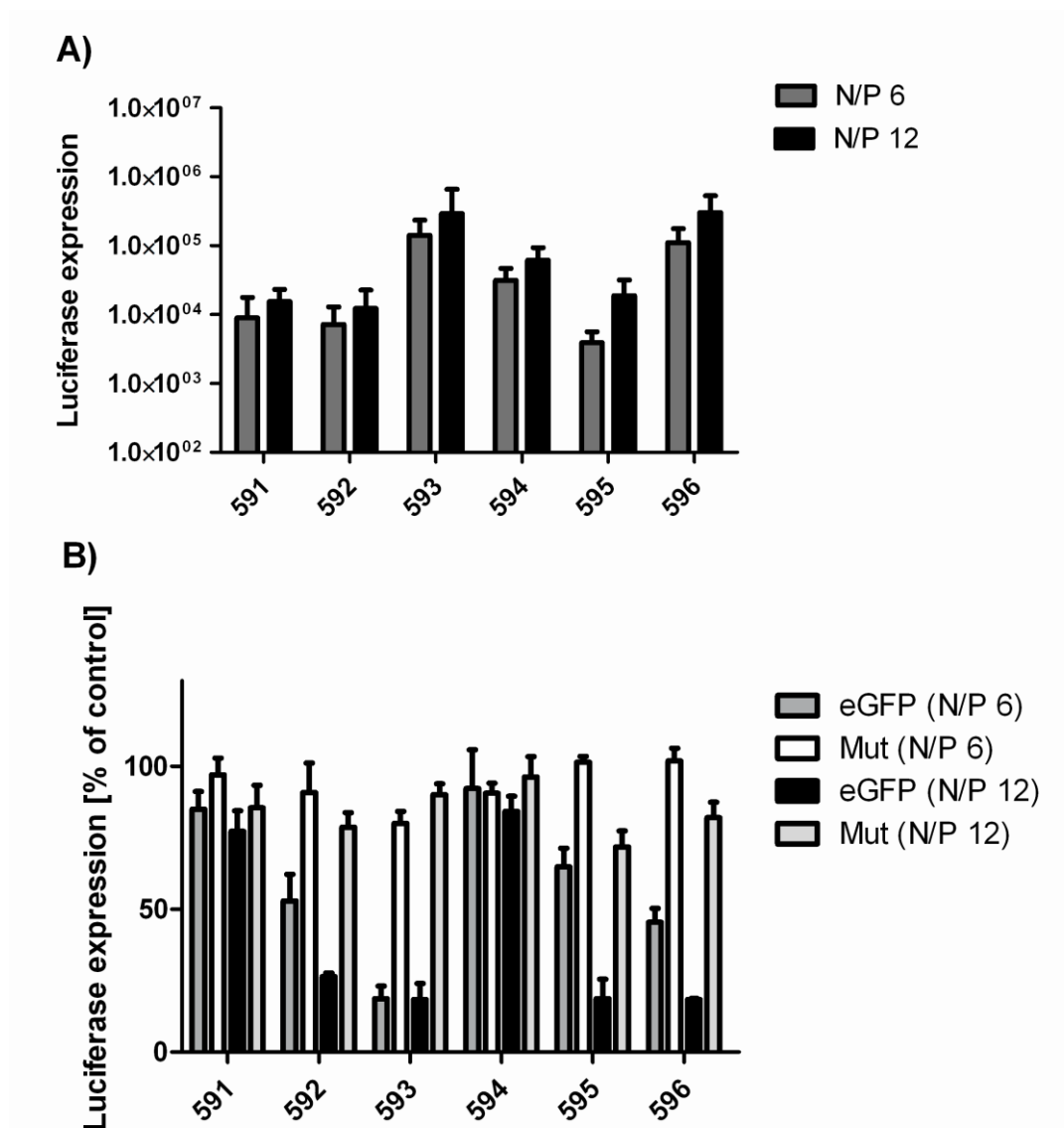


Figure 23: Gene transfer (A) and gene silencing (B) in neuroblastoma cells. Luciferase pDNA polyplexes were tested for luciferase expression in Neuro2A cells, eGFP-targeted siRNA (eGFP) or control siRNA (Mut) polyplexes for eGFPLuc gene silencing in Neuro2A-eGFPLuc cells, polyplexes were tested at N/P 6 and 12. Transfection experiments were performed by Petra Kos, Thomas Fröhlich and Daniel Edinger.

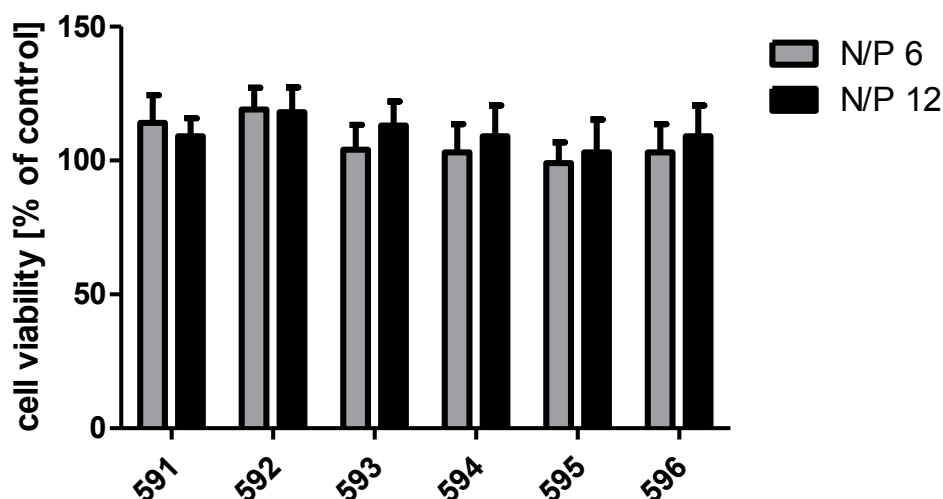


Figure 24: Metabolic activity of Neuro2A cells after transfection with pDNA polyplexes (N/P 6 and 12). MTT assay was performed by Petra Kos.

Regarding siRNA delivery, addition of twin disulfides did not increase target gene knockdown compared to siRNA polyplexes with single cysteine oligomers (Figure 23B and Figure 10B). In case of oligomer **594** polyplexes, silencing efficacy was even abolished. In summary, the new class of C-R-C motif containing oligomers was efficient in pDNA and siRNA transfection. Nevertheless, in most cases they were less efficient than oligomers with single cysteines.

2.3.4. Serum stability

For simulating in vivo conditions, siRNA polyplexes were analyzed for their stability in fetal bovine serum (FBS). Therefore, polyplexes were first formed in HEPES buffer, followed by the addition of FBS. The samples were incubated at room temperature or 37°C for 0, 10, 30 and 90 min. Afterwards gel electrophoresis was performed to investigate if the polyplexes were stable, partially stable or instable. Free siRNA migrates in the gel due to its negative charge, whereas intact polyplexes stay in the pockets of the agarose gel (Figure 25). Moreover, polyplexes were treated with 50 I.U. of heparin per sample after 90 min in order to dissociate polyplexes, and to investigate whether the siRNA was degraded by serum proteins.

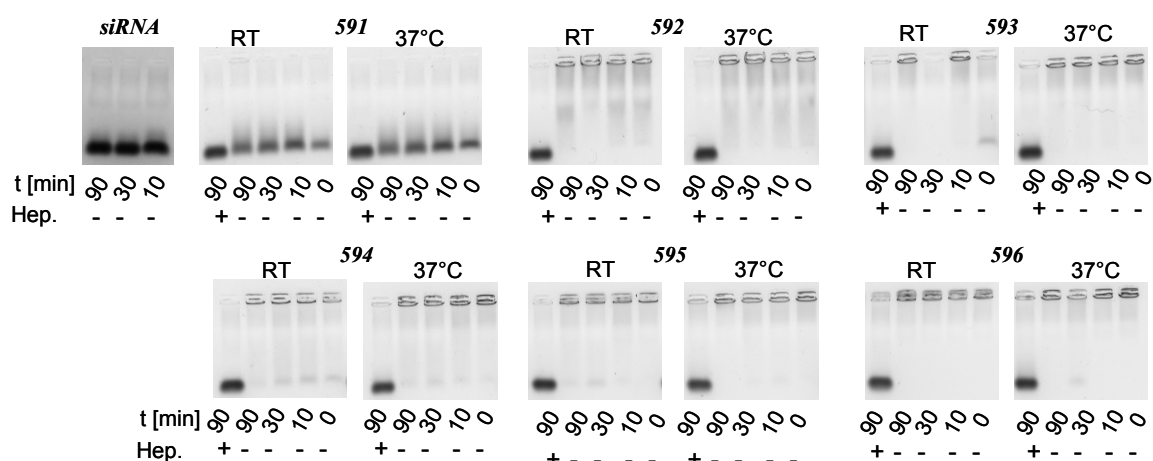


Figure 25: siRNA polyplex stability in 90% FBS at RT and 37°C at different time points. Polyplexes, formed with stabilized control siRNA, were incubated at room temperature for 30 min before FBS was added. Heparin (50 I.U.) was added to dissociate polyplexes.

After gel electrophoresis, siRNA migration was only observable for **591** polyplexes. As a result, **591** polyplexes dissociated, as a band at the free siRNA level appeared immediately after addition of serum. In contrast, all other polyplexes were stable in 90% FBS. This data showed that the twin disulfides led to a favorable stabilization and improved resistance to serum protein mediated disassembly, if compared with structures with single cysteines (Figure 12).

Consequently, the stability of polyplexes in serum was investigated with fluorescence correlation spectroscopy (FCS). Therefore, C-R-C motif containing siRNA polyplexes with particle sizes smaller than 300 nm were investigated. The limit was chosen due to the size of the confocal volume. Table 10 shows polyplex sizes in HEPES.

Table 10: Hydrodynamic radii (r), diffusion times, number of particles in the confocal volume, and fit χ^2 of polyplexes determined with FCS.

	r [nm]	Diffusion time [μ s]	Number of particles	fit χ^2
free siRNA	2.3	214.7	16.1	5.0E-08
593 polyplexes	75.7	6922.3	0.219	1.1E-03
594 polyplexes	161.6	14788.4	0.049	5.2E-02
595 polyplexes	40.0	3658.7	0.377	5.6E-04
596 polyplexes	55.9	5111.7	0.179	1.2E-03

In serum, all radii were viscosity corrected for data analysis. Addition of FBS led to a slight increase in siRNA polyplex size of 20-60 nm over time. The new C-R-C modified polyplexes displayed enhanced serum stability, as all polyplexes, except **591** polyplexes, were completely stable at 37°C for 90 min as determined with FCS measurements and gel shift assay. Single cysteine polymers of **454** and **464** were already completely stable in 90% FBS at 37°C for 90 min. As a result, an increase in stability for **595** and **596** polyplexes with twin disulfides could not be observed. In contrast, polyplexes of the analogs **49**, **468**, and **465** without C-R-C motif displayed lower serum stability. Data from FCS measurements and gel shift assay showed that **49** polyplexes were partially stable in serum (Figure 12 and Table 4). **468** siRNA polyplexes were not measurable with DLS, whereas **465** polyplexes had a diameter of over 1 μm (Table 2). Consequently, **468** and **465** polyplexes could not be analyzed with FCS due to the limited size of the confocal volume. Gel electrophoresis experiments displayed that **468** and **465** polyplexes were instable in serum. This data demonstrated the improved stability of the new oligomers with peripheral twin disulfides.

3. Comparison of four different particle sizing methods for siRNA polyplex characterization

The ability to reliably determine the size of siRNA polyplexes is the key to the rational design of particles and their formulation, as well as their safe application in vivo. Particle size data from literature is hardly comparable, if different methods have been used, due to the different underlying principles⁸⁸. Up to now, no standard technique is available, as the choice of methods largely depends on availability, application and required measurement.

Four analytical methods were evaluated for their suitability to analyze the characteristics of homogeneous and heterogeneous siRNA polyplexes: Dynamic light scattering (DLS), atomic force microscopy (AFM), nanoparticle trafficking analysis (NTA) and fluorescence correlation spectroscopy (FCS). Therefore, three siRNA polyplex compositions were used. The oligomers were precisely synthesized and consisted of hydrophobically modified oligoaminoamides.

3.1. Synthesis of oligomers

Three polycationic oligomers **49**, **332** and **279** (sequences listed in Table 11) with 1,2-diaminoethane subunits (Stp) were synthesized using solid phase assisted synthesis as described above^{55-56, 101}. Therefore, natural amino acids like cysteine (C), lysine (K), alanine (A) and tyrosine (Y) were combined with the unsaturated fatty acids oleic acid (OleA) or linoleic acid (LinA).

All oligomers had varying amounts of hydrophobic groups. The T-shape oligomer **49** had a dioleic acid motif (OleA) and cysteines, whereas in **332** the cysteines were replaced with oligotyrosine motifs. In U-shape **279** the dilinoleic acid (LinA) motif was added twice at the ends of the protonable backbone. These oligoaminoamides are able to bind negatively charged nucleic acids through electrostatic interactions. The fatty acids stabilize the so called polyplexes through hydrophobic interactions. In addition, cysteines form covalent disulfide bridges, whereas the oligotyrosine motif stabilizes through π - π stacking^{99, 107}. All polyplexes were prepared at N/P ratios of 12. The excess of polycation led to positively charged polyplexes, which are able to interact with the negatively charged cell membrane and therefore, endocytotic uptake into cells is possible. The formed polyplexes of the oligomers lead to efficient eGFPLuc silencing in stably transfected mouse neuroblastoma cells Neuro2A/eGFPLuc with low toxicity^{55-56, 108}.

Table 11: Sequences of the selected oligomers. The U-shape oligomer **279** was synthesized by Irene Martin.

Oligomer	Sequence
49	C-Stp ₂ -[(OleA) ₂ -K]K-Stp ₂ -C
332	Y ₃ -Stp ₂ -[(OleA) ₂ -K]K-Stp ₂ -Y ₃
279	A-[(LinA) ₂ K]K-Stp ₃ -[(LinA) ₂ -K]K-A

]K: Lysine with branching at α, ϵ -amino groups.

3.2. Dynamic laser light scattering

Dynamic light scattering is a technique for measuring particles in the nanometer region. DLS measures the Brownian motion and relates this to the hydrodynamic diameter of the particles, according to the Stokes-Einstein equation¹⁰⁹. Brownian motion is the random movement of particles in solution, which results from the bombardment of the particles with surrounding solvent molecules¹¹⁰. Smaller particles lead to faster Brownian motion and therefore, higher intensity fluctuations¹⁰⁹. The rate, at which the intensity of the scattered light fluctuates, is detected with suitable optical arrangements and converted into a correlation function. In a first step, intensity, volume and size distribution of the dynamic light scattering measurements of the three different siRNA polyplexes, formulated in HEPES buffer, were compared (Figure 26).

The DLS results of the **332** siRNA polyplexes showed only one peak in the intensity, number, and volume distribution (Figure 26B). Hence, the hydrodynamic diameters were in the same order of magnitude of ~ 150 nm, independently of the investigated distribution.

The intensity distribution of **49** polyplexes showed a small peak > 1 μm resulting in a high intensity mean and therefore, an irreproducible Z-average (Figure 26A and Table 12). In contrast, the diameter determined with volume or number distribution was significantly smaller. For the **279** polyplexes no correlation of the distributions was observable (Figure 26C).

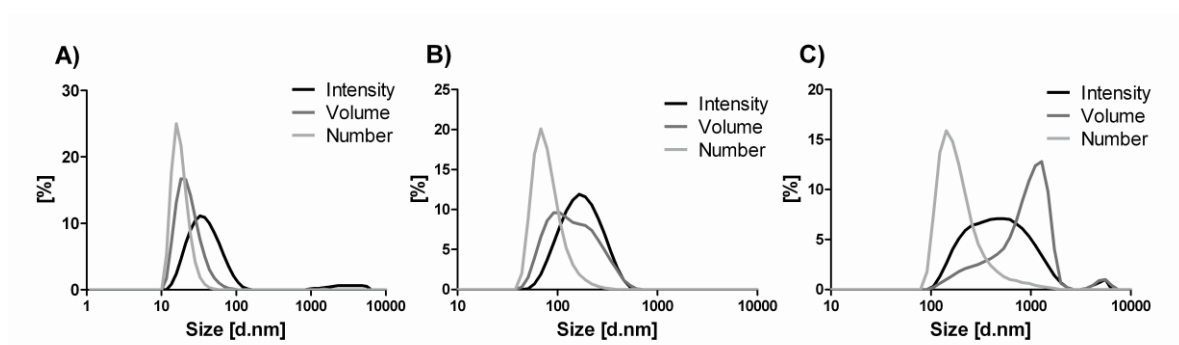


Figure 26: Particle size measurement of siRNA polyplexes with DLS in HEPES pH 7.4. Comparison of intensity, number, and volume distribution versus size distributions. A) **49**; B) **332**; C) **279** polyplexes.

All samples were prepared in 50 μL buffer to reach a siRNA concentration of 200 $\mu\text{g}/\text{mL}$. Before DLS measurement all samples were diluted 1:20, as a volume of ~ 1 mL was necessary for the accurate and reproducible size and zeta potential measurements in a folded capillary cell. For this reason, the influence of different dilution buffers was analyzed in order to find a most suitable buffer providing reliable results for all further measurements (Table 12). As high salt concentrations can lead to polyplex aggregation, we compared particle sizes in buffers with low salt concentration (20 mM HEPES, 10 mM NaCl) with particles in high salt concentrations (150 mM NaCl). Therefore, polyplexes were mixed in 20 mM HEPES, 10 mM NaCl or 150 mM NaCl and diluted after polyplex formation with the same buffer to 1 mL. The results of this experiment are displayed in Table 12.

Table 12: Influence of buffer on particle diameter determined with DLS. Variation of the median amongst three measurements of the same sample is shown, not the standard deviation.

	Z-average [nm]	Pdl	Intensity mean [nm]	Number mean [nm]	Volume mean [nm]	Zeta potential [mV]
49 polyplex						
20 mM HEPES	35.2 \pm 1.8*	0.28 \pm 0.05	275 \pm 123	18.0 \pm 0.5	34.4 \pm 6.3	20.8 \pm 0.6
10 mM NaCl	40.2 \pm 15	0.28 \pm 0.08	475 \pm 151	12.7 \pm 0.6	23.3 \pm 2.1	33.4 \pm 6.6
150 mM NaCl	46.4 \pm 0.2	0.22 \pm 0.02	345 \pm 66	16.6 \pm 1.0	32.1 \pm 3.2	-
332 polyplex						
20 mM HEPES	150 \pm 2.2	0.15 \pm 0.02	180 \pm 8.5	84.2 \pm 13	154 \pm 7.2	38.1 \pm 0.8
10 mM NaCl	125 \pm 0.8	0.20 \pm 0.01	192 \pm 31	66.6 \pm 3.9	187 \pm 63	48.6 \pm 1.4
150 mM NaCl	149 \pm 1.3	0.13 \pm 0.01	173 \pm 2.4	99.0 \pm 3.6	155 \pm 1.8	-
279 polyplex						
20 mM HEPES	414 \pm 11	0.31 \pm 0.02	668 \pm 8.2	239 \pm 15	1011 \pm 12	25.6 \pm 0.6
10 mM NaCl	579 \pm 89	0.56 \pm 0.04	609 \pm 185	51.3 \pm 27	468 \pm 71	44.5 \pm 0.7
150 mM NaCl	223 \pm 4.6	0.62 \pm 0.05	582 \pm 64	19.3 \pm 6.6	302 \pm 61	-

49 polyplexes showed a decreased number and volume mean diameter, when prepared and diluted in 10 mM NaCl, whereas intensity and Z-average mean diameter increased. As mentioned before, the intensity distribution of **49** polyplexes showed a small peak $> 1 \mu\text{m}$, resulting in a high intensity mean and therefore, an irreproducible Z-average. The size determined with number and volume distribution gave similar results in 20 mM HEPES and physiological NaCl concentration. **332** polyplexes gave constant sizes independent of the dilution buffer and the investigated distribution. As a result, **49** and **332** polyplexes were stable in physiological salt concentration, because no aggregation occurred. In contrast, for **279** polyplexes no correlation between buffers and distribution was observable. This effect might be due to the lipophilic character of those polyplexes. Zeta potential was lower in 20 mM HEPES as in 10 mM NaCl, independent of the polycation in the polyplex. Zeta potential in the physiological salt concentration of 150 mM NaCl could not be measured, as the high salt concentration shielded the electric charge of the polyplexes. Moreover, the voltage led to a corrosion of the electrodes.

In addition, the influence of glucose on particle measurements with DLS was investigated. The dilution with HBG led to the appearance of a glucose peak with a diameter of 1 nm in the volume and number distribution, due to the high glucose concentration of 5% (w/v) in the sample. Therefore, accurate analysis of the size of the polyplexes was not possible in HBG.

All salt containing buffers were suitable for data analysis, whereas glucose containing buffers hindered data analysis due to the appearance of a glucose peak and high salt concentrations obscured zeta potential measurements. Therefore, we performed all further measurements in 20 mM HEPES.

Additionally, the influence of the preparation buffer on particle size was investigated: The polyplexes were mixed in HEPES or HBG buffer and diluted with HEPES. It was discovered that the buffer, in which the samples were mixed, had no influence on size and zeta potential.

DLS was also applied to determine **49** and **332** polyplex stability in buffer over time. Stability was not analyzed for **279** polyplexes due to the inhomogeneous results gained with DLS. Therefore, **49** and **332** polyplexes were formed in 20 mM HEPES, incubated at room temperature for 30 min up to 21 days, and analyzed afterwards

with DLS. Both polyplexes were extremely stable over time and no aggregation was observable. Hence, particle size stayed constant in HEPES buffer over 3 weeks.

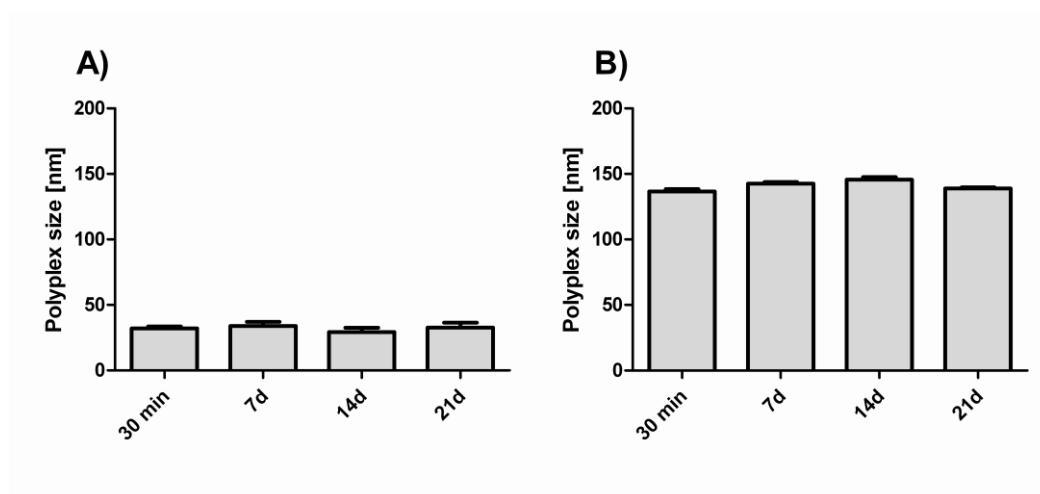


Figure 27: Polyplex stability in buffer at room temperature over time. A) Volume mean of **49** polyplexes; B) Z-average of **332** polyplexes.

3.3. Atomic force microscopy

Atomic force microscopy allows the visualization of particles with sub-nanometer resolution in three dimensions¹¹¹. The main element of the AFM is the sensor, a pyramidal tip attached to a 100-400 μm long cantilever, which is in contact with the sample¹¹². The highest resolution can be achieved with a tip that ends in a single atom. The simplest mode is the contact mode, where the tip is permanently in contact with the sample surface, causing the cantilever to deflect. This mode is limited to relatively firm samples¹¹³. The tapping AFM, also known as intermittent contact AFM was used, where the sample is exposed to minimized forces. Therefore, the contact of the tip and the sample lasts only for several nanoseconds and thus, the analysis of supple materials is possible, such as living cells, biomembranes or liposomes¹¹⁴. A piezoelectric crystal is oscillating and hence, exciting the cantilever. If the tip interacts with the sample at its low point, a damping of oscillation can be observed. The height of the AFM stage is adjusted to keep the damping at a constant rate. The tip scans across the sample and from the up and down movements of the AFM, the topography of the sample can be extracted. The cantilever is bending due to forces between tip and sample, when the tip is engaging a surface. This deflection, which is proportional to the force applied to the

sample (Hooke's law), is used to directly visualize a surface topography. The AFM pictures revealed individual nanoparticles for all formulations. The picture of **49** polyplexes displayed a large number of spherical polyplexes between 15 and 45 nm in diameter, which were homogeneous in size (Figure 28A). For **332** polyplexes the number of particles observed under the microscope was a lot smaller, in spite of a dilution of 1:50. The particles had a diameter of 120-170 nm (Figure 28B). Contrary, the AFM picture of **279** polyplexes showed a large number of small particles with a diameter of 80-110 nm (Figure 28C). In addition, particles up to 430 nm were observed, reflecting the heterogeneity of this polyplex sample.

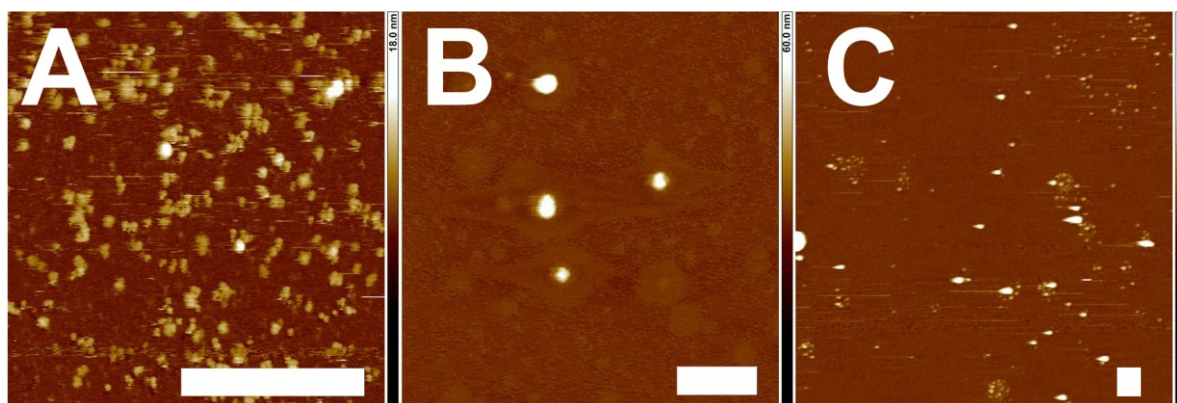


Figure 28: AFM pictures of siRNA polyplexes in HEPES pH 7.4. A) **49** polyplexes $d = 15\text{-}45$ nm; B) **332** polyplexes $d = 120\text{-}170$ nm; C) **279** polyplexes $d = 80\text{-}430$ nm. Scale bars represent 500 nm. These measurements were performed by Julia Kasper and Max Scheible.

3.4. Nanoparticle tracking analysis

Nanoparticle tracking analysis is based on a laser illuminating microscopic technique. Compared to DLS measurements, NTA does not measure the intensity of the scattered light. A laser excites particles suspended in a fluid, which then scatter light and hence, the particle position is determined under a microscope¹¹⁵. The Brownian motion of these illuminated particles is analyzed by a camera in real-time. The rate of the movement is related solely to the viscosity of the liquid, the temperature, and the size of the particles. Each particle is simultaneously, but separately visualized and tracked from frame to frame by particle tracking image analysis software¹¹⁶. The rate of the particle movement is related to a sphere

equivalent hydrodynamic diameter and calculated through a variation of the Stokes-Einstein equation. The lower size limit for the analysis with NTA is around 35 nm for particles with high refractive index, like gold nanoparticles. As a result, nanoparticle tracking analysis measurements were suitable for medium sized particles. **332** polyplexes displayed a mean diameter of 139 ± 47 nm, if settings with low threshold were used. The polyplex size did not change significantly, when settings with high threshold or the extended dynamic range mode was utilized. The standard deviation was the variation of the median amongst different measurements. The 3D plot of the relative intensity versus the particle size displayed one peak with two maxima (Figures 29A).

The resolution of the NTA was therefore higher than for the DLS. In contrast, polyplexes of **49** were too small to be tracked due to the size limit, independently of the settings. The calculated mean diameter of 155 ± 48 nm did not reflect reality. For **279** polyplexes, the mean diameter was 128 ± 35 nm. According to AFM measurement, the size of the main population was in this magnitude, whereas the few large particles could not be tracked, even if the threshold was at its maximum. Figure 29B shows the video frames of the tracked **332** polyplexes corresponding to the three dimensional graph (Figure 29A), which were followed in real-time by a camera. The polyplex size, hence their homogeneity or heterogeneity, and their scattering intensities could be observed.

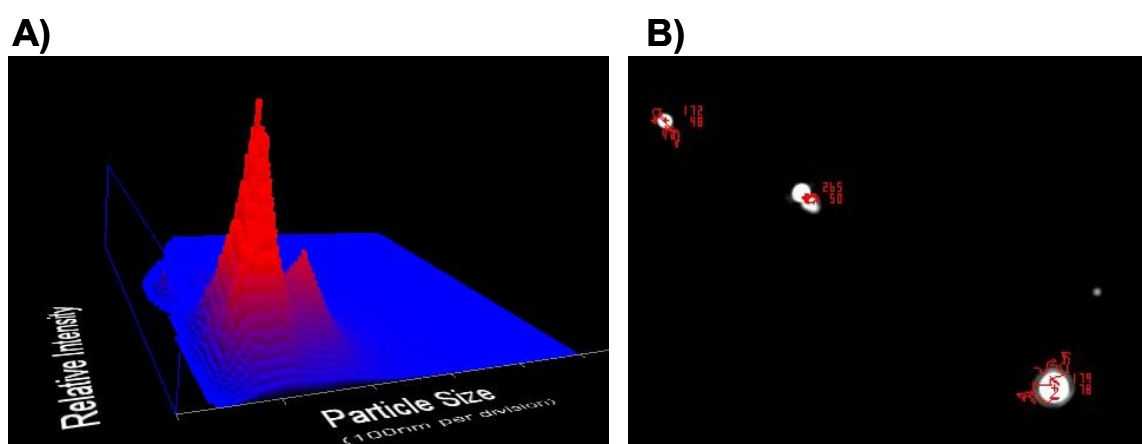


Figure 29: NTA of **332** polyplexes in HEPES pH 7.4. A) 3D plot of relative intensity versus particle size. B) Microscope pictures of tracked particles. This experiment was performed by Julia Kasper.

3.5. Fluorescence correlation spectroscopy

Fluorescent correlation spectroscopy is a technique that allows to measure spontaneous fluctuations of molecules in a small open volume, the so called confocal volume (< 1 fL)^{102, 117}. A confocal diaphragm (pinhole) on the image surface limits the passage of the fluorescent signal and enables the collection of light exclusively from the confocal volume. Fluorescently labeled molecules are excited entering the laser focus. The number of the fluorescent labeled molecules has to be low enough to assure that each one contributes substantially to the fluorescence signal. Emitted light is collected by the confocal detection optics in conjunction with an avalanche photodiode. Fluctuations in the recorded intensity signal either represent molecules entering, or leaving the detection volume¹¹⁸. The duration of the fluctuations is determined by the degree of mobility of the diffusing species and the size of the confocal volume. These molecules lead to characteristic time decays, depending on their diffusion constants due to Brownian motion. Hence, the higher the count rate, the smaller the particles. Search for self-similarities is done by autocorrelation, a mathematical method that compares intensities at different time points. The shape of the resulting autocorrelation function is determined by the underlying dynamic process. Hence, the autocorrelation function $G(t)$ gives information about two important parameters: i) The diffusion time of the particles, which is directly proportional to their size (hydrodynamic radius), and ii) the total number of particles contributing to the signal within the confocal volume (N)¹¹⁹⁻¹²⁰. Cy5-labeled siRNA was spiked with unlabeled siCtrl and then complexed with **49**, **332**, and **279** at a N/P ratio of 12. Relative correlation function curves $G(t)$ and fitting functions curves $G(t)$ fit are shown in Figure 30A.

For **49** and **332** polyplexes $G(t)$ and $G(t)$ fit overlap in a perfect match. In contrast, $G(t)$ of **279** polyplexes deviated visibly from $G(t)$ fit, indicating an imperfect fit, which could not be improved using a two or three component fit. Additionally, the signal of **49** polyplexes declined more rapidly than for **332** and **279** polyplexes resulting in a smaller diffusion time and thus, smaller particles.

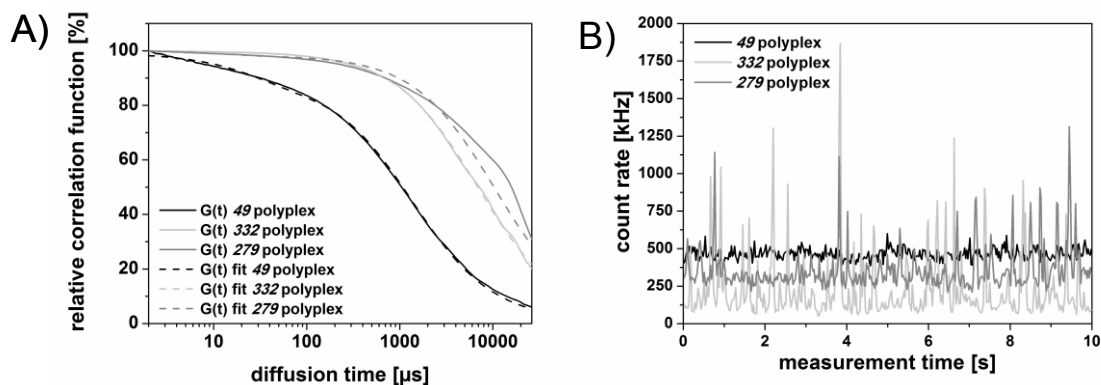


Figure 30: FCS measurement of all three polyplexes in HEPES. A) Relative correlation functions $G(t)$ and fitting functions $G(t)$ fit. B) Count rate of the polyplexes.

The count rate displayed sharp peaks for **332** and **279** polyplexes in the intensity fluctuations, indicating the presence of more than one labeled siRNA in the polyplex. In contrast, uniform count rates were observed for **49** polyplexes and therefore, only one labeled siRNA was present in the polyplex (Figure 30B). It is likely, that multiple unlabeled siRNAs were present in all polyplexes. Moreover, the values for the count rate were lower for **332** and **279** polyplexes, which was consistent with their hydrodynamic radii. The count rate was highest for **49** polyplexes, indicating smaller particles, compared to the above mentioned polyplexes.

Data analysis of all polyplexes resulted in hydrodynamic radii of 19.3, 95.8, and 147.5 nm for **49**, **332**, and **279** polyplexes, respectively (Table 13).

Table 13: Hydrodynamic radii (r), diffusion times, number of particles in the confocal volumes, and fit χ^2 of polyplexes determined with FCS.

	r [nm]	Diffusion time [μs]	Number of particles	fit χ^2
free siRNA	2.2	245.0	51.8	1.1E-08
49 polyplex	19.3	1371.0	3.8	4.0E-06
332 polyplex	95.8	6799.9	0.1	4.1E-04
279 polyplex	147.5	10473.9	0.5	6.2E-03

The size of free labeled siRNA was 2.2 nm. The number of particles decreased from 51.8 to < 4 , when polyplexes were measured. This decrease in N may be due to the influence of the polycation on the fluorescence properties of the siRNA. The chi-square (χ^2) test is a statistical hypothesis test used for testing the presence of autocorrelation and therefore, the lower the value, the better the fit. Fit χ^2 was highest for **279** polyplexes, which was consistent with the imperfect overlap of the $G(t)$ with $G(t)$ fit (Figure 30A). As a result, the few large particles in the **279** polyplexes affected FCS measurements, because those large particles were bigger than the confocal volume. Moreover, some polyplexes had a very high number of labeled siRNAs incorporated and therefore, the light intensity was higher than the detection limit. Consequently, measurement time was decreased to 5 s in order to minimize the probability of large particle entering the confocal volume.

In addition to particle size measurements, FCS made monitoring of the polyplex self-assembling process possible. Polyplexes were prepared in higher concentrations compared to all other FCS measurements, mixed directly in the eight well chamber slides, and analyzed after different time points. It was clearly visible that **332** polyplex formation was incomplete after 10 minutes (Figure 31B) due to the high deviation of $G(t)$ from $G(t)$ fit, even though the diffusion time was already at 7404 μs .

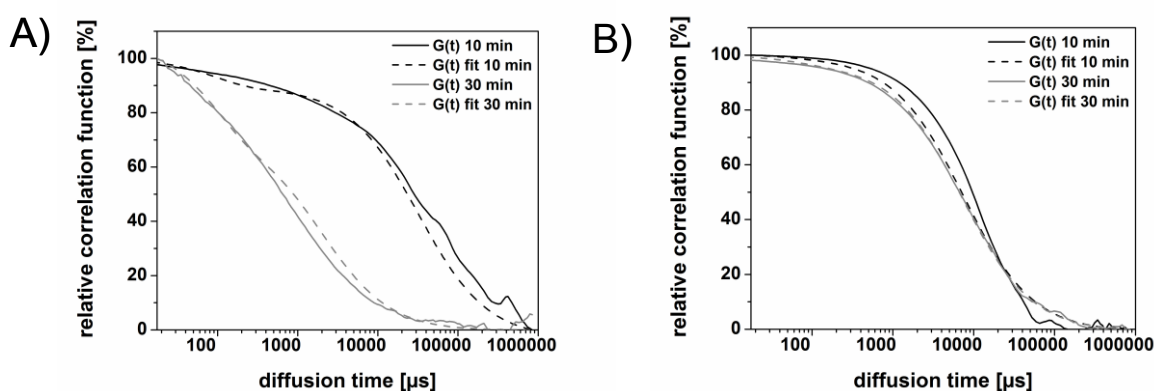


Figure 31: Polyplex self-assembly with FCS. Relative correlation functions $G(t)$ and fitting functions $G(t)$ fit of A) **49** polyplexes and B) **332** polyplexes after 10 and 30 min.

This diffusion time corresponded to a radius of 92 nm. In contrast, after 30 min the fitting of the correlation function resulted in a perfect overlay of $G(t)$ and $G(t)$ fit.

The effect of time on polyplex self-assembly was more drastic for **49** polyplexes: After 10 min the diffusion time of the polyplexes was ten fold higher than after 30 min of incubation, resulting in radii of 395 nm and 24.2 nm, respectively (Figure 31A). Moreover, the number of particles was 7.5, compared to 52.9 after 30 min. In addition, χ^2 fit was with $1.3E-05$ higher than after 30 min. Therefore, a fitting of **49** polyplexes was not possible after 10 min. Polyplex sizes did not vary, if analyzed after 60 min. These measurements proved that an incubation time of 30 min was sufficient for the self-assembly into polyplexes.

Using FCS, analysis both polyplex size and stability in full serum is possible. Polyplexes of **49** were formed in HEPES buffer prior to the dilution with a 40-fold volume of fetal bovine serum (FBS). Table 4 shows the polyplex stability in serum after different time points at room temperature and 37°C. All radii were viscosity corrected for data analysis. An increase in size was observed after addition of FBS due to the attachment of serum proteins to the polyplexes. **49** polyplexes were stable for 30 min at room temperature (Table 4). In contrast, a dissociation of those polyplexes was observed at 37°C already after 30 min. The count rate (number of particles in confocal volume) of the polyplexes increased slightly, indicating a partial release of labeled siRNA. With a two component fit, 6% of free siRNA was detected, which is consistent with the increase in particle number. After 90 min, a partial dissociation of the polyplexes was observed for both temperatures. Polyplexes were more stable at room temperature than at 37°C resulting in 66% and 18% intact polyplexes, respectively. The count rate shifted to higher values (18.0 at room temperature and 57.4 at 37°C) demonstrating a significant release of siRNA, well consistent with results of an agarose gel shift assay detecting free siRNA (Chapter 1.4). All FCS measurements in this section were performed together with Julia Kasper.

4. Native chemical ligation

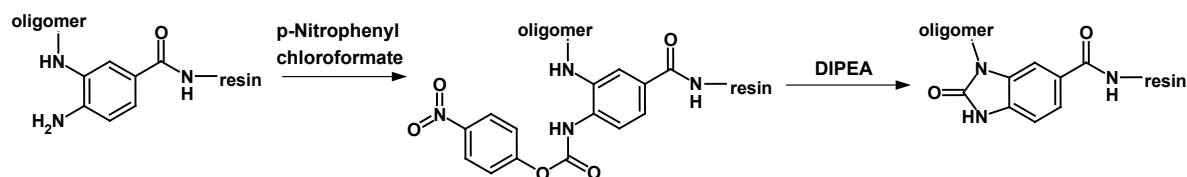
Protection of the carrier surface from interactions with blood components and off-target cells plays an important role in the choice of carrier system. The hydrophobic or charged surface of delivery systems can be shielded to avoid interactions with blood components during circulation. Polyethylene glycol (PEG) is the most prominent molecule used for shielding¹²¹⁻¹²³. An ideally stabilized and shielded particle should be able to circulate for an extended time without cell interaction. Therefore, interaction of a maximally shielded particle with its target is not possible. Consequently, an active targeting domain has to be incorporated into the structure of the carrier system to allow uptake and accumulation at the targeted site. As a result, receptor ligands or their analogs are integrated into the carrier structure in order to enable receptor specific interactions with the target site.

In the current thesis, native chemical ligation (NCL), a precise conjugation technique, is employed to connect existing non-targeted structures with shielding and targeting domains. NCL is a chemoselective chemistry that forms an amide bond by transthioesterification followed by intramolecular nucleophilic rearrangement between thioesters and cysteine⁷⁴. This simple reaction occurs in mild aqueous solution, and gives almost quantitative yields without side reactions with other functional groups⁷³. Since the first report by Dawson in 1994⁷², studies involving the use of NCL have focused on the total synthesis of proteins¹²⁴⁻¹²⁶. The application of the NCL reaction for other areas remains largely unexplored. Therefore, we investigated if NCL is a suitable technique to attach shielding and targeting domains to already existing oligomers of our library.

4.1. Principles of NCL

Blanco-Canosa et al.⁷³ published a chemical reaction which is compatible with reaction conditions used for solid phase peptide synthesis. Two prerequisites for the successful ligation were necessary: i) An oligomer with a *N*-terminal cysteine, and ii) an oligomer with a *C*-terminal, aromatic *N*-acylurea moiety. Therefore, 3,4-diaminobenzoic acid (Dbz) was attached to a MBHA Rink amide resin or a preloaded Dawson Dbz AM resin was used. The Dbz-group was stable at standard Fmoc SPPS coupling and deprotection protocols. After oligomer elongation, the

Dbz-group was converted into *N*-acyl-benzimidazolinone (Nbz) with the help of *p*-nitrophenyl chloroformate (Scheme 4).



Scheme 4: Conversion of a Dbz peptide on the resin to a Nbz peptide with the help of *p*-nitrophenyl chloroformate.

4.1.1. Synthesis of model oligomers for NCL

Two activated model oligomers Fola-PEG₂-Nbz and the non-targeted A-PEG₂-Nbz were synthesized to prove suitability of the method for the attachment of a shielding and targeting domain to a polycation. Therefore, a defined PEG₂ with two ethylene oxide monomer units was attached to the deprotected Dbz Dawson resin. After successful coupling, the Fmoc protection group of PEG₂ was removed. As last coupling step either Boc-Ala-OH, or protected folic acid synthesized by means of convergent synthesis were coupled. Afterwards the Dbz was converted into the Nbz group with *p*-nitrophenyl chloroformate and the resin was washed twice with DIPEA in DMF (Scheme 4). The products were cleaved of the resin and all protection groups were removed by treating the resin with triisopropylsilane, DCM, water, and TFA. Afterwards, the raw products were precipitated in cooled *n*-hexane and ether. After centrifugation, the Nbz-PEG₂-A peptide was purified with size exclusion chromatography. NMR (page 112) and FAB mass analysis proved the purity and identity of the model structure A-PEG₂-Nbz. The purification of Fola-PEG₂-Nbz with SEC was not possible due to the poor solubility in water and acetonitrile. Consequently, it was applied for NCL without further purification (NMR page 112).

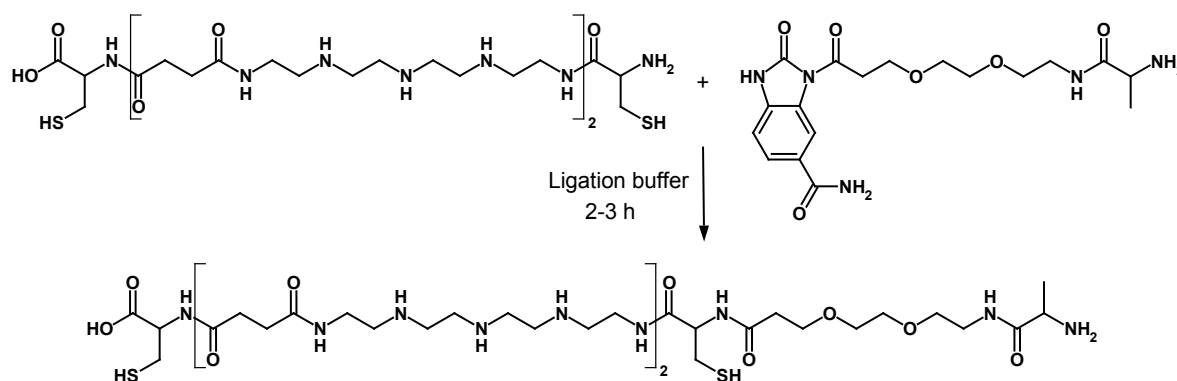
Moreover, the polycation C-Stp₂-C with a *N*-terminal cysteine was synthesized with standard SPPS procedures on a chlorotriyl chloride resin preloaded with Fmoc-Cys(trt)-OH. NMR (page 111) and FAB mass analysis proved the purity and identity of this small oligocation.

Table 14: Solid phase assisted peptide synthesis based model oligomers for native chemical ligation. Mass was determined with FAB analysis.

Sequence	Formula	Calculated mass	Detected mass
		[M+H] ⁺	[M+H] ⁺
Nbz-PEG ₂ -A	C ₁₈ H ₂₅ N ₅ O ₆	408.1	408.4
C-Stp ₂ -C	C ₃₀ H ₆₂ N ₁₂ O ₇ S ₂	767.4	767.6

4.1.2. Ligation of model oligomers

After purification and lyophilization of oligomers C-Stp₂-C and A-PEG₂-Nbz, native chemical ligation was performed (Scheme 5). The educts (molar ratio of A-PEG₂-Nbz to polycation C-Stp₂-C = 1 : 1.3) were solved in ligation buffer containing guanidine hydrochloride, disodium hydrogen phosphate, TCEP*HCl and 4-mercaptophenylacetic acid. After a ligation time of 2-3 h, the products were purified with size exclusion. Simultaneously, the buffer salts were removed. Native chemical ligation of the unpurified FoIA-PEG₂-Nbz with C-Stp₂-C was performed accordingly.



Scheme 5: Native chemical ligation of the activated model oligomer A-PEG₂-Nbz and the polycation C-Stp₂-C.

After lyophilization, the products were analyzed with NMR and MALDI-TOF mass spectrometry. Mass spectra (Table 15) and NMR (page 112) proved the expected identity of the two products.

Table 15: Native chemical ligation of model oligomers. Mass was determined with MALDI-TOF analysis.

Sequence	Formula	Calculated mass	Detected mass
A-PEG ₂ -C-Stp ₂ -C	C40H80N14O11S2	997.3	997.4
FoIA-PEG ₂ -C-Stp ₂ -C	C56H92N20O15S2	1349.6	1349.2

4.2. Synthesis of shielded and targeted oligomers for NCL

Different targeting ligands like folic acid (FoIA), B6, GE11 and cMBP were coupled on a MBHA rink amide resin preloaded with Dbz-Gly-Fmoc to a defined PEG₂₄ as previously described. Those ligands target the folic acid receptor, transferrin receptor, EGF receptor, and hepatocyte growth factor, respectively. After oligomer elongation, the Dbz-group was converted into Nbz and the oligomer was cleaved off the resin. The resulting activated oligomeric structures FoIA-PEG₂₄-G-Nbz, B6-PEG₂₄-G-Nbz, GE11-PEG₂₄-G-Nbz and cMBP-PEG₂₄-G-Nbz and the control A-PEG₂₄-G-Nbz (Table 16) are now available for coupling by means of native chemical ligation to oligomers with *N*-terminal cysteines out of the existing library of over 600 structures.

Table 16: Solid phase assisted peptide synthesis based shielded and targeted oligomers for native chemical ligation. Mass was determined with ESI analysis.

Sequence	Formula	Calculated mass	Detected mass [M+H] ⁺	z
FoIA-PEG ₂₄ -G-Nbz	C80H128N12O33	1785.9	894.4	2
B6-PEG ₂₄ -G-Nbz	C103H184N22O37	2322.7	775.5	3
GE11-PEG ₂₄ -G-Nbz	C136H206N22O46	2885.2	1443.7	2
cMBP-PEG ₂₄ -G-Nbz	C125H207N31O44	2848.1	950.5	3
A-PEG ₂₄ -G-Nbz	C64H116N6O29	1433.6	1433.8	1

IV. DISCUSSION

1. Stabilizing effects of tyrosine trimers on pDNA and siRNA polyplexes

For efficient nucleic acid delivery in vitro and in vivo certain bottlenecks have to be mastered. The negative charge of the cell membrane hinders the uptake of negatively charged nucleic acids due to charge repulsion. Therefore, polycationic carriers are commonly used to bind the nucleic acids forming polyplexes with positive surface charge. For nucleic acid binding, at least four 1,2-diaminoethane units were incorporated in the oligomer structure. The primary and secondary amines are partially protonated under physiological conditions and therefore, are able to bind nucleic acids by means of electrostatic interactions. The uptake into the cells is then mediated through endocytosis. As a result, a correlation between zeta potential and uptake was seen: The higher the zeta potential the better the uptake. Aggregates, like in the case of oligomer **468** polyplexes, led to an increased uptake and hence, transfection efficacy in vitro, but were unsuitable for in vivo use, because clogging of capillaries must be prevented⁸⁵. As the next bottleneck, the payload has to be released out of the endosomes. The endosomal escape is mediated through the endosomal buffering by the phenolic groups in the aromatic amino acid tyrosine⁹⁷ and/or the endosomolytic activity of unsaturated fatty acids⁵⁶.

Stabilization of polyplexes plays an important role for the successful delivery of nucleic acids in vitro and especially in vivo. Hence, certain prerequisites to ensure polyplex stabilization were incorporated in the oligomer structures: i) The hydrophobic dioleic acid motif, ii) cysteines, and iii) the oligotyrosine motif. Each component resulted in a different principle of stabilization: i) Hydrophobic interactions, ii) disulfide bridges, or iii) π - π stacking⁹⁹. To ensure polyplex stability cysteines, a dioleic acid motif, an oligotyrosine modification, or a combination of these were integrated in the oligomer structure in the center, the periphery, or both. Oligomers modified with solely tyrosines (**333**, **589**) were less efficient in binding nucleic acid and displayed a decreased transfection efficiency. All other oligomers, except the controls, increased luciferase expression > 100-fold after pDNA transfection and showed efficient target gene silencing with siRNA. Therefore, we

can conclude that efficient nucleic acid transfer requires the combination of two different stabilizing components.

The stability of polyplexes in 90% serum was analyzed by gel electrophoresis, demonstrating favorable stability of our new oligotyrosine based oligomers. For a more precise determination of intact polyplexes after several incubation times in 90% serum, we used fluorescence correlation spectroscopy (FCS) for the quantification of both free siRNA and intact polyplexes¹¹⁸. The size limit of the confocal volume hindered FCS measurements of siRNA polyplexes > 300 nm¹⁰². Comparing gel-shift and FCS data generated a sequence of stability for the differently modified siRNA polyplexes as follows: **49** < **332** < **454**, **464**, **589**. Accordingly, oligomers with lateral oligotyrosines formed more stable polyplexes in comparison with structures with terminal cysteines. Nevertheless, oligomers combining oligotyrosines and cysteines in the periphery displayed superior polyplex stability.

On account of these beneficial properties, experiments were performed to evaluate the in vivo distribution of Cy7-labeled siRNA by the various polyplexes. Some oligomers quenched the fluorescent signal of the Cy7-labeled siRNA, making an in vivo comparison of these oligomer polyplexes impossible due to detection reasons. Even though, the oligomers quenched the signal, no signal of Cy7-labeled siRNA was observed in the kidneys or the bladder. This allows the conclusion that the polyplexes were still intact and hence, no dissociation took place. In contrast, the distribution of polyplexes of oligomers **49**, **332**, and **454** could be detected, revealing a prolonged presence of siRNA in tissues for all polymers compared to free siRNA and control oligomers. NIR fluorescence imaging revealed short circulation times followed by a fast renal clearance¹²⁷⁻¹²⁸ for free siRNA with a hydrodynamic radius of approximately 2.3 nm and for control polyplexes. As the sizes of our control polyplexes were larger than the renal filtration limit of 6 nm in diameter, dissociation must have occurred before elimination through the kidneys. The hydrophobic modification of **49**, **332**, and **454** polyplexes led to an accumulation in the liver¹²⁹. However, a fluorescence signal could be detected in the whole mouse for several hours. Circulation times of polyplexes with oligomers **332** and **454** were longer than with **49**, revealing the higher stability of these polyplexes consistent with the in vitro experiments. As a result, high serum stability is beneficial for polyplex distribution, but oligomer characteristics, like

hydrophobicity, also play an important role. The addition of oligotyrosines resulted in the design of more stable oligomers showing a superior in vivo distribution.

In accordance to the stability and favorable biocharacteristics of **332** polyplexes, siRNA transfer efficacy in vivo was examined. The **49** polyplexes were applied as controls⁵⁵. As the current polyplex versions lacked any targeting or shielding domains, intratumoral delivery of therapeutic RAN siRNA¹³⁰ or control siRNA polyplexes was performed, with administration into Neuro2A tumor bearing NMRI mice twice a week. In a former experiment, we showed that tumor growth of animals treated with **49** siRNA polyplexes was significantly reduced when animals were treated more frequently (3 times a week)⁵⁵. In the current study, the intratumoral injections were diminished to only twice a week. With this new application regime, **49** polyplexes did no longer reduce tumor growth significantly compared to animals treated with control siRNA. In contrast, the treatment with **332** RAN siRNA polyplexes reduced the tumor volume significantly from day 14 onwards. These data show the efficacy of oligomer **332** in the i.t. treatment of Neuro2A tumor bearing mice.

2. Further stabilizing motifs for pDNA and siRNA polyplexes

Certain prerequisites have to be fulfilled for efficient nucleic acid delivery in vitro and in vivo: Size, stability, transfection efficacy and negligible toxicity of the carrier systems. In order to increase stability of the polyplexes, various stabilizing motifs were incorporated into the oligomer structure: i) Ureido-pyrimidinone motifs, ii) 3-pyridyl isothiocyanate motifs, and iii) C-R-C motifs. Each component was considered to result in a different principle of stabilization: i) Hydrogen bond formation, ii) π - π stacking⁹⁹, and iii) disulfide bridges, respectively.

Dankers et al.¹⁰⁴ introduced ureido-pyrimidinones (ICH-CAMP motif) which led to the formation of non-covalent hydrogen bonds between two monomers. This concept was used for the stabilization of our T-shaped polyplexes. In order to attach ureido-pyrimidinones at the *N*-terminus on solid phase, a new synthesis strategy was invented: 'Reverse synthesis'. The ureido-pyrimidinone modified oligomer **408** and its analog **407** showed comparable luciferase expression. Even

though, siRNA gene silencing was slightly increased by the ICH-CAMP motif, the effect was less pronounced as for analogs with cysteine modification⁵⁶. siRNA binding ability was decreased by the ureido pyrimidinone modification. The ureido pyrimidinones did not have the desired effect on transfection efficiency and even displayed decreased nucleic acid binding. A possible explanation for the loss in binding ability is the fact that the dominating content of body fluids is body water and water itself forms hydrogen bonds. Ureido pyrimidinones also form hydrogen bonds. In the presence of water, the ureido pyrimidinone monomers interact with water and do not form hydrogen bonds with other ICH-CAMP monomers. Consequently, the specificity was insufficient to ensure stability in aqueous solution. As a result, this approach was not further pursued.

Creusat et al.¹⁰⁵ introduced pyridyl thiourea grafted 25 kDa polyethylenimine which led to effective siRNA-mediated gene silencing in vitro and in vivo. However, the incorporation of 3-pyridyl isothiocyanate motifs into our T-shape structure led to a complete loss of gene silencing compared to polyplexes with cysteine motifs. The transfection efficiency was comparable to the control T-shape **216** with alanine instead of cysteines⁵⁵. The π - π interactions of the pyridyl isothiocyanate monomers are insufficient for polyplex stabilization. This is in accordance with the finding that linear oligomer structures with single tyrosine modification did not show any siRNA silencing compared to structures with six tyrosines. As a result, at least six tyrosines were introduced in our structures divided in tyrosine motifs with three consecutive tyrosines. The use of a pyridyl isothiocyanate trimer might increase transfection efficiency. However, attachment of three consecutive 3-pyridyl isothiocyanate is impossible due to its structure. As a result, this approach to increase target gene knockdown and polyplex stability was not further pursued.

Wu et al.¹⁰⁶ introduced twin disulfides C-X-C (cysteine-any-cysteine) for orthogonal disulfide pairing which led to the formation of stable dimers linked together by two disulfide bonds. Employing this strategy for our purposes, polycationic oligomers with twin disulfides were used to form positively charged polyplexes with enhanced stability. T-shape oligomers with four 1,2-diaminoethane units incorporated in the oligomer structure were modified with the C-R-C motif.

siRNA polyplexes of oligomer **591** could not be analyzed and **592** polyplexes formed aggregates and hence, were unsuitable for in vivo use, because clogging of capillaries must be prevented⁸⁵. The release of the payload out of the endosome is

another crucial delivery step. The endosomal buffer capacity was not increased by the additional cysteines and arginines in the twin disulfide modification, because buffer capacities were comparable to analogs with single cysteines. As a result, only the phenolic groups in the aromatic amino acid tyrosine⁹⁷ and/or the endosomolytic activity of unsaturated fatty acids⁵⁶ mediated endosomal escape.

Oligomers modified with the twin disulfides and either an oligotyrosine or a dioleic acid motif showed good siRNA binding. Oligomer **591** with solely the C-R-C motif did not show complete siRNA binding, comparable to its analog **413** with single cysteines. In contrast, all oligomers displayed complete pDNA binding at N/P > 3 and therefore, increased luciferase expression > 50-fold after pDNA transfection, although the absolute transfection levels were still moderate. Oligomers without central modification (**591** and **594**) did not lead to efficient target gene silencing with siRNA. Therefore, we can conclude that efficient nucleic acid transfer requires, in the case of twin disulfide modified oligomers, the combination of at least one central and one peripheral stabilizing component. siRNA as well as pDNA binding was increased by the twin disulfide modification when compared to analogs with single cysteine modification. This higher nucleic binding ability might be advantageous for in vivo application.

The stability of polyplexes in 90% serum was analyzed by gel electrophoresis demonstrating favorable stability of our new twin disulfide based oligomers. Especially **592**, **593**, and **594** polyplexes showed increased serum stability in the gel shifts compared to polyplexes containing single cysteines analogues **49**, **468**, and **465**. For a more precise determination of intact polyplexes in 90% serum, we used fluorescence correlation spectroscopy (FCS) for the quantification of both free siRNA and intact C-R-C motif containing polyplexes⁸⁵. Particles of oligomer **592** were larger than the confocal volume and therefore analysis with FCS was not possible. All other oligomers with twin disulfides formed more stable polyplexes in comparison to structures with single cysteines.

First in vitro siRNA delivery experiments did not result in enhanced gene silencing. The beneficial stability properties however encourage further in vitro transfection and possibly in vivo experiments in the future.

3. Comparison of four different particle sizing methods for siRNA polyplex characterization

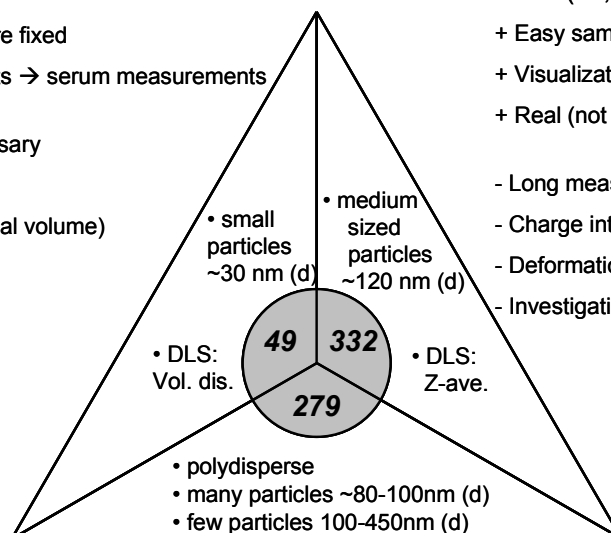
An appropriate method for the physico-chemical characterization of siRNA polyplexes should be found. Therefore, four different analytical methods were evaluated and each one used different parameters for size determination: DLS converted the fluctuations of the scattered light into a correlation function. Therefore, particles movements through Brownian motion are related to the hydrodynamic diameter according to the Stokes-Einstein equation¹⁰⁹⁻¹¹⁰. With NTA illuminated particles under a microscope are tracked¹¹⁵. The particles scatter light, which is captured by a real-time camera¹¹⁶. Both methods determined the hydrodynamic diameter of the polyplexes. In contrast, AFM visualized the particles with the help of a cantilever tip^{112, 114}. The topography of the sample was scanned and hence, the diameter of the particles was determined¹¹³. FCS measured spontaneous fluctuation of fluorescent molecules, which occurred in the confocal volume due to Brownian motion of the polyplexes. The autocorrelation function held information about the diffusion time and hence, the hydrodynamic radius¹¹⁹⁻¹²⁰. Understanding the principles that stand behind each method was essential for the data evaluation. For instance, the intensity of the scattered light of big particles hindered the simultaneous analysis of small particles with DLS, if intensity distribution, Pdl, or Z-average were investigated. The intensity of the scattered light of the particles is directly proportional to the diameter by the power of 6 in the Rayleigh approximation and therefore, the contribution of the total scattered light by small particles is insignificant in the presence of big particles¹³¹. The Mie theory is used to convert the intensity distribution into the volume distribution¹³². If the intensity peak shows more than one peak, or a tail, the conversion into the volume distribution will give a more realistic view of the importance of the second peak or the tail. For example, if there are two populations of spherical particles present in equal numbers, which differ in size more than the factor 3, the number distribution will show two peaks of a 1:1 (smaller : bigger particle) ratio. If the number distribution is converted into the volume distribution, the peaks would change to a ration of 1:1000. The intensity of scattering is proportional to d^6 and therefore, the ratio between the two peaks would change to $1:10^6$, if it was further converted into the intensity distribution. In general, it can be observed that $d(\text{intensity}) > d(\text{volume}) > d(\text{number})$.

FCS (49, 332)

- + Fast when settings are fixed
- + No background effects → serum measurements
- Labeled siRNA necessary
- Critical data fitting
- Size limitation (confocal volume)

AFM (49, 332, 279)

- + Easy sample preparation
- + Visualization and 3D profile
- + Real (not hydrodynamic) size
- Long measurement times
- Charge interaction with sample holder
- Deformation via cantilever tip
- Investigation of small section of sample

**NTA (332)**

- + Easy sample preparation, but high dilution required
- + Better resolution, information on concentration
- + Indirect visualization
- Results depend on settings and operator
- No parallel tracking of small and large particles

DLS (49, 332, 279)

- + Easy sample preparation
- + Fast
- Results depend on used fitting function

Figure 32: Polyplex sizes and comparison of different methods.

All methods had their advantages and disadvantages (Figure 32): Sample preparation was easy and fast for DLS, NTA, and AFM, whereas for FCS at least one fluorescently labeled compound was necessary. DLS was the most user-friendly method, which yielded consistent results in a relative short period of time. However, the results depended on the distributions used for data analysis. An overview of the results, obtained with the four different methods, is given in Table 17.

Table 17: Comparison of polyplex diameters obtained with DLS, AFM, FCS, and NTA. N.m. = number mean; V.m. = volume mean; Z-ave = Z-average; ZP = zeta potential; d = diameter; Mean = mean diameter. Variation of the median amongst 3 measurements of the same sample is shown, not the standard deviation.

Polyplex	DLS	AFM	FCS	NTA
49	N.m.: 18.1 ± 0.5 nm V.m.: 34.4 ± 6.3 nm ZP: 20.8 ± 0.6 mV	15-45 nm	38.6 nm	Mean: 155 ± 48 nm
332	Z-ave: 150.3 ± 2.2 nm ZP: 38.1 ± 0.8 mV	120-170 nm	191.6 nm	Mean: 139 ± 47 nm
279	Z-ave: 414.0 ± 11.1 nm ZP: 25.6 ± 0.6 mV	~80-100 nm and ≤ 430 nm	295.0 nm	Mean: 128 ± 35 nm

DLS measurements enabled the determination of the zeta potential of the polyplexes. Only positively charged polyplexes were taken up through endocytosis due to the negative charge of the cell membrane. DLS measurements were used to find a suitable dilution buffer to obtain reliable results for all further measurements as measurement times were short, especially when compared to AFM. All salt containing buffers were found suitable for data analysis, whereas glucose containing buffers hindered data analysis due to the appearance of a glucose peak at approximately 1 nm, and high salt concentrations obscured zeta potential measurements. Therefore, all further measurements were performed in 20 mM HEPES. Whereas, the measurements with DLS were fast and straightforward, NTA required several optimization steps and the results depended on the operator and the settings by a large extent. Contrary to DLS, the small **49** polyplexes could not be tracked and analyzed with NTA due to the detection limit of around 35 nm. This limit applied only for samples with high refractive index (e.g. gold nanoparticles). Moreover, the simultaneous analysis of small and large polyplexes was not possible even with high threshold settings or with the extended dynamic range mode. Contrary to DLS, NTA enabled indirect sample visualization and provided approximate particle concentrations. Both techniques showed good sizing and narrow distributions for the homogeneous, medium sized **332** polyplexes, whereas NTA had a higher resolution: One peak with two maxima was observed for **332** polyplexes with NTA, whereas DLS showed only one peak independently of the

distributions. AFM was another method that allowed sample visualization and gave additionally a three dimensional profile of the sample. Contrary to all other methods, the real, and not the hydrodynamic, size of the polyplexes was determined. Long measurement times, charge interactions of the probe with the sample holder, as well as deformation of the sample through the cantilever tip were disadvantages of AFM. Moreover, only a small section of the sample was investigated and therefore, this section might not be representative for the whole sample. FCS is the only method, whereby particle measurements in full serum were possible. No background effects, like light scattering by serum proteins, hindered the analysis, as only the labeled component is being analyzed, in contrast to DLS and NTA measurements. Moreover, AFM measurements in serum were not possible due to the long measurement times for each sample and therefore, dissociation of the polyplexes. After fixing the settings needed for the calibration of the device, the size measurements with FCS were as fast as with DLS. Similar to NTA, data analysis depended on the operators and their expertise.

DLS, AFM and FCS were suitable methods to determine the size of homogeneous particles, such as the polyplexes with T-shape oligomers **49** and **332**. DLS measurements displayed small peak $> 1 \mu\text{m}$ in the intensity distribution of **49** polyplexes. Therefore, the intensity mean, Z-average and polydispersity index had to be evaluated with care, whereas the number and volume distribution reflected a more realistic particle size. Moreover, the dilution buffer influenced the results of the DLS particle size and zeta potential measurements. Especially sugar containing buffers, like HBG, led to the appearance of a glucose peak of $\sim 1 \text{ nm}$ due to the high sugar concentration of 5% (w/v). Similar results were reported in literature. For example, Kaszuba et al.¹³³ showed that 5% sucrose (w/v) in water displayed particle sizes of around 1 nm. The effects of HBG were more drastic for **49** polyplexes than for **332** polyplexes and thus, influenced dynamic light scattering results. Contrary to **49** polyplexes, the analysis of **332** polyplexes with NTA led to accurate results with high resolution. In accordance to this, Filipe et al.¹¹⁵ reported a higher accuracy for NTA compared to DLS for standard polystyrene beads. The analysis of heterogeneous polyplexes (**279**), displaying small and big particles, was a challenge with all methods. Only AFM gave information about the heterogeneity of the sample. DLS results did not reflect reality and varied to a great extent, depending on the distribution, although the fitting of the correlation function was

possible with the Cumulants analysis. However, the NTA measurements gave diameters reflecting the predominant, smaller particle fraction, whereas the bigger aggregates were neglected. Contrary to DLS and NTA, FCS had a size limitation of around 300 nm due to the size of the confocal volume. In addition, the analysis was not possible for particles with a high number of fluorescently labeled molecules, as the fluorescence intensity was higher than the detection limit. Furthermore, FCS was the only method whereby real-time analysis of polyplex self-assembly was possible. The results confirmed that an incubation of 30 min was sufficient for polyplex formation.

Polyplex stability plays a crucial role in the *in vivo* application of siRNA polyplexes, as instable polyplexes are destroyed by serum proteins. Consequently, the siRNA is released into the blood stream, where it is degraded by RNases. FCS was the only method, where polyplexes in full serum are quantifiable, as reported by Buyens et al.⁸⁵. The size of the **49** polyplexes increased in full fetal bovine serum (from a hydrodynamic radius of less than 20 nm to approximately 50 nm), as negatively charged serum proteins attached onto the positively charged polyplexes¹³⁴. In contrast to their long-term stability in buffer, **49** polyplexes showed serum stability only to a certain degree: 66% and 18% of intact polyplexes were detected after 90 min at room temperature and 37°C, respectively.

4. Native chemical ligation

Polyethylene glycol (PEG) is used as shielding domain resulting in the protection of the carrier surface from interactions with blood components and non-target cells. Additionally, shielding increases the circulation time of carriers due to a decreased clearance¹³⁵ and avoids recognition by the immune system or the liver. Consequently, an ideally shielded particle is not able to interact with the target cell. Thus, a targeting ligand has to be attached to the carrier system in order to increase specific interactions with target cells that overexpress these receptors.

Blanco-Canosa et al.⁷³ introduced an approach which is compatible with solid phase peptide synthesis for the generation of thioesters oligomer precursors for native chemical ligation. With the help of these protocols, the suitability of the

method for the ligation of polycations with activated shielding and targeting domains was evaluated. After proving the suitability of NCL with model oligomers, larger shielding domains were incorporated into the oligomer structures. Additionally, different targeting ligands like folic acid, B6, GE11, and cMet binding peptide (cMBP) were attached to the shielding domains. Those ligands target the folic acid receptor, transferrin receptor, EGF receptor, and cMet/hepatocyte growth factor receptor, respectively. The resulting thioesters oligomer precursors FoIA-PEG₂₄-G-Nbz, B6-PEG₂₄-G-Nbz, GE11-PEG₂₄-G-Nbz and cMBP-PEG₂₄-G-Nbz were synthesized and can now be coupled by means of native chemical ligation to oligomers with *N*-terminal cysteines out of the existing library of over 600 structures.

Native chemical ligation can be performed prior to polyplex formation, as described above, or possibly after polyplex formation (post-ligation). The post-ligation would be useful for oligomers with more than one *N*-terminal cysteine. As a result, only the cysteines displayed on the polyplex surface can be modified with the shielding and targeting domain. Therefore, the ionic interactions between polycations and nucleic acids are not hampered. Further steps would be the biophysical characterization of the targeted structures, as well as *in vitro* and *in vivo* experiments.

V. SUMMARY

Free nucleic acids cannot enter cells, because of their negative charge and are therefore degraded by DNases or RNases, or rapidly cleared through the urinary tract due to their size. Consequently, appropriate carriers for the transport of nucleic acids are needed. Endosomal escape, transfection efficacy, carrier stability, size, and distribution profile play an important role for successful in vivo application of synthetic vectors and formulation development.

Polyplex stability was increased by integrating tyrosine trimers as stabilizing components into the oligomer sequences. Therefore, we synthesized precise, self-assembling, polycationic, oligotyrosine motif containing oligomers by means of solid phase assisted synthesis. Those oligomers had a favorable increase in buffer capacity and showed improved serum stability due to the incorporation of trimers of the aromatic amino acid. Our results show that these new carriers with at least two different polyplex stabilizing components were efficient in siRNA and pDNA delivery, and showed low toxicity in vitro and in vivo. Stability and hydrophobicity of the polyplexes affected systemic distribution upon intravenous administration and therapeutic efficacy in a subcutaneous tumor model.

Ureido pyrimidinone motifs, pyridyl thiourea motifs, or cysteine-arginine-cysteine motifs were incorporated into the oligomer structures in order to increase polyplex stability. The resulting oligomers were stabilized with the help of hydrogen bonds, π - π interactions, and covalent disulfide bridges, respectively. As pyridyl thiourea modification led to a loss in transfection efficiency and ureido pyrimidinone modification was less beneficial on binding and transfection efficiency than cysteine modification, these approaches were not further pursued. However, stabilization of oligomers with twin disulfides led to an increased nucleic acid binding ability and stability in fetal bovine serum. In contrast, gene delivery and target gene silencing of C-R-C modified oligomers seemed to be less efficient than with single cysteine modified analogs. Nevertheless, the influence of the C-R-C modification in vitro and in vivo has to be further investigated.

DLS, AFM, NTA and FCS were evaluated as analytical methods for polyplex characterization. All methods were suitable for medium sized, homogeneous polyplexes. In contrast, the smaller polyplexes could not be analyzed with NTA, due

to the detection limit. The analysis of heterogeneous samples was delicate independent of the method. Only by visualization with AFM, the heterogeneity of polyplexes was detectable. The small amount of large particles obscured the size measurements with all other methods, producing misleading results, even though fitting of the data was possible with DLS. FCS enables monitoring of the self-assembly process of polyplexes. In addition, polyplex stability in full fetal bovine serum could be quantified with FCS. In sum, none of the tested methods for particle size characterization was fully satisfactory. Each of them had its advantages and disadvantages. Therefore, a combination of at least two methods, one of which should be microscopic, to analyze the potential heterogeneity of samples, is recommended.

Interaction of the carrier surface with blood components and off-target cells should be reduced. Therefore, shielding and targeting domains should be ligated to already existing, polycationic structures with the help of native chemical ligation. A model polycation and activated oligomers containing PEG or PEG and a targeting ligand were used to investigate the suitability of this method to attach those domains. Afterwards, further activated, shielded oligomers with targeting ligand were synthesized. The strategy offers the possibility attaching ligands and PEG to oligomers out of our library with > 600 structures. The resulting oligomers need to be further evaluated as part of pDNA and siRNA polyplexes in vitro and in vivo.

VI. REFERENCES

- (1) Rosenecker, J., Huth, S., and Rudolph, C. (2006) Gene therapy for cystic fibrosis lung disease: current status and future perspectives. *Curr Opin Mol Ther* 8, 439-445.
- (2) Blaese, R. M., Culver, K. W., Miller, A. D., Carter, C. S., Fleisher, T., Clerici, M., Shearer, G., Chang, L., Chiang, Y., and Tolstoshev, P. (1995) T lymphocyte-directed gene therapy for ADA- SCID: initial trial results after 4 years. *Science* 270, 475-480.
- (3) Scott, D. W., and Lozier, J. N. (2012) Gene therapy for haemophilia: prospects and challenges to prevent or reverse inhibitor formation. *Br J Haematol* 156, 295-302.
- (4) Scherer, L. J., and Rossi, J. J. (2011) Ex vivo gene therapy for HIV-1 treatment. *Hum Mol Genet* 20, R100-R107.
- (5) Strayer, D. S., Akkina, R., Bunnell, B. A., Dropulic, B., Planelles, V., Pomerantz, R. J., Rossi, J. J., and Zaia, J. A. (2005) Current status of gene therapy strategies to treat HIV/AIDS. *Mol Ther* 11, 823-842.
- (6) Sawicki, J. A., Anderson, D. G., and Langer, R. (2008) Nanoparticle Delivery of Suicide DNA for Epithelial Ovarian Cancer Therapy Ovarian Cancer, (Coukos, G., Berchuck, A., and Ozols, R., Eds.) pp 209-219, Springer New York.
- (7) Ferraro, B., Morrow, M. P., Hutnick, N. A., Shin, T. H., Lucke, C. E., and Weiner, D. B. (2011) Clinical Applications of DNA Vaccines: Current Progress. *Clin Infect Dis* 53, 296-302.
- (8) Fire, A., Xu, S., Montgomery, M. K., Kostas, S. A., Driver, S. E., and Mello, C. C. (1998) Potent and specific genetic interference by double-stranded RNA in *Caenorhabditis elegans*. *Nature* 391, 806-811.
- (9) Elbashir, S. M., Harborth, J., Lendeckel, W., Yalcin, A., Weber, K., and Tuschl, T. (2001) Duplexes of 21-nucleotide RNAs mediate RNA interference in cultured mammalian cells. *Nature* 411, 494-498.
- (10) Hammond, S. M., Boettcher, S., Caudy, A. A., Kobayashi, R., and Hannon, G. J. (2001) Argonaute2, a Link Between Genetic and Biochemical Analyses of RNAi. *Science* 293, 1146-1150.
- (11) Rand, T. A., Ginalski, K., Grishin, N. V., and Wang, X. (2004) Biochemical identification of Argonaute 2 as the sole protein required for RNA-induced silencing complex activity. *Proc Natl Acad Sci* 101, 14385-14389.
- (12) Wang, Y., Sheng, G., Juranek, S., Tuschl, T., and Patel, D. J. (2008) Structure of the guide-strand-containing argonaute silencing complex. *Nature* 456, 209-213.
- (13) Gao, K., and Huang, L. (2008) Nonviral Methods for siRNA Delivery. *Mol Pharm* 6, 651-658.
- (14) Lin, C., Blaauboer, C.-J., Timoneda, M. M., Lok, M. C., van Steenberg, M., Hennink, W. E., Zhong, Z., Feijen, J., and Engbersen, J. F. J. (2008) Bioreducible poly(amido amine)s with oligoamine side chains: Synthesis, characterization, and structural effects on gene delivery. *J Control Release* 126, 166-174.
- (15) Schaffert, D., and Wagner, E. (2008) Gene therapy progress and prospects:

synthetic polymer-based systems. *Gene Ther* 15, 1131-8.

(16) Troiber, C., and Wagner, E. (2011) Nucleic Acid Carriers Based on Precise Polymer Conjugates. *Bioconjug Chem* 22, 1737-1752.

(17) Wolff, J. A., and Rozema, D. B. (2008) Breaking the bonds: non-viral vectors become chemically dynamic. *Mol Ther* 16, 8-15.

(18) Wagner, E. (2004) Strategies to improve DNA polyplexes for in vivo gene transfer: will "artificial viruses" be the answer? *Pharm Res* 21, 8-14.

(19) Wagner, E. (2008) Converging Paths of Viral and Non-viral Vector Engineering. *Mol Ther* 16, 1-2.

(20) Wagner, E., Plank, C., Zatloukal, K., Cotten, M., and Birnstiel, M. L. (1992) Influenza virus hemagglutinin HA-2 N-terminal fusogenic peptides augment gene transfer by transferrin-polylysine-DNA complexes: toward a synthetic virus-like gene-transfer vehicle. *Proc Natl Acad Sci* 89, 7934-7938.

(21) Zuber, G., Dauty, E., Nothisen, M., Belguise, P., and Behr, J. P. (2001) Towards synthetic viruses. *Adv Drug Deliv Rev* 52, 245-253.

(22) Krebs, M. D., and Alsberg, E. (2011) Localized, Targeted, and Sustained siRNA Delivery. *Chem Eur J* 17, 3054-3062.

(23) Mintzer, M. A., and Simanek, E. E. (2009) Nonviral vectors for gene delivery. *Chem Rev* 109, 259-302.

(24) Dekie, L., Toncheva, V., Dubruel, P., Schacht, E. H., Barrett, L., and Seymour, L. W. (2000) Poly--glutamic acid derivatives as vectors for gene therapy. *J Control Release* 65, 187-202.

(25) Burke, R. S., and Pun, S. H. (2008) Extracellular Barriers to in Vivo PEI and PEGylated PEI Polyplex-Mediated Gene Delivery to the Liver. *Bioconjug Chem* 19, 693-704.

(26) Chen, H. H., Ho, Y.-P., Jiang, X., Mao, H.-Q., Wang, T.-H., and Leong, K. W. (2008) Quantitative Comparison of Intracellular Unpacking Kinetics of Polyplexes by a Model Constructed From Quantum Dot-FRET. *Mol Ther* 16, 324-332.

(27) Midoux, P., Breuzard, G., Gomez, J. P., and Pichon, C. (2008) Polymer-based gene delivery: a current review on the uptake and intracellular trafficking of polyplexes. *Curr Gene Ther* 8, 335-52.

(28) Nishiyama, N., Arnida, Jang, W.-D., Date, K., Miyata, K., and Kataoka, K. (2006) Photochemical enhancement of transgene expression by polymeric micelles incorporating plasmid DNA and dendrimer-based photosensitizer. *J Drug Target* 14, 413-424.

(29) Grosse, S., Thévenot, G., Monsigny, M., and Fajac, I. (2006) Which mechanism for nuclear import of plasmid DNA complexed with polyethylenimine derivatives? *J Gene Med* 8, 845-851.

(30) Parker, A. L., Newman, C., Briggs, S., Seymour, L., and Sheridan, P. J. (2003) Nonviral gene delivery: techniques and implications for molecular medicine. *Expert Rev Mol Med* 5, 1-15.

(31) Christie, R. J., Nishiyama, N., and Kataoka, K. (2010) Minireview: Delivering the

Code: Polyplex Carriers for Deoxyribonucleic Acid and Ribonucleic Acid Interference Therapies. *Endocrinology* 151, 466-473.

(32) Itaka, K., Harada, A., Yamasaki, Y., Nakamura, K., Kawaguchi, H., and Kataoka, K. (2004) In situ single cell observation by fluorescence resonance energy transfer reveals fast intra-cytoplasmic delivery and easy release of plasmid DNA complexed with linear polyethylenimine. *J Gene Med* 6, 76-84.

(33) Kunath, K., von Harpe, A., Fischer, D., Petersen, H., Bickel, U., Voigt, K., and Kissel, T. (2003) Low-molecular-weight polyethylenimine as a non-viral vector for DNA delivery: comparison of physicochemical properties, transfection efficiency and in vivo distribution with high-molecular-weight polyethylenimine. *J Control Release* 89, 113-125.

(34) Akinc, A., Thomas, M., Klivanov, A. M., and Langer, R. (2005) Exploring polyethylenimine-mediated DNA transfection and the proton sponge hypothesis. *J Gene Med* 7, 657-663.

(35) Kichler, A., Leborgne, C., Coeytaux, E., and Danos, O. (2001) Polyethylenimine-mediated gene delivery: a mechanistic study. *J Gene Med* 3, 135-144.

(36) Sonawane, N. D., Szoka, F. C., Jr., and Verkman, A. S. (2003) Chloride Accumulation and Swelling in Endosomes Enhances DNA Transfer by Polyamine-DNA Polyplexes. *J.Biol.Chem.* 278, 44826-44831.

(37) Zou, S. M., Erbacher, P., Remy, J. S., and Behr, J. P. (2000) Systemic linear polyethylenimine (L-PEI)-mediated gene delivery in the mouse. *J Gene Med* 2, 128-134.

(38) Jeong, J. H., Mok, H., Oh, Y.-K., and Park, T. G. (2008) siRNA Conjugate Delivery Systems. *Bioconjug Chem* 20, 5-14.

(39) Russ, V., Elfberg, H., Thoma, C., Kloeckner, J., Ogris, M., and Wagner, E. (2008) Novel degradable oligoethylenimine acrylate ester-based pseudodendrimers for in vitro and in vivo gene transfer. *Gene Ther* 15, 18-29.

(40) Werth, S., Urban-Klein, B., Dai, L., Hobel, S., Grzelinski, M., Bakowsky, U., Czubayko, F., and Aigner, A. (2006) A low molecular weight fraction of polyethylenimine (PEI) displays increased transfection efficiency of DNA and siRNA in fresh or lyophilized complexes. *J Control Release* 112, 257-270.

(41) Wightman, L., Kircheis, R., Rossler, V., Carotta, S., Ruzicka, R., Kursa, M., and Wagner, E. (2001) Different behavior of branched and linear polyethylenimine for gene delivery in vitro and in vivo. *J Gene Med* 3, 362-372.

(42) Shir, A., Ogris, M., Wagner, E., and Levitzki, A. (2006) EGF receptor-targeted synthetic double-stranded RNA eliminates glioblastoma, breast cancer, and adenocarcinoma tumors in mice. *PLoS Med* 3, e6.

(43) Crespo, L., Sanclimens, G., Pons, M., Giralt, E., Royo, M., and Albericio, F. (2005) Peptide and amide bond-containing dendrimers. *Chem Rev* 105, 1663-81.

(44) Denkewalter, R. G., Kolc, J., and Lukasavage, W. J. (1981) US Pat. 4 289 872.

(45) Merrifield, R. B. (1963) Solid Phase Peptide Synthesis. I. The Synthesis of a Tetrapeptide. *J Am Chem Soc* 85, 2149-2154.

(46) Tam, J. P. (1988) Synthetic peptide vaccine design: synthesis and properties of a high-density multiple antigenic peptide system. *Proc Natl Acad Sci* 85, 5409-5413.

- (47) Ravina, M., Paolicelli, P., Seijo, B., and Sanchez, A. (2010) Knocking down gene expression with dendritic vectors. *Mini Rev Med Chem* 10, 73-86.
- (48) Binauld, S., Damiron, D., Connal, L. A., Hawker, C. J., and Drockenmuller, E. (2011) Precise Synthesis of Molecularly Defined Oligomers and Polymers by Orthogonal Iterative Divergent/Convergent Approaches. *Macromol Rapid Commun* 32, 147-168.
- (49) Hartmann, L. (2011) Polymers for Control Freaks: Sequence-Defined Poly(amidoamine)s and Their Biomedical Applications. *Macromol Chem Phys* 212, 8-13.
- (50) Hartmann, L., and Börner, H. G. (2009) Precision Polymers: Monodisperse, Monomer-Sequence-Defined Segments to Target Future Demands of Polymers in Medicine. *Adv Mater* 21, 3425-3431.
- (51) Hartmann, L., Hafele, S., Peschka-Suss, R., Antonietti, M., and Börner, H. G. (2008) Tailor-made poly(amidoamine)s for controlled complexation and condensation of DNA. *Chemistry* 14, 2025-33.
- (52) Hartmann, L., Häfele, S., Peschka-Süss, R., Antonietti, M., and Börner, H. G. (2007) Sequence Positioning of Disulfide Linkages to Program the Degradation of Monodisperse Poly(amidoamines). *Macromolecules* 40, 7771-7776.
- (53) Hartmann, L., Krause, E., Antonietti, M., and Börner, H. G. (2006) Solid-phase supported polymer synthesis of sequence-defined, multifunctional poly(amidoamines). *Biomacromolecules* 7, 1239-44.
- (54) Schaffert, D., Badgujar, N., and Wagner, E. (2011) Novel Fmoc-Polyamino Acids for Solid-Phase Synthesis of Defined Polyamidoamines. *Org Lett* 13, 1586-1589.
- (55) Fröhlich, T., Edinger, D., Kläger, R., Troiber, C., Salcher, E., Badgujar, N., Martin, I., Schaffert, D., Cengizeroglu, A., Hadwiger, P., Vornlocher, H.-P., and Wagner, E. (2012) Structure-activity relationships of siRNA carriers based on sequence-defined oligo (ethane amino) amides. *J Control Release* 160, 532-541.
- (56) Schaffert, D., Troiber, C., Salcher, E. E., Fröhlich, T., Martin, I., Badgujar, N., Dohmen, C., Edinger, D., Kläger, R., Maiwald, G., Farkasova, K., Seeber, S., Jahn-Hofmann, K., Hadwiger, P., and Wagner, E. (2011) Solid-Phase Synthesis of Sequence-Defined T-, i-, and U-Shape Polymers for pDNA and siRNA Delivery. *Angew Chem Int Ed* 50, 8986-8989.
- (57) Hein, C., Liu, X.-M., and Wang, D. (2008) Click Chemistry, A Powerful Tool for Pharmaceutical Sciences. *Pharm Res* 25, 2216-2230.
- (58) Lutz, J.-F., and Zarafshani, Z. (2008) Efficient construction of therapeutics, bioconjugates, biomaterials and bioactive surfaces using azide-alkyne "click" chemistry. *Adv Drug Deliv Rev* 60, 958-970.
- (59) Moses, J. E., and Moorhouse, A. D. (2007) The growing applications of click chemistry. *Chem Soc Rev* 36, 1249-1262.
- (60) Orski, S. V., Poloukhtine, A. A., Arumugam, S., Mao, L., Popik, V. V., and Locklin, J. (2010) High Density Orthogonal Surface Immobilization via Photoactivated Copper-Free Click Chemistry. *J Am Chem Soc* 132, 11024-11026.
- (61) Kolb, H. C., Finn, M. G., and Sharpless, K. B. (2001) Click Chemistry: Diverse Chemical Function from a Few Good Reactions. *Angew Chem Int Ed* 40, 2004-2021.

- (62) Rostovtsev, V. V., Green, L. G., Fokin, V. V., and Sharpless, K. B. (2002) A Stepwise Huisgen Cycloaddition Process: Copper(I)-Catalyzed Regioselective "Ligation" of Azides and Terminal Alkynes. *Angew Chem Int Ed* 41, 2596-2599.
- (63) Tornøe, C. W., Christensen, C., and Meldal, M. (2002) Peptidotriazoles on Solid Phase: [1,2,3]-Triazoles by Regiospecific Copper(I)-Catalyzed 1,3-Dipolar Cycloadditions of Terminal Alkynes to Azides. *J Org Chem* 67, 3057-3064.
- (64) Mindt, T. L., Müller, C., Stuker, F., Salazar, J.-F. d. r., Hohn, A., Mueggler, T., Rudin, M., and Schibli, R. (2009) A "Click Chemistry" Approach to the Efficient Synthesis of Multiple Imaging Probes Derived from a Single Precursor. *Bioconjug Chem* 20, 1940-1949.
- (65) Schlossbauer, A., Schaffert, D., Kecht, J., Wagner, E., and Bein, T. (2008) Click chemistry for high-density biofunctionalization of mesoporous silica. *J Am Chem Soc* 130, 12558-12559.
- (66) Chang, P. V., Prescher, J. A., Sletten, E. M., Baskin, J. M., Miller, I. A., Agard, N. J., Lo, A., and Bertozzi, C. R. (2010) Copper-free click chemistry in living animals. *Proc Natl Acad Sci* 107, 1821-1826.
- (67) Lee, C.-C., Grandinetti, G., McLendon, P. M., and Reineke, T. M. (2010) A Polycation Scaffold Presenting Tunable "Click" Sites: Conjugation to Carbohydrate Ligands and Examination of Hepatocyte-Targeted pDNA Delivery. *Macromol Biosci* 10, 585-598.
- (68) Liu, J., Jiang, X., Xu, L., Wang, X., Hennink, W. E., and Zhuo, R. (2010) Novel Reduction-Responsive Cross-Linked Polyethylenimine Derivatives by Click Chemistry for Nonviral Gene Delivery. *Bioconjug Chem* 21, 1827-1835.
- (69) Srinivasachari, S., and Reineke, T. M. (2009) Versatile supramolecular pDNA vehicles via "click polymerization" of beta-cyclodextrin with oligoethyleneamines. *Biomaterials* 30, 928-938.
- (70) van Dijk, M., Rijkers, D. T. S., Liskamp, R. M. J., van Nostrum, C. F., and Hennink, W. E. (2009) Synthesis and Applications of Biomedical and Pharmaceutical Polymers via Click Chemistry Methodologies. *Bioconjug Chem* 20, 2001-2016.
- (71) Jayaprakash, K. N., Peng, C. G., Butler, D., Varghese, J. P., Maier, M. A., Rajeev, K. G., and Manoharan, M. (2010) Non-Nucleoside Building Blocks for Copper-Assisted and Copper-Free Click Chemistry for the Efficient Synthesis of RNA Conjugates. *Org Lett* 12, 5410-5413.
- (72) Dawson, P., Muir, T., Clark-Lewis, I., and Kent, S. (1994) Synthesis of proteins by native chemical ligation. *Science* 266, 776-779.
- (73) Blanco-Canosa, J. B., and Dawson, P. E. (2008) An Efficient Fmoc-SPPS Approach for the Generation of Thioester Peptide Precursors for Use in Native Chemical Ligation. *Angew Chem Int Ed* 47, 6851-6855.
- (74) Byun, E., Kim, J., Kang, S. M., Lee, H., Bang, D., and Lee, H. (2010) Surface PEGylation via Native Chemical Ligation. *Bioconjug Chem* 22, 4-8.
- (75) Miyata, K., Nishiyama, N., and Kataoka, K. (2012) Rational design of smart supramolecular assemblies for gene delivery: chemical challenges in the creation of artificial viruses. *Chem Soc Rev* 41, 2562-2574.
- (76) Wagner, E. (2012) Polymers for siRNA delivery: inspired by viruses to be targeted, dynamic, and precise. *Acc Chem Res* 45, 1005-13.

- (77) Soo Choi, H., Liu, W., Misra, P., Tanaka, E., Zimmer, J. P., Iltis Ipe, B., Bawendi, M. G., and Frangioni, J. V. (2007) Renal clearance of quantum dots. *Nat Biotechnol* 25, 1165-1170.
- (78) Maeda, H. (2001) The enhanced permeability and retention (EPR) effect in tumor vasculature: the key role of tumor-selective macromolecular drug targeting. *Adv Enzyme Regul* 41, 189-207.
- (79) Alexis, F., Pridgen, E., Molnar, L. K., and Farokhzad, O. C. (2008) Factors Affecting the Clearance and Biodistribution of Polymeric Nanoparticles. *Mol Pharm* 5, 505-515.
- (80) Maeda, H., Bharate, G. Y., and Daruwalla, J. (2009) Polymeric drugs for efficient tumor-targeted drug delivery based on EPR-effect. *Eur J Pharm Biopharm* 71, 409-419.
- (81) Heidel, J., and Davis, M. (2011) Clinical Developments in Nanotechnology for Cancer Therapy. *Pharm Res* 28, 187-199.
- (82) Nomura, T., Koreeda, N., Yamashita, F., Takakura, Y., and Hashida, M. (1998) Effect of Particle Size and Charge on the Disposition of Lipid Carriers After Intratumoral Injection into Tissue-isolated Tumors. *Pharm Res* 15, 128-132.
- (83) Choi, J. S., Nam, K., Park, J.-y., Kim, J.-B., Lee, J.-K., and Park, J.-s. (2004) Enhanced transfection efficiency of PAMAM dendrimer by surface modification with L-arginine. *J Control Release* 99, 445-456.
- (84) Gaumet, M., Vargas, A., Gurny, R., and Delie, F. (2008) Nanoparticles for drug delivery: The need for precision in reporting particle size parameters. *Eur J Pharm Biopharm* 69, 1-9.
- (85) Buyens, K., Lucas, B., Raemdonck, K., Braeckmans, K., Vercammen, J., Hendrix, J., Engelborghs, Y., De Smedt, S. C., and Sanders, N. N. (2008) A fast and sensitive method for measuring the integrity of siRNA-carrier complexes in full human serum. *J Control Release* 126, 67-76.
- (86) Haley, B., and Frenkel, E. (2008) Nanoparticles for drug delivery in cancer treatment. *Urol Oncol* 26, 57-64.
- (87) Rozema, D. B., Lewis, D. L., Wakefield, D. H., Wong, S. C., Klein, J. J., Roesch, P. L., Bertin, S. L., Reppen, T. W., Chu, Q., Blokhin, A. V., Hagstrom, J. E., and Wolff, J. A. (2007) Dynamic PolyConjugates for targeted in vivo delivery of siRNA to hepatocytes. *Proc Natl Acad Sci* 104, 12982-12987.
- (88) Boyd, R. D., Pichaimuthu, S. K., and Cuenat, A. (2011) New approach to inter-technique comparisons for nanoparticle size measurements; using atomic force microscopy, nanoparticle tracking analysis and dynamic light scattering. *Colloids Surf A: Physicochem Eng Aspects* 387, 35-42.
- (89) Kaiser, E., Colescott, R. L., Bossinger, C. D., and Cook, P. I. (1970) Color test for detection of free terminal amino groups in the solid-phase synthesis of peptides. *Anal Biochem* 34, 595-598.
- (90) v. Smoluchowski, M. (1908) Molekular-kinetische Theorie der Opaleszenz von Gasen im kritischen Zustande, sowie einiger verwandter Erscheinungen. *Ann Phys* 330, 205-226.
- (91) Salcher, E. E., Kos, P., Frohlich, T., Badgujar, N., Scheible, M., and Wagner, E. (2012) Sequence-defined four-arm oligo(ethanamino)amides for pDNA and siRNA

delivery: Impact of building blocks on efficacy. *J Control Release* 164, 380-6.

(92) Zintchenko, A., Philipp, A., Dehshahri, A., and Wagner, E. (2008) Simple Modifications of Branched PEI Lead to Highly Efficient siRNA Carriers with Low Toxicity. *Bioconjug Chem* 19, 1448-1455.

(93) Boussif, O., Lezoualc'h, F., Zanta, M. A., Mergny, M. D., Scherman, D., Demeneix, B., and Behr, J. P. (1995) A versatile vector for gene and oligonucleotide transfer into cells in culture and in vivo: polyethylenimine. *Proc Natl Acad Sci* 92, 7297-7301.

(94) Creusat, G., and Zuber, G. (2008) Self-Assembling Polyethylenimine Derivatives Mediate Efficient siRNA Delivery in Mammalian Cells. *Chembiochem* 9, 2787-2789.

(95) Richards Grayson, A., Doody, A., and Putnam, D. (2006) Biophysical and Structural Characterization of Polyethylenimine-Mediated siRNA Delivery In Vitro. *Pharm Res* 23, 1868-1876.

(96) Tarcha, P. J., Pelisek, J., Merdan, T., Waters, J., Cheung, K., von Gersdorff, K., Culmsee, C., and Wagner, E. (2007) Synthesis and characterization of chemically condensed oligoethylenimine containing beta-aminopropionamide linkages for siRNA delivery. *Biomaterials* 28, 3731-3740.

(97) Creusat, G., Rinaldi, A.-S., Weiss, E., Elbaghdadi, R., Remy, J.-S., Mulherkar, R., and Zuber, G. (2010) Proton Sponge Trick for pH-Sensitive Disassembly of Polyethylenimine-Based siRNA Delivery Systems. *Bioconjug Chem* 21, 994-1002.

(98) Zaghloul, E. M., Viola, J. R., Zuber, G., Smith, C. I. E., and Lundin, K. E. (2010) Formulation and Delivery of Splice-Correction Antisense Oligonucleotides by Amino Acid Modified Polyethylenimine. *Mol Pharm* 7, 652-663.

(99) Hunter, C. A., and Sanders, J. K. M. (1990) The nature of π - π interactions. *J Am Chem Soc* 112, 5525-5534.

(100) Zaupa, A., Neffe, A. T., Pierce, B. F., Nöchel, U., and Lendlein, A. (2010) Influence of Tyrosine-Derived Moieties and Drying Conditions on the Formation of Helices in Gelatin. *Biomacromolecules* 12, 75-81.

(101) Schaffert, D., Troiber, C., and Wagner, E. (2012) New Sequence-Defined Polyaminoamides with Tailored Endosomolytic Properties for Plasmid DNA Delivery. *Bioconjug Chem* 23, 1157-1165.

(102) Remaut, K., Lucas, B., Raemdonck, K., Braeckmans, K., Demeester, J., and De Smedt, S. C. (2007) Can we better understand the intracellular behavior of DNA nanoparticles by fluorescence correlation spectroscopy? *J Control Release* 121, 49-63.

(103) Troiber, C., Kasper, J. C., Milani, S., Scheible, M., Martin, I., Schaubhut, F., Küchler, S., Rädler, J., Simmel, F. C., Friess, W., and Wagner, E. Comparison of four different particle sizing methods for siRNA polyplex characterization. *Eur J Pharm Biopharm*.

(104) Dankers, P. Y. W., Adams, P. J. H. M., Löwik, D. W. P. M., van Hest, J. C. M., and Meijer, E. W. (2007) Convenient Solid-Phase Synthesis of Ureido-Pyrimidinone Modified Peptides. *European J Org Chem*, 3622-3632.

(105) Creusat, G., Thomann, J.-S., Maglott, A., Pons, B., Dontenwill, M., Guérin, E., Frisch, B., and Zuber, G. (2012) Pyridylthiourea-grafted polyethylenimine offers an effective assistance to siRNA-mediated gene silencing in vitro and in vivo. *J Control*

Release 157, 418-426.

(106) Wu, C., Leroux, J.-C., and Gauthier, M. A. (2012) Twin disulfides for orthogonal disulfide pairing and the directed folding of multicyclic peptides. *Nat Chem* 4, 1044-1049.

(107) Neffe, A. T., Loebus, A., Zaupa, A., Stoetzel, C., Müller, F. A., and Lendlein, A. (2011) Gelatin functionalization with tyrosine derived moieties to increase the interaction with hydroxyapatite fillers. *Acta Biomaterialia* 7, 1693-1701.

(108) Troiber, C., Edinger, D., Kos, P., Schreiner, L., Kläger, R., Herrmann, A., and Wagner, E. (2012) Stabilizing effect of tyrosine trimers on pDNA and siRNA polyplexes. *Biomaterials*, in press.

(109) Pecora, R. (1985) in *Dynamic light scattering: Applications of Photon Correlation Spectroscopy*, Plenum Press.

(110) Goldberg, W. I. (1999) Dynamic light scattering. *Am J Phys* 67, 1152-1160.

(111) Binnig, G., Quate, C. F., and Gerber, C. (1986) Atomic Force Microscope. *Phys Rev Lett* 56, 930-933.

(112) Meyer, E. (1992) Atomic force microscopy. *Prog Surf Sci* 41, 3-49.

(113) Jungmann, R., Scheible, M., and Simmel, F. C. (2012) Nanoscale imaging in DNA nanotechnology. *Wiley Interdiscip Rev Nanomed Nanobiotechnol* 4, 66-81.

(114) Sitterberg, J., Özçetin, A., Ehrhardt, C., and Bakowsky, U. (2010) Utilising atomic force microscopy for the characterisation of nanoscale drug delivery systems. *Eur J Pharm Biopharm* 74, 2-13.

(115) Filipe, V., Hawe, A., and Jiskoot, W. (2010) Critical Evaluation of Nanoparticle Tracking Analysis (NTA) by NanoSight for the Measurement of Nanoparticles and Protein Aggregates. *Pharm Res* 27, 796-810.

(116) Malloy, A., and Carr, B. (2006) NanoParticle Tracking Analysis – The Halo™ System. *Part Part Syst Charact* 23, 197-204.

(117) DeRouchey, J., Schmidt, C., Walker, G. F., Koch, C., Plank, C., Wagner, E., and Rädler, J. O. (2008) Monomolecular Assembly of siRNA and Poly(ethylene glycol)-Peptide Copolymers. *Biomacromolecules* 9, 724-732.

(118) Buyens, K., Meyer, M., Wagner, E., Demeester, J., De Smedt, S. C., and Sanders, N. N. (2010) Monitoring the disassembly of siRNA polyplexes in serum is crucial for predicting their biological efficacy. *J Control Release* 141, 38-41.

(119) Perevoshchikova, I., Kotova, E., and Antonenko, Y. (2011) Fluorescence correlation spectroscopy in biology, chemistry, and medicine. *Biochemistry (Mosc)* 76, 497-516.

(120) Schwille, P., Haupts, U., Maiti, S., and Webb, W. W. (1999) Molecular Dynamics in Living Cells Observed by Fluorescence Correlation Spectroscopy with One- and Two-Photon Excitation. *Biophys J* 77, 2251-2265.

(121) Harris, J. M., and Chess, R. B. (2003) Effect of pegylation on pharmaceuticals. *Nat Rev Drug Discov* 2, 214-221.

(122) Immordino, M. L., Dosio, F., and Cattel, L. (2006) Stealth liposomes: review of the

basic science, rationale, and clinical applications, existing and potential. *Int J Nanomedicine* 1, 297-315.

(123) Ulasov, A. V., Khramtsov, Y. V., Trusov, G. A., Rosenkranz, A. A., Sverdlov, E. D., and Sobolev, A. S. (2011) Properties of PEI-based Polyplex Nanoparticles That Correlate With Their Transfection Efficacy. *Mol Ther* 19, 103-112.

(124) Dawson, P. E., and Kent, S. B. (2000) Synthesis of native proteins by chemical ligation. *Annu Rev Biochem* 69, 923-60.

(125) Kochendoerfer, G. G., Chen, S. Y., Mao, F., Cressman, S., Traviglia, S., Shao, H., Hunter, C. L., Low, D. W., Cagle, E. N., Carnevali, M., Gueriguian, V., Keogh, P. J., Porter, H., Stratton, S. M., Wiedeke, M. C., Wilken, J., Tang, J., Levy, J. J., Miranda, L. P., Crnogorac, M. M., Kalbag, S., Botti, P., Schindler-Horvat, J., Savatski, L., Adamson, J. W., Kung, A., Kent, S. B., and Bradburne, J. A. (2003) Design and chemical synthesis of a homogeneous polymer-modified erythropoiesis protein. *Science* 299, 884-7.

(126) Torbeev, V. Y., and Kent, S. B. (2007) Convergent chemical synthesis and crystal structure of a 203 amino acid "covalent dimer" HIV-1 protease enzyme molecule. *Angew Chem Int Ed Engl* 46, 1667-70.

(127) Dohmen, C., Edinger, D., Fröhlich, T., Schreiner, L., Lächelt, U., Troiber, C., Rädler, J., Hadwiger, P., Vornlocher, H.-P., and Wagner, E. (2012) Nanosized Multifunctional Polyplexes for Receptor-Mediated siRNA Delivery. *ACS Nano* 6, 5198-5208.

(128) Huang, Y., Hong, J., Zheng, S., Ding, Y., Guo, S., Zhang, H., Zhang, X., Du, Q., and Liang, Z. (2011) Elimination Pathways of Systemically Delivered siRNA. *Mol Ther* 19, 381-385.

(129) Zhang, Y., Bradshaw-Pierce, E. L., DeLille, A., Gustafson, D. L., and Anchordoquy, T. J. (2008) In Vivo comparative study of lipid/DNA complexes with different In Vitro serum stability: Effects on biodistribution and tumor accumulation. *J Pharm Sci* 97, 237-250.

(130) Tietze, N., Pelisek, J., Philipp, A., Roedl, W., Merdan, T., Tarcha, P., Ogris, M., and Wagner, E. (2008) Induction of apoptosis in murine neuroblastoma by systemic delivery of transferrin-shielded siRNA polyplexes for downregulation of Ran. *Oligonucleotides* 18, 161-174.

(131) Rayleigh, L. (1914) On the Diffraction of Light by Spheres of Small Relative Index. *Proc R Soc A* 90, 219-225.

(132) Mie, G. (1908) Beiträge zur Optik trüber Medien, speziell kolloidaler Metallösungen. *Ann Phys* 330, 377-445.

(133) Kaszuba, M., McKnight, D., Connah, M., McNeil-Watson, F., and Nobbmann, U. (2008) Measuring sub nanometre sizes using dynamic light scattering. *J Nanopart Res* 10, 823-829.

(134) Hönig, D., DeRouchey, J., Jungmann, R., Koch, C., Plank, C., and Rädler, J. O. (2010) Biophysical Characterization of Copolymer-Protected Gene Vectors. *Biomacromolecules* 11, 1802-1809.

(135) Philipp, A., Zhao, X., Tarcha, P., Wagner, E., and Zintchenko, A. (2009) Hydrophobically Modified Oligoethylenimines as Highly Efficient Transfection Agents for siRNA Delivery. *Bioconjug Chem* 20, 2055-2061.

VII.APPENDIX

1.1. Abbreviations

A	Alanine, Ala
AA	Amino acid
ACN	Acetonitrile
AFM	Atomic force microscopy
AHA1	Activator of 90 kDa heat shock protein ATPase isoform 1
B6	Peptide sequence with affinity for the transferrin receptor
Boc	<i>tert</i> -Butyloxycarbonyl
bPEI	Branched polyethylenimine
C	Cysteine, Cys
CDCl ₃	Deuterated chloroform
cMBP	Peptide binding to the hepatocyte growth factor receptor(cMet)
cMet	Hepatocyte growth factor receptor
C-R-C	Cysteine-arginine-cysteine
Cy	Cyanine
Dbz	3,4-Diaminobenzoic acid
DCM	Dichloromethane
Dde	<i>N</i> -1-(4,4-dimethyl-2,6-dioxocyclohexylidene)ethyl
DIPEA	Diisopropylethylamine
DLS	Dynamic light scattering
DMF	<i>N,N</i> -Dimethylformamide
DMFxD ₆	Deuterated DMF
DMSO	Dimethyl sulfoxide
DMSOxD ₆	Deuterated DMSO

DNA	Deoxyribunucleic acid
D ₂ O	Deuterium oxide
E	Glutamic acid, Glu
e.g.	Exempli gratia (for example)
EDTA	Ethylenediaminetetraacetic acid
EGF	Epidermal growth factor
eGFP	Enhanced green fluorescent protein
EPR	Enhanced permeability and retention effect
ESI	Electron spray ionization
EtOH	Ethanol
F	Phenylalanine, Phe
FA	Fatty acid
FAB-MS	Fast atom bombardment mass spectrometry
FACS	Fluorescence-activated cell sorting
FBS	Fetal bovine serum
FCS	Fluorescence correlation spectroscopy
Fmoc	Fluorenylmethoxycarbonyl
FoIA	Folic acid
G	Glycine, Gly
G(t)	Relative correlation function
G(t) fit	Fitting function curve
GE11	Peptide binding to the EGF receptor
HBG	HEPES buffered glucose
HEPES	<i>N</i> -(2-hydroxyethyl)piperazine- <i>N'</i> -(2-ethansulfonic acid)
HOBt	Hydroxybenzotriazole
ICH-CAMP	2-(6-isocyanahexylaminocarbonylamino)-6-methyl-4(1H)pyrimidinone

i. t.	Intratumoral
I.U.	International unit
i. v.	Intravenous
K	Lysine, Lys
LinA	Linoleic acid
LPEI	Linear polyethylenimine
Luc	Luciferase
MALDI-TOF	Matrix assisted laser desorption ionization – time of flight
MeOH	Methanol
MS	Mass spectrometry
MtBE	Methyl <i>tert</i> -butyl ether
MTT	Dimethylthiazoldiphenyl-tetrazolium bromide
Mut	Scrambled sequence of eGFP siRNA without silencing potential
M_w	Molecular weight
n.d.	Not defined
N/P ratio	Number of protonable nitrogens to phosphates
Nbz	<i>N</i> -acyl-benzimidazolinone
NCL	Native chemical ligation
NIR	Near-infrared
NMR	Nuclear magnetic resonance
NTA	Nanoparticle tracking analysis
OleA	Oleic acid
PAMAM	Polyamidoamine
PBS	Phosphate buffered saline
PdI	Polydispersity Index
pDNA	Plasmid deoxyribonucleic acid

PEG	Polyethylene glycol
PEG ₂ or PEG ₂₄	Polyethylene glycol with exactly 2 or 24 monomers
PITC	3-Pyridyl isothiocyanate
Pybop®	Benzotriazole-1-yl-oxy-tris-(dimethylamino)-phosphonium hexafluorophosphate
R	Arginine, Arg
RAN	Ras (rat sarcoma)-related nuclear protein
RLU	Relative light units
RNA	Ribonucleic acid
rpm	Rounds per minute
RT	Room temperature
SEC	Size exclusion chromatography
siRNA	Small interfering ribonucleic acid
SPPS	Solid phase peptide synthesis
Stp	Succinoyl tetraethylenpentamine
TBE	Tris(hydroxymethyl)aminomethane-borate-EDTA
tBu	<i>tert</i> -Butyl
TCEP	Tris(2-carboxyethyl)phosphine
TFA	Trifluoroacetic acid
TFE	2,2,2-Trifluoroethanol
TIS	Triisopropylsilane
Trt	Trityl
v/v	Volume per volume
W	Tryptophan, W
w/v	Weight per volume
Y	Tyrosine, Tyr

1.2. Analytical data

Sequence: Fmoc-Tyr(tBu)₃-OH

Molecular formula: C₅₄H₆₃N₃O₉ M_w 898.09

FAB⁺ (mass found) 898.6

¹H NMR spectrum (400 MHz) in CDCl₃. δ (ppm) = 1.1-1.4 (m, 27 H, -CH₃ tBu), 2.6-3.1 (m, 6 H, -CH₂- tyrosine), 4.1-4.7 (m, 6 H, -CH₂- fmoc, -CH- fmoc and αH amino acids), 6.8-7.1 (m, 12 H, -CH- tyrosine), 7.25-7.8 (m, 8 H, -CH- fmoc).

Sequence: Boc-Tyr(tBu)₃-OH

Molecular formula: C₄₄H₆₁N₃O₉ M_w 775.97

DEI⁺ (mass found) 776.4

¹H NMR spectrum (400 MHz) in CDCl₃. δ (ppm) = 1.1-1.5 (m, 36 H, -CH₃ tBu), 2.7-3.2 (m, 6 H, -CH₂- tyrosine), 4.2-5.0 (m, 3 H, αH amino acids), 6.7-7.1 (m, 12 H, -CH- tyrosine).

Sequence: 2-(6-Isocyanahexylaminocarbonylamino)-6-methyl-4(1*H*)pyrimidinone (ICH-CAMP)

Molecular formula: C₁₃H₁₉N₅O₃ M_w 293.32

DEI⁺ (mass found) 293.1

¹H NMR spectrum (400 MHz) in DMF-*d*₆. δ (ppm) = 1.3-1.7 (m, 8 H, aliphatic -CH₂-), 2.1-2.2 (s, 3 H, aromatic -CH₃), 3.2-3.3 (q, 2 H, aliphatic -CH₂-), 3.37-3.45 (m, 2 H, aliphatic -CH₂-), 5.75-5.85 (s, 1 H, aromatic -CH-).

Sequence: Fmoc-Dbz

Molecular formula: C₂₂H₁₈N₂O₄ M_w 374.39

DEI⁺ (mass found) 374.5

¹H NMR spectrum (400 MHz) in CDCl₃. δ (ppm) = 4.1-4.5 (m, 3 H, -CH- and -CH₂- Fmoc), 6.7-6.75 (d, 1 H, -CH- Dbz), 7.2-7.9 (m, 10 H, -CH- fmoc and Dbz), 8.6-8.8 (s, 1 H, -COOH Dbz).

Sequence: FoIA(trt)

Molecular formula: C₄₂H₄₁N₇O₆

M_w 739.82

ESI⁺ (mass found) 740.32

¹H NMR spectrum (400 MHz) in DMF*D₆. δ (ppm) = 1.4-1.6 (s, 9 H, -CH₃ tBu), 2.0-2.6 (m, 4 H, -CH₂- glutamic acid), 4.4-4.6 (m, 2 H, -CH₂- N¹⁰-(trifluoroacetyl)pteroic acid)), 7.2-7.9 (m, 20 H, -CH- trt and N¹⁰-(trifluoroacetyl)pteroic acid)).

Sequence: C-Stp₂-[(OleA)₂-K]K-Stp₂-C

49

Molecular formula: C₁₀₂H₂₀₀N₂₆O₁₅S₂

M_w 2094.98

Maldi (mass found) 2094.44

¹H NMR spectrum (400 MHz) in D₂O. δ (ppm) = 0.7-0.8 (s, 6 H, -CH₃ oleic acid), 1.0-2.25 (m, 68 H, γδϵH lysine, -CH₂- oleic acid), 2.4-2.6 (m, 16 H, -CO-CH₂-CH₂-CO-), 2.8-3.1 (m, 8 H, βH lysine and cysteine), 3.15-3.6 (m, 64 H, -CH₂- Tp), 4.0-4.5 (m, 4 H, αH amino acids), 5.15-5.3 (m, 4 H, -CH- oleic acid).

Sequence: A-Stp₂-[(OleA)₂-K]K-Stp₂-A

216

Molecular formula: C₁₀₂H₂₀₀N₂₆O₁₅

M_w 2030.84

¹H NMR spectrum (400 MHz) in D₂O. δ (ppm) = 0.7-0.9 (s, 6 H, -CH₃ oleic acid), 1.0-2.25 (m, 74 H, γδϵH lysine, -CH₃ alanine, -CH₂- oleic acid), 2.4-2.6 (m, 16 H, -CO-CH₂-CH₂-CO-), 3.0-3.2 (m, 4 H, βH lysine), 3.1-3.6 (m, 64 H, -CH₂- Tp), 4.0-4.25 (m, 4 H, αH amino acids), 5.1-5.4 (m, 4 H, -CH- oleic acid).

Sequence: [C-Y₃-Stp₃]₂K

331

Molecular formula: C₁₄₀H₂₃₇N₄₁O₂₇S₂

M_w 2990.768

¹H NMR spectrum (400 MHz) in D₂O. δ (ppm) = 1.3-1.8 (m, 6 H, γδϵH lysine), 2.4-2.6 (m, 24 H, -CO-CH₂-CH₂-CO-), 2.65-3.1 (m, 15 H, βH lysine, cysteine and tyrosine), 3.1-3.6 (m, 96 H, -CH₂- Tp), 4.0-4.5 (m, 9 H, αH amino acids), 6.65-7.15 (m, 24 H, -CH- tyrosine).

Sequence: Y₃-Stp₂-[(OleA)₂-K]K-Stp₂-Y₃

332

Molecular formula: C₁₅₀H₂₄₄N₃₀O₂₅

M_w 2867.73

Maldi (mass found) 2867.57

^1H NMR spectrum (400 MHz) in D_2O . δ (ppm) = 0.7-0.8 (s, 6 H, $-\text{CH}_3$ oleic acid), 1.0-2.0 (m, 68 H, $\gamma\delta\epsilon\text{H}$ lysine, $-\text{CH}_2-$ oleic acid), 2.3-2.7 (m, 16 H, $-\text{CO}-\text{CH}_2-\text{CH}_2-\text{CO}-$), 2.7-3.1 (m, 16 H, βH lysine and tyrosine), 3.1-3.6 (m, 64 H, $-\text{CH}_2-$ Tp), 4.0-4.5 (m, 8 H, αH amino acids), 5.15-5.3 (m, 4 H, $-\text{CH}-$ oleic acid), 6.65-7.15 (m, 24 H, $-\text{CH}-$ tyrosine).

Sequence: $\text{Y}_3\text{-Stp}_2\text{-}[(\text{Y}_3)_2\text{-K}]\text{K-Stp}_2\text{-Y}_3$ **333**
 Molecular formula: $\text{C}_{170}\text{H}_{240}\text{N}_{36}\text{O}_{34}$ M_w 3331.9453

^1H NMR spectrum (400 MHz) in D_2O . δ (ppm) = 1.0-1.8 (m, 12 H, $\gamma\delta\epsilon\text{H}$ lysine), 2.3-2.6 (m, 16 H, $-\text{CO}-\text{CH}_2-\text{CH}_2-\text{CO}-$), 2.6-3.1 (m, 28 H, βH lysine and tyrosine), 3.1-3.6 (m, 64 H, $-\text{CH}_2-$ Tp), 3.8-4.5 (m, 14 H, αH amino acids), 6.65-7.15 (m, 48 H, $-\text{CH}-$ tyrosine).

Sequence: $[(\text{Stp}_5)_2\text{K}]\text{K}[\text{K}(\text{OleA})_2]$ **407**
 Molecular formula: $\text{C}_{174}\text{H}_{352}\text{N}_{56}\text{O}_{26}$ M_w 3645.02

Maldi (mass found) 3643.98

^1H NMR spectrum (400 MHz) in D_2O . δ (ppm) = 0.75-0.85 (s, 6 H, $-\text{CH}_3$ oleic acid), 1.1-2.3 (m, 74 H, $\gamma\delta\epsilon\text{H}$ lysine, $-\text{CH}_2-$ oleic acid), 2.4-2.6 (m, 40 H, $-\text{CO}-\text{CH}_2-\text{CH}_2-\text{CO}-$), 2.9-3.15 (m, 6 H, βH lysine), 3.15-3.6 (m, 160 H, $-\text{CH}_2-$ Tp), 4.0-4.3 (m, 3 H, αH amino acids), 5.2-5.4 (m, 4 H, $-\text{CH}-$ oleic acid).

Sequence: $[(\text{ICH-CAMP-Stp}_5)_2\text{K}]\text{K}[\text{K}(\text{OleA})_2]$ **408**
 Molecular formula: $\text{C}_{200}\text{H}_{390}\text{N}_{66}\text{O}_{32}$ M_w 4231.66

^1H NMR spectrum (400 MHz) in D_2O . δ (ppm) = 0.75-0.85 (s, 6 H, $-\text{CH}_3$ oleic acid), 1.0-2.3 (m, 96 H, $\gamma\delta\epsilon\text{H}$ lysine, $-\text{CH}_2-$ oleic acid, $-\text{CH}_2-$ ICH-CAMP and $-\text{CH}_3$ ICH-CAMP), 2.4-2.6 (m, 40 H, $-\text{CO}-\text{CH}_2-\text{CH}_2-\text{CO}-$), 2.9-3.15 (m, 6 H, βH lysine), 3.15-3.6 (m, 168 H, $-\text{CH}_2-$ Tp and $-\text{CH}_2-$ ICH-CAMP), 4.0-4.3 (m, 3 H, αH amino acids), 5.2-5.4 (m, 4 H, $-\text{CH}-$ oleic acid), 5.9-5.95 (s, 2 H, aromatic $-\text{CH}-$).

Sequence: $\text{C-Stp}_2\text{-}[\text{K}]\text{K-Stp}_2\text{-C}$ **413**
 Molecular formula: $\text{C}_{66}\text{H}_{136}\text{N}_{26}\text{O}_{13}\text{S}_2$ M_w 1566.08

Maldi (mass found) 1565.07

^1H NMR spectrum (400 MHz) in D_2O . δ (ppm) = 1.1-1.9 (m, 12 H, $\gamma\delta\epsilon\text{H}$ lysine), 2.4-2.7 (m, 16 H, $-\text{CO}-\text{CH}_2-\text{CH}_2-\text{CO}-$), 2.8-3.1 (m, 8 H, βH lysine and cysteine), 3.1-3.6 (m, 64 H,

-CH₂- Tp), 3.8-4.4 (m, 4 H, αH amino acids).

Sequence: C-Y₃-Stp₂-[(OleA)₂-K]K-Stp₂-Y₃-C **454**

Molecular formula: C₁₅₆H₂₅₄N₃₂O₂₇S₂ M_w 3074.01

¹H NMR spectrum (400 MHz) in D₂O. δ (ppm) = 0.7-0.8 (s, 6 H, -CH₃ oleic acid), 0.8-2.0 (m, 68 H, γδϵH lysine, -CH₂- oleic acid), 2.3-2.6 (m, 16 H, -CO-CH₂-CH₂-CO-), 2.6-3.1 (m, 20 H, βH lysine, tyrosine and cysteine), 3.1-3.6 (m, 64 H, -CH₂- Tp), 4.0-4.6 (m, 10 H, αH amino acids), 5.15-5.3 (m, 4 H, -CH- oleic acid), 6.65-7.35 (m, 24 H, -CH- tyrosine).

Sequence: C-Y₃-Stp₂-[(Y₃)₂-K]K-Stp₂-Y₃-C **464**

Molecular formula: C₁₇₄H₂₄₄N₃₈O₃₇S₂ M_w 3524.16

¹H NMR spectrum (400 MHz) in D₂O. δ (ppm) = 1.1-1.9 (m, 12 H, γδϵH lysine), 2.3-2.6 (m, 16 H, -CO-CH₂-CH₂-CO-), 2.6-3.1 (m, 32 H, βH lysine, cysteine and tyrosine), 3.1-3.6 (m, 64 H, -CH₂- Tp), 3.8-4.5 (m, 16 H, αH amino acids), 6.65-7.15 (m, 48 H, -CH- tyrosine).

Sequence: C-Y₃-Stp₂-[K]K-Stp₂-Y₃-C **465**

Molecular formula: C₁₂₀H₁₉₀N₃₂O₂₅S₂ M_w 2545.122

¹H NMR spectrum (400 MHz) in D₂O. δ (ppm) = 1.1-1.8 (m, 12 H, γδϵH lysine), 2.3-2.6 (m, 16 H, -CO-CH₂-CH₂-CO-), 2.6-3.1 (m, 20 H, βH lysine, cysteine and tyrosine), 3.1-3.6 (m, 64 H, -CH₂- Tp), 3.7-4.5 (m, 10 H, αH amino acids), 6.65-7.15 (m, 24 H, -CH- tyrosine).

Sequence: C-Stp₂-[(Y₃)₂-K]K-Stp₂-C **468**

Molecular formula: C₁₂₀H₁₉₀N₃₂O₂₅S₂ M_w 2545.12

¹H NMR spectrum (400 MHz) in D₂O. δ (ppm) = 0.9-1.9 (m, 12 H, γδϵH lysine), 2.3-2.6 (m, 16 H, -CO-CH₂-CH₂-CO-), 2.6-3.1 (m, 20 H, βH lysine, cysteine and tyrosine), 3.1-3.6 (m, 64 H, -CH₂- Tp), 3.75-4.5 (m, 10 H, αH amino acids), 6.65-7.15 (m, 24 H, -CH- tyrosine).

Sequence: [(PITC-Stp₂)₂K]K[K(Y₃)₂] **587**

Molecular formula: C₁₃₂H₂₀₀N₃₆O₂₄S₂ M_w 2739.357

¹H NMR spectrum (400 MHz) in D₂O. δ (ppm) = 1.1-1.8 (m, 18 H, γδϵH lysine), 2.4-2.6 (m, 16 H, -CO-CH₂-CH₂-CO-), 2.65-3.1 (m, 18 H, βH lysine and tyrosine), 3.1-3.6 (m, 64 H, -CH₂- Tp), 3.8-4.6 (m, 9 H, αH amino acids), 6.6-7.1 (m, 24 H, -CH- tyrosine), 7.8-9.2 (m,

4 H, PITC).

Sequence: [C-Y₃-Stp₃]₂K-Stp₃-Y₃-C **589**
 Molecular formula: C₂₀₄H₃₃₅N₅₉O₄₁S₃ M_w 4366.41
¹H NMR spectrum (400 MHz) in D₂O. δ (ppm) = 1.1-1.8 (m, 6 H, γδϵH lysine), 2.4-2.6 (m, 36 H, -CO-CH₂-CH₂-CO-), 2.6-3.1 (m, 42 H, βH lysine, cysteine and tyrosine), 3.1-3.6 (m, 144 H, -CH₂- Tp), 4.0-4.5 (m, 12 H, αH amino acids), 6.65-7.15 (m, 36 H, -CH- tyrosine).

Sequence: [Y₃-Stp₃]₂K-Stp₃-Y₃ **590**
 Molecular formula: C₁₉₅H₃₂₀N₅₆O₃₈ M_w 4056.9797
¹H NMR spectrum (400 MHz) in D₂O. δ (ppm) = 1.1-1.8 (m, 6 H, γδϵH lysine), 2.4-2.6 (m, 36 H, -CO-CH₂-CH₂-CO-), 2.6-3.1 (m, 38 H, βH lysine and tyrosine), 3.1-3.6 (m, 144 H, -CH₂- Tp), 4.0-4.5 (m, 10 H, αH amino acids), 6.65-7.2 (m, 36 H, -CH- tyrosine).

Sequence: C-R-C-Stp₂-[K]K-Stp₂-C-R-C **591**
 Molecular formula: C₈₉H₁₈₁N₃₇O₁₇S₄ M_w 2169.89
¹H NMR spectrum (400 MHz) in D₂O. δ (ppm) = 1.2-2.0 (m, 20 H, γδϵH lysine and γδH arginine), 2.4-2.6 (m, 16 H, -CO-CH₂-CH₂-CO-), 2.8-3.2 (m, 16 H, βH lysine, arginine and cysteine), 3.2-3.7 (m, 64 H, -CH₂- Tp), 3.8-4.4 (m, 8 H, αH amino acids).

Sequence: C-R-C-Stp₂-[(OleA)₂-K]K-Stp₂-C-R-C **592**
 Molecular formula: C₁₂₅H₂₄₅N₃₇O₁₉S₄ M_w 2698.78
¹H NMR spectrum (400 MHz) in D₂O. δ (ppm) = 0.7-0.9 (s, 6 H, -CH₃ oleic acid), 1.0-2.3 (m, 76 H, γδϵH lysine and γδH arginine, -CH₂- oleic acid), 2.4-2.6 (m, 16 H, -CO-CH₂-CH₂-CO-), 2.8-3.2 (m, 16 H, βH lysine, arginine and cysteine), 3.2-3.7 (m, 64 H, -CH₂- Tp), 4.0-4.5 (m, 8 H, αH amino acids), 5.15-5.3 (m, 4 H, -CH- oleic acid).

Sequence: C-R-C-Stp₂-[(Y₃)₂-K]K-Stp₂-C-R-C **593**
 Molecular formula: C₁₄₃H₂₃₅N₄₃O₂₉S₄ M_w 3148.927
¹H NMR spectrum (400 MHz) in D₂O. δ (ppm) = 0.9-1.9 (m, 20 H, γδϵH lysine and γδH arginine), 2.4-2.6 (m, 16 H, -CO-CH₂-CH₂-CO-), 2.6-3.2 (m, 28 H, βH lysine, arginine,

cysteine and tyrosine), 3.2-3.7 (m, 64 H, -CH₂- Tp), 3.8-4.6 (m, 14 H, αH amino acids), 6.6-7.1 (m, 24 H, -CH- tyrosine).

Sequence: C-R-C-Y₃-Stp₂-[K]K-Stp₂-Y₃-C-R-C **594**

Molecular formula: C₁₄₃H₂₃₅N₄₃O₂₉S₄ M_w 3148.927

¹H NMR spectrum (400 MHz) in D₂O. δ (ppm) = 1.1-1.8 (m, 20 H, γδϵH lysine and γδH arginine), 2.3-2.6 (m, 16 H, -CO-CH₂-CH₂-CO-), 2.6-3.1 (m, 28 H, βH lysine, arginine, cysteine and tyrosine), 3.1-3.6 (m, 64 H, -CH₂- Tp), 3.8-4.6 (m, 14 H, αH amino acids), 6.65-7.15 (m, 24 H, -CH- tyrosine).

Sequence: C-R-C-Y₃-Stp₂-[(OleA)₂-K]K-Stp₂-Y₃-C-R-C **595**

Molecular formula: C₁₇₉H₂₉₉N₄₃O₃₁S₄ M_w 3677.819

¹H NMR spectrum (400 MHz) in D₂O. δ (ppm) = 0.5-0.7 (s, 6 H, -CH₃ oleic acid), 0.8-1.9 (m, 76 H, γδϵH lysine and γδH arginine, -CH₂- oleic acid), 2.3-2.6 (m, 16 H, -CO-CH₂-CH₂-CO-), 2.6-3.1 (m, 28 H, βH lysine, arginine, tyrosine and cysteine), 3.1-3.6 (m, 64 H, -CH₂- Tp), 4.0-4.6 (m, 14 H, αH amino acids), 5.15-5.3 (m, 4 H, -CH- oleic acid), 6.65-7.35 (m, 24 H, -CH- tyrosine).

Sequence: C-R-C-Y₃-Stp₂-[(Y₃)₂-K]K-Stp₂-Y₃-C-R-C **596**

Molecular formula: C₁₉₇H₂₈₉N₄₉O₄₁S₄ M_w 4127.966

¹H NMR spectrum (400 MHz) in D₂O. δ (ppm) = 0.9-1.9 (m, 20 H, γδϵH lysine and γδH arginine), 2.3-2.55 (m, 16 H, -CO-CH₂-CH₂-CO-), 2.6-3.1 (m, 40 H, βH lysine, arginine, cysteine and tyrosine), 3.1-3.6 (m, 64 H, -CH₂- Tp), 3.8-4.6 (m, 20 H, αH amino acids), 6.65-7.15 (m, 48 H, -CH- tyrosine).

Sequence: C-Stp₂-C

Molecular formula: C₃₀H₆₂N₁₂O₇S₂ M_w 767.2

FAB⁺ (mass found) 767.6

¹H NMR spectrum (400 MHz) in D₂O. δ (ppm) = 2.4-2.65 (m, 8 H, -CO-CH₂-CH₂-CO-), 2.8-3.1 (m, 4 H, βH cysteine), 3.2-3.7 (m, 32 H, -CH₂- Tp), 4.1-4.5 (m, 2 H, αH cysteine).

Sequence: Nbz-PEG₂-A

Molecular formula: C₁₈H₂₅N₅O₆ M_w 407.42

FAB⁺ (mass found) 408.4

¹H NMR spectrum (400 MHz) in D₂O. δ (ppm) = 0.8-1.2 (s, 3 H, -CH₃ alanine), 2.2-2.6 (m, 2 H, -CH₂- PEG), 3.0-4.2 (m, 11 H, -CH₂- PEG and αH alanine), 6.8-8.0 (m, 3 H, -CH-Nbz).

Sequence: Nbz-PEG₂-FolA

Molecular formula: C₃₄H₃₇N₁₁O₁₀ M_w 759.73

¹H NMR spectrum (400 MHz) in DMSO-*d*₆. δ (ppm) = 1.8-2.6 (m, 6 H, -CH₂- PEG and glutamic acid), 3.0-4.2 (m, 11 H, -CH₂- PEG and αH glutamic acid), 7.0-9.0 (m, 9 H, -CH-Nbz and N¹⁰-(trifluoroacetyl)pteroic acid)).

Sequence: Nbz-G-PEG₂₄-A

Molecular formula: C₆₄H₁₁₆N₆O₂₉ M_w 1433.63

ESI⁺ (mass found) 1433.8

¹H NMR spectrum (400 MHz) in D₂O. δ (ppm) = 1.4-1.6 (s, 3 H, -CH₃ alanine), 2.5-2.7 (m, 2 H, -CH₂- glycine), 3.2-4.2 (m, 101 H, -CH₂- PEG and αH alanine), 7.0-8.0 (m, 3 H, -CH-Nbz).

Sequence: Nbz-G-PEG₂₄-FolA

Molecular formula: C₈₀H₁₂₈N₁₂O₃₃ M_w 1785.93

ESI⁺ (mass found) 894.4 (z = 2)

¹H NMR spectrum (400 MHz) in D₂O. δ (ppm) = 2.1-3.0 (m, 6 H, -CH₂- glutamic acid and glycine), 3.2-4.2 (m, 101 H, -CH₂- PEG and αH glutamic acid), 7.1-9.0 (m, 8 H, -CH-Nbz and N¹⁰-(trifluoroacetyl)pteroic acid)).

Sequence: Nbz-G-PEG₂₄-B6 (= Nbz-G-PEG₂₄-GHKAKGPRK)

Molecular formula: C₁₀₃H₁₈₄N₂₂O₃₇ M_w 2322.69

ESI⁺ (mass found) 775.5 (z = 3)

Sequence: Nbz-G-PEG₂₄-cMBP (= Nbz-G-PEG₂₄- HHHIHDHRSLSK)
Molecular formula: C₁₂₅H₂₀₇N₃₁O₄₄ M_w 2848.16
ESI⁺ (mass found) 950.5 (z = 3)

Sequence: Nbz-G-PEG₂₄-GE11 (= Nbz-G-PEG₂₄-YHWYGYTPQNVI)
Molecular formula: C₁₃₆H₂₀₆N₂₂O₄₆ M_w 2885.21
ESI⁺ (mass found) 1444.2 (z = 2)

1.3. Publications

1.3.1. Original paper

J. C. Kasper, C. Troiber, S. Kuchler, E. Wagner, W. Frieß; *Formulation development of lyophilized, long-term stable siRNA/polyamidoamine polyplexes*, submitted.

C. Troiber, D. Edinger, P. Kos, L. Schreiner, R. Kläger, A. Herrmann, E. Wagner; *Stabilizing effect of tyrosine timers on pDNA and siRNA polyplexes*, *Biomaterials*, 34, 1624-1633, 2013.

C. Troiber, J.C. Kasper, S. Milani, M. Scheible, I. Martin, F. Schaubhut, S. Kuchler, J. Rädler, F.C. Simmel, W. Frieß, E. Wagner; *Comparison of four different particle sizing methods for siRNA polyplex characterization*, *Eur. Journal of Pharmaceutics and Biopharmaceutics*, 2012, doi: 10.1016/j.ejpb.2012.08.014.

C. Dohmen, D. Edinger, T. Fröhlich, L. Schreiner, U. Lächelt, C. Troiber, J. Rädler, P. Hadwiger, H.-P. Vornlocher, E. Wagner; *Nanosized Multifunctional Polyplexes for Receptor-Mediated SiRNA Delivery*, *ACS Nano*, 6, 5198-5208, 2012.

T. Fröhlich, D. Edinger, R. Kläger, C. Troiber, E. Salcher, N. Badgujar, I. Martin, D. Schaffert, A. Cengizeroglu, P. Hadwiger, H.-P. Vornlocher, E. Wagner; *Structure–activity relationships of siRNA carriers based on sequence-defined oligo (ethane amino) amides*, *Journal of Controlled Release*, 2012, doi: 10.1016/j.jconrel.2012.06.023.

D. Schaffert, C. Troiber, E. Wagner; *New Sequence-Defined Polyaminoamides with Tailored Endosomolytic Properties for Plasmid DNA Delivery*, *Bioconjugate Chemistry*, 23, 1157-1165, 2012.

I. Martin, C. Dohmen, C. Mas-Moruno, C. Troiber, P. Kos, D. Schaffert, U. Lächelt, M. Teixido, M. Günther, H. Kessler, E. Giralt, E. Wagner; *Solid-phase-assisted synthesis of targeting peptide-PEG-oligo(ethane amino)amides for receptor-mediated gene delivery*, *Organic & Biomolecular Chemistry*, 10, 3258-3268, 2012.

D. Schaffert, C. Troiber, E.E. Salcher, T. Fröhlich, I. Martin, N. Badgajar, C. Dohmen, D. Edinger, R. Kläger, G. Maiwald, K. Farkasova, S. Seeber, K. Jahn-Hofmann, P. Hadwiger, E. Wagner; *Solid-Phase Synthesis of Sequence-Defined T-, i-, and U-Shape Polymers for pDNA and siRNA Delivery*, *Angewandte Chemie International Edition*, 50, 8986-8989, 2011.

1.3.2. Reviews

C. Troiber, E. Wagner; *Nucleic Acid Carriers Based on Precise Polymer Conjugates*, *Bioconjugate Chemistry*, 22, 1737-1752, 2011.

1.3.3. Patents

C. Dohmen, M. Günther, U. Lächelt, D. Schaffert, C. Troiber, E. Wagner; *Polymers for Nucleic Acid Delivery*, European Patent Application (WO2011154331A1, EP2395041A1) in cooperation with Roche Kulmbach.

1.3.4. Poster presentations

C. Troiber, J.C. Kasper, S. Milani, M. Scheible, I. Martin, F. Schaubhut, S. Kuchler, J. Rädler, F.C. Simmel, W. Frieß, E. Wagner; *Analytical methods for the physico-chemical characterization of siRNA polyplexes*, Poster presentation, Center for NanoScience Workshop, Venice, 2011.

1.3.5. Oral presentations

C. Troiber, T. Fröhlich, D. Edinger, R. Kläger, P. Kos, U. Lächelt, D. Schaffert, E. Wagner; *Nucleic Acid Carriers for In Vitro and In Vivo Delivery Based on Sequence-Defined T-shape Polymers*, Oral abstract presentation, 15th Annual meeting of the American Society of Gene and Cell Therapy; Philadelphia, 2012.

VIII. ACKNOWLEDGEMENTS

This thesis would not have been possible without the help and support of various people who deserve my acknowledgement.

First of all, I want to thank my supervisor Prof. Dr. Ernst Wagner for giving me the opportunity to perform this work in his research group, his time, professional guidance and scientific support.

Furthermore, I want to thank all my colleagues for their help and support, as well as the nice atmosphere during the last three years.

Thanks to David for tutoring me during my master thesis and the beginning of my PhD. Furthermore, would like to thank all other members of the “polymer” group for the discussions, help, support and great collaboration: Edith, Claudia, Christian D., Ulrich, Irene, Thomas, Petra, Daniel, Laura, Raphaela, and Annika.

Thanks to our technicians Miriam, Ursula, Anna and Markus for keeping the lab running. My special gratitude goes to Wolfgang for being around and helping with all kind of problems. I greatly appreciated the help and support of Dr. Martina Ruffer.

Moreover, I would like to thank Dr. Jörg Pabel and the organic chemistry practical course supervising team, especially Markus, for making the time over in building C more pleasant.

Thanks to Prof. Dr. Joachim Rädler, Prof. Dr. Wolfgang Frieß, Prof. Dr. Friedrich Simmel, Frank Schaubhut, Silvia, and Max for the support and help in analyzing siRNA polyplexes. Additionally, I greatly appreciated the cooperation and support of Prof. Dr. Wolfgang Frieß in the siRNA formulation project. My special gratitude goes to Julia, for being there in the dark, cold FCS room, and of course for her scientific discussions.

Additionally, I want to thank our HiWis Verena and Sarah for helping with building block synthesis and other boring routine lab work. Moreover, I want to thank all the interns working with me, especially Ulrich, Raquel, and Teresa.

Life is more than just science. Therefore, I want to thank my family for always being there and supporting me, no matter what. I also want to thank my friends, study colleagues, and fencing partners for showing me the bright side of life. Last, but not least, I want to thank Frank for his support, patience, and just every single day.